Understanding the Role of PRMT5 in Neuroblastoma

Dr. Gulsah Albayrak
Linacre College
University of Oxford

A thesis submitted for the degree of
Doctor of Philosophy
Hilary 2023

Contents

Acknowledgements

First of all, I would like to thank my supervisor, Professor Nick La Thangue for his time, full support, and guidance throughout my DPhil. His support had been crucial and much appreciated. I would also like to thank so much to Dr. Laurel Bate-Eya for her time and efforts throughout this project whom I have learnt so much about how to be more efficient and productive in science. I was very lucky to have such great role models in Oxford.

I would also like to thank many of my colleagues, first to Dr. Simon Carr for his help and his guidance about the various aspects of the project. Thanks also to all my group members Dr. Amit Shrestha, Dr. Wojciech Barczak, Dr. Geng Liu, Hasan Syfuddin, and Koyo Harada for their support. Many other friends have also provided me a great community feeling at tough times when we could not even go home for many months. Thanks go to Simge Bahcevanci for being my Oxford sun and reminding me of the progress that we went through altogether. May Sin Ke and Nick Tenci, another thanks go to them for their great accompany. I would like to thank Dr. Ali Oztuna for his full support during my studies. I also would like to thank my friends Cem Esen, Dr. Fatih Senturk, and Dr. Ridvan Arda Demirci for their support.

As last but not least I would like to express my gratitude to the founder of the Turkish Republic, Mustafa Kemal Atatürk. My scholarship was first initiated with his guidance in 1920s, we are very fortunate to have had such a visionary leader. Final thanks go to my beloved family; Neslişah, Berke, Seynur, and Aydın for their unconditional love and support throughout my whole journey. I am very grateful for their existence. And of course, to my late mother Gül … I cannot thank them enough.

Understanding the Role of PRMT5 in Neuroblastoma

Gulsah Albayrak Department of Oncology

Linacre College University of Oxford

A thesis submitted for the degree of Doctor of Philosophy Hilary 2023

Abstract

Neuroblastoma (NB) is a deadly childhood cancer that has an orphan disease status, and the most malignant forms of the tumours have MYCN amplification. There is significant unmet medical need and urgency to develop new treatments for high-risk NB patients, as clinical research on rare diseases of children is very challenging. We revealed that higher PRMT5, MYCN, and E2F1 levels are poor prognostic factors in NB according to their Kaplan-Meier survival plots and then we hypothesized that PRMT5-E2F1-MYCN pathway might have potential prognostic value in NB. We characterized NB cell lines in terms of sensitivity to the PRMT5 inhibition by using genomic and transcriptomic assays in order to gain better insight into the underlying molecular mechanism of sensitivity to PRMT5 inhibition. We used T1-44 compound to inhibit PRMT5 biochemically. We found that MYCN amplified NB cancer cells were significantly more sensitive to the PRMT5 inhibition ($p < 0.0062$) and T1-44 treatment induced higher number of differentially expressed and alternatively spliced events in the high *E2F1/MYCN* expressing cell line when compared with the low *E2F1/MYCN* expressing cell line. We characterized differentially spliced apoptotic genes upon 200 nM treatment with T1-44 for 72 hours as these genes might have a functional impact on cell fate, we found that T1-44 induced differential splicing of apoptosis genes *BCL2L11* and *CDK10* in MYCN amplified compared with non-MYCN amplified NB cells. Our

results highlight the role of the PRMT5, E2F1, and MYCN axis in the alternative splicing pathway and its clinical relevance in MYCN amplified NB patients. MYCN amplification is observed in many other cancer types beyond NB. Therefore, we believe that our findings will also contribute to the targeted therapy efforts in other cancer types as well.

List of figures

List of tables

Abbreviations

˚C	Celsius degree
µg	Microgram
µl	Microliter
µM	Micromolar
ΔΨ	Percent spliced in
ADC	Antibody drug conjugate
ADMA	Asymmetric dimethylarginine
AHNAK	AHNAK nucleoprotein (Desmoyokin)
AKT	Serine-threonine protein kinase family
ALK	Anaplastic lymphoma kinase
ALT	Alternative lengthening of telomeres
AML	Acute myeloid leukaemia
Anti-GD2	Anti-disialoganglioside
APAF1	Apoptotic peptidase activating factor 1
ATRX	Transcriptional regulator ATRX
AURKA	Aurora kinase A
BARD1	BRCA1 associated RING domain 1
BIM	Bcl-2-like 11
BOK	Bcl-2 related ovarian killer
C1QL1	Complement C1q like 1
Cas9	CRISPR-associated protein 9
CAR-T	Chimeric antigen receptor T-cell
CASP3	Caspase 3
CASP7	Caspase 7

CCND1	Cyclin D1
CDC6	Cell division cycle 6
CDK	Cyclin-dependent kinase
CDK10	Cyclin-dependent kinase 10
CDKN1A	Cyclin dependent kinase inhibitor 1A
cDNA	Complementary DNA
CESC	Cervical squamous cell and endocervical adenocarcinoma
ChIP	Chromatin immunoprecipitation
CPSF3	Cleavage and polyadenylation specific factor 3
CPSF4	Cleavage and polyadenylation specific factor 4
CRISPR	Clustered regularly interspaced short palindromic repeats
CRPC	Castration-resistant prostate cancer
CRYZ	Crystallin zeta
CSF1	Colony stimulating factor 1
DEGs	Differentially expressed genes
dsRNA	Double-stranded RNA
DMEM	Dulbecco's modified Eagle’s medium
DMSO	Dimethyl sulfoxide
DNAJB1	DnaJ heat shock protein family (Hsp40) member B1
DP	Dimerization partner
E2F1-8	E2F transcription factor 1-8
ENCODE	Encyclopedia of DNA elements
FBS	Fetal bovine serum
FDR	False discovery rate
GAB2	GRB2 associated binding protein 2

GBM	Glioblastoma multiforme
GEO	Gene expression omnibus
GM-CSF	Granulocyte-macrophage colony-stimulating factor
GO	Gene ontology
GPC2	Glypican 2
GSEA	Gene set enrichment analysis
GWAS	Genome wide association studies
HCC	Hepatocellular carcinoma
HNRNPA3	Heterogeneous nuclear ribonucleoprotein A3
HRK	Harakiri, BCL2 interacting protein
HVA	Homovanillic acid
ID2	Inhibitor of DNA binding 2
IGFBP5	Insulin like growth factor binding protein 5
IL-2	Interleukin-2
INFORM	Individualized therapy for relapsed malignancies in childhood
IR	Intron retention
ITS	Insulin, transferrin, selenous acid
KIRC	Kidney renal clear cell carcinoma
KIRP	Kidney renal papillary cell carcinoma
KO	Knockout
LIF	Leukemia inhibitory factor
LIHC	Liver hepatocellular carcinoma
LIN28B	Lin-28 homolog B
LUAD	Lung adenocarcinoma
MCL	Mantle cell lymphoma

MDS	Myelodysplastic syndrome
METTL7A	Methyltransferase like 7A
MIBG	Iodine-131-meta-iodobenzylguanidine
MMA	Monodimethylarginine
MPAK	Mitogen-activated protein kinase
mRNA	Messenger RNA
MTA	Methylthioadenosine
MTAP	Methylthioadenosine phosphorylase
MTT	3-(4,5-dimethylthiazol-2-yl)- 2,5-diphenyltetrazolium bromide
MYCN	MYCN proto-oncogene, bHLH transcription factor
NB	Neuroblastoma
NCL	Nucleolin
NEPC	Neuroendocrine prostate cancer
NHL	Non-Hodgkin lymphoma
NMD	Nonsense-mediated decay
OMS	Opsoclonus myoclonus syndrome
PBD	Pyrrolobenzodiazepine
PMAIP1	Phorbol-12-myristate-13-acetate-induced protein 1
PAGE1	P antigen family member 1
PAPOLA	Poly (A) polymerase alpha
PARP2	Poly (ADP-Ribose) polymerase 2
PBS	Phosphate-buffered saline
PCR	Polymerase chain reaction
PDAC	Pancreatic ductal adenocarcinoma
PHLDA3	Pleckstrin homology like domain family A member 3

PHOX2B	Paired like homeobox 2B
PI3K-mTOR	Phosphoinositide 3-kinase-mammalian target of rapamycin
PLK1	Polo like kinase 1
PLK2	Polo like kinase 2
PNET	Primitive neuroectodermal tumour
PRMT	Protein arginine methyltransferase
PRMT5	Protein arginine methyltransferase 5
PSI	Percent of spliced in scores
PUMA	p53 upregulated modulator of apoptosis
PVDF	Polyvinylidene difluoride
qPCR	Quantitative real time PCR
RB	Retinoblastoma
RBP	RNA-binding protein
RGG/RG	Arginine and glycine rich motifs
RNA	Ribonucleic acid
RNA-seq	RNA sequencing
RPM	Revolutions per minute
RPS27L	Ribosomal protein S27 like
RTK	Receptor tyrosine kinase
RT-PCR	Reverse transcription polymerase chain reaction
SAM	S-adenosylmethionine
SARC	Sarcoma
SCLC	Small cell lung cancer
SD	Standard deviation
SDMA	Symmetric dimethylarginine

SDS	Sodium dodecyl sulfate
SEC31A	SEC31 homolog A, COPII coat complex component
SF1	Splicing factor 1
SF3B1	Splicing factor 3b subunit 1
sgRNA	Single guide RNA
siRNA	Small interfering RNA
SKP2	S phase kinase associated protein 2
snRNP	Small nuclear ribonucleoprotein
SNRNPN200	Small nuclear ribonucleoprotein U5 subunit 200
SPECT/CT	Single-photon emission computed tomography with computed tomography
SR	Serine and arginine rich
SRSF1	Serine and arginine rich splicing factor 1
SRSF2	Serine and arginine rich splicing factor 2
SRSF3	Serine and arginine rich splicing factor 3
SRSF4	Serine and arginine rich splicing factor 4
TARGET	Therapeutically applicable research to generate effective treatments
TBS-T	Tris-buffered saline-Tween 20
TCGA	The cancer genome atlas
TE	Tris-EDTA
TERT	Telomerase reverse transcriptase
TF	Transcription factors
TIGAR	TP53 induced glycolysis regulatory phosphatase
TP53	Tumour protein 53
TSN	Translin

U2AF	U2 auxiliary factor
UHR	Ultra-high risk
VEGFA	Vascular endothelial growth factor A
VMA	Vanillylmandelic acid
WT	Wild type

CHAPTER 1. INTRODUCTION

1.1. Neuroblastoma

1.1.1. Epidemiology

Neuroblastoma (NB) is the most common extracranial solid tumour in childhood that is a developmental tumour that arises from the embryonic sympathoadrenal lineage of the neural crest cells (Louis and Shohet, 2015). NB accounts for 12%-15% of all childhood cancer related deaths (Johnsen et al., 2019).

Neuroblastoma incidence is approximately 10.2 cases per million children under 15 years of age (Colon and Chung, 2011). Every year, approximately 1,500 cases are diagnosed in Europe and 700 cases in the United States and Canada, which makes up 28% of all cancers in infants in those regions. NB has a median age at diagnosis of 18 month; however, it can be diagnosed in either childhood or adulthood and 90% of tumours arise in children who are younger than 10 years (Matthay et al., 2016). There is a slight predisposition for males, with a male-to-female ratio of 1.2:1 (Heck et al., 2009).

1.1.2. Etiology

While there are a few known risk factors for neuroblastoma, the exact etiology of neuroblastoma is not well known. NB can be sporadic or inherited through the germline. Minority of the neuroblastoma cases (1% to 2%) have family history as inherited in an autosomal dominant manner (Barr and Applebaum, 2018). Familial neuroblastoma cases are usually linked to the inheritance of penetrant mutations in either the *ALK* or *PHOX2B* genes (Bourdeaut et al, 2012). Mutations in *ALK* account for 15% of sporadic neuroblastomas, while more frequent changes involve polymorphisms in *BARD1*, *LIN28B*, or *FLJ22536* genes (Mahapatra and Challagundla, 2023). Notably, more than 27% of neuroblastomas have with a MYCN amplification

located on chromosome 2, which is associated with a poor prognosis. 17q gain and 1p loss also correlates with MYCN amplification (Huang and Weiss, 2013). Studies with environmental factors that are known to increase the chance of getting neuroblastoma have reported inconsistent findings (Bluhm et al., 2008).

1.1.3. Pathogenesis

Neuroblastoma tumours are histologically characterized as small round blue cell tumours alongside with other undifferentiated paediatric malignancies such as rhabdomyosarcoma, non-Hodgkin's lymphoma, Ewing's sarcoma, primitive neuroectodermal tumour (PNET), and the blastemal component of Wilms' tumour (Gregoria et al., 2008).

The origin of neuroblastoma cells has not been defined precisely but likely to derive from sympathoadrenal progenitor cells within the neural crest that differentiate to sympathetic ganglion cells and adrenal catecholamine-secreting chromaffin cells (Johnsen et al., 2019). Genomic and epigenetic impairments might be the underlying mechanism for this defective differentiation of neural crest derived cells (Ponzoni et al., 2022). Several cytogenetic and molecular factors have been associated with the pathogenicity of neuroblastoma and certain cytogenetic and molecular tumour characteristics correlate with prognosis and treatment selection.

Chromosomal alterations are common in NB and these alterations have been shown to have prognostic importance (Schleiermacher et al., 2012). While whole chromosome gains are associated with low-risk NB, segmental alterations such as gains or losses of chromosome arms such as the loss of 1p, 3p, 4p, 11q and gain of 1q, 2p, 17q are associated with poor prognosis (Brady et al., 2020). In additional to chromosomal gains and structural changes, ploidy is also important in terms of prognosis and response to

therapy. Overall better prognosis and response to initial treatment have been shown at hyperdiploid tumour cells in NB (Look et al., 1991).

Somatic mutations in NB are diverse and these mutations can affect various pathways involved in cancer progression. *ALK* mutations impair PI3K/AKT, RAS/MAPK, and JAK/STAT signalling pathways lead NB cell survival and proliferation. *ALK* mutated NB is predictive of a poor prognosis despite of the multimodal treatment modalities and *ALK* mutations are found in 15% and 2-3% of sporadic and familial neuroblastomas, respectively (Hallberg and Palmer, 2016; Trigg and Turner, 2018).

Genetic changes that have an effect on telomere maintenance are poor prognostic indicator that is frequently observed in high-risk NB. Loss of function alterations in transcriptional regulator ATRX (*ATRX*) and *TERT* (encoding Telomerase Reverse Transcriptase) genes were linked to telomere maintenance. NB cells upregulate telomerase activity via overexpression of *TERT* in order to maintain telomere length. *ATRX* is a chromatin remodeler that is involved in DNA repair and telomere maintenance, and mutations in this gene can lead to genomic instability and altered gene expression. *TERT* is a telomerase reverse transcriptase that is involved in telomere maintenance and cell immortalization, and mutations in this gene can lead to increased cell proliferation and survival (Koneru et al., 2020; Hartlieb et al., 2021).

Unlike other human cancers, *p53* is rarely mutated in the primary tumour in NB and *p53* mutations usually appear in tumours post chemotherapy treatment (Blanco-Luquin et al., 2021). However, Ackermann and colleagues reported that the survival rates were lowest at patients whose tumours carry both telomere maintenance and RAS or p53 pathway alterations where they performed genome sequencing on 416 pretreated NBs (Ackermann et al., 2018).

The role of MYCN amplification in neuroblastoma pathogenesis

The MYC proto-oncogene family includes three paralogs *c-MYC (MYC)*, *MYCN*, and *MYCL*. Due to structural and sequence similarity between the *MYC* family genes, the function and biochemical properties of MYC proteins are closely related. MYC and MYCN have mutual exclusivity at mRNA and protein level. However, their expression and functionality are tissue specific (Beltran et al., 2014).

MYCN can affect cellular processes like sustained growth and repress genes that drive differentiation. The target genes of MYCN have diverse roles in proliferation, differentiation, cell cycle, apoptosis, angiogenesis, and immune surveillance (Hsu et al., 2016). MYCN promotes cell cycle progression by activating G1-S transition, G2-M transition, and mitosis relevant gene expressions. Some of the transcriptional targets of MYCN include Cyclin D1 (*CCND1*), Aurora kinase A (*AURKA*), Nucleolin (*NCL*), Polo-like kinase 1 (*PLK1*), S phase kinase associated protein 2 (*SKP2*), and inhibitor of DNA binding 2 (*ID2*).

MYCN is overexpressed in nervous system tumours neuroblastoma, medulloblastoma, retinoblastoma, astrocytoma, glioblastoma multiforme, and also in nonneuronal tumours such as castration-resistant prostate cancer (CRPC) and neuroendocrine prostate cancer (NEPC), haematologic malignancies, rhabdomyosarcoma, Wilms' tumour, small cell lung cancer (SCLC), and pancreatic tumours (Rickman et al., 2018).

Inducible overexpression of MYCN in genetically engineered mouse model induced clinically relevant NB (Weiss et al., 1997; Althoff et al., 2015). In another study, subcutaneous introduction of overexpressed MYCN cells into mice led to human tumour relevant model in terms of phenotype and molecular characteristics of MYCN amplified NB (Kroesen et al., 2014). Ectopic expression of MYCN also induces NB in zebrafish, demonstrating the conserved nature of MYCN among other species. These

findings highlight the role of MYCN expression as a driver of neuroblastoma (Rickman and Schulte, 2018). More than 27% of NB present with MYCN amplification which is strongly associated with a poor patient prognosis (Maris, 2010; Huang and Weiss, 2013). Also, MYCN expression levels correlate with invasive and metastatic behaviour. Metastases are found in most cases at diagnosis, consistent with an origin from multipotent migratory neural crest cells. Metastasis occurs in half of the of NB patients at diagnosis to bone marrow, bone, lymph nodes, liver, and brain (Huang and Weiss, 2013).

1.1.4. Diagnosis and risk stratification

Most neuroblastoma cases are diagnosed before the age of five (Colon, 2011). The manifestations of NB depend on the stage and location of the tumour. Common symptoms may include abdominal pain, anorexia, decreased appetite, exhaustion, and bone pain (Chu et al., 2011).

Neuroblastoma diagnosis is based on the elevated levels of urinary catecholamines [homovanillic acid (HVA), vanillylmandelic acid (VMA)], dopamine, and on initial tumour imaging by ultrasound, brain scan or MRI (Strenger et al., 2007). Tumour biopsy confirms the diagnosis and allows histological classification. Genomic sequencing of tumour tissue is used for many novel therapies in relapsed or refractory neuroblastoma. Image-guided biopsy options like MIBG (iodine-131-meta-iodobenzylguanidine) single-photon emission computed tomography with computed tomography (SPECT/CT) is also useful for finding metastases in order to guide therapy decisions (Samoyedny et al., 2021).

The International Neuroblastoma Risk Group was established to guide the treatment intensity depending on disease stratification. This international categorization takes into

account the age, stage, histology, *MYCN* gene amplification status, tumour cell ploidy, and chromosomal abnormalities of the patient (Tolbert and Matthay, 2018).

Molecular determinants of clinical ultra-high risk (UHR) stratification have also been characterized recently. This UHR stratification is based on the *MYCN* amplification status, *TERT* rearrangement, higher ALT (alternative lengthening of telomeres) and *TERT* expression and mutations in *TP53* and RAS/MAPK (mitogen-activated protein kinase) pathways (Schmelz et al. 2021). The INFORM (Individualized Therapy for Relapsed Malignancies in Childhood) precision medicine study group has also identified common actionable targets including RTK (receptor tyrosine kinases), PI3K-mTOR (phosphoinositide 3-kinase-mammalian target of rapamycin), and MAPK pathways in real-time molecular profiling of high-risk paediatric cancer patients (Worst et al., 2016).

Extensive genetic intratumour heterogeneity is also reflected in patient survival rates of NB. Survival rates could be lower than 50% in high-risk patients, whereas that could go up to more than 95% in low-risk patients (Lundberg et al., 2022).

1.1.5. Treatment

The current strategy in localized NB treatment involves the resection of the primary tumour after completion of all induction chemotherapy. The chemotherapy regimen consists of carboplatin, cyclophosphamide, doxorubicin, and etoposide. However, complete surgical excision might be limited due to the major blood vessel and other structures involvement (Chung et al., 2021).

Neuroblastoma treatment is based on tumour risk qualifications whether low, intermediate, and high risk. Treatment for low-risk tumours is either observation or resection with chemotherapy only for symptomatic patients. The 5-year overall survival

rate for low-risk patients has been found as 98% in 5,000 patients enrolled in the Children's Oncology Group study (Board, 2022).

Multiagent chemotherapy is often given before definitive resection to achieve a partial response to the NB patients with intermediate-risk tumours. The 5-year overall survival rate for intermediate-risk patients has been found as 95% (Board, 2022).

Treatment of high-risk NB consists of intensive multiagent chemotherapy and surgical resection of the primary tumour to reduce tumour burden. In later stages high-dose chemotherapy is used alongside with autologous stem cell rescue followed by radiotherapy. The last phase involves using immunotherapy and isotretinoin as targeted therapies (DuBois et al., 2022). Immunotherapy that combines a monoclonal antibody that targets anti-disialoganglioside (anti-GD2) with interleukin-2 (IL-2), granulocyte-macrophage colony-stimulating factor (GM-CSF), and isotretinoin has been established as standard of care for high-risk NB patients according to a Children's Oncology Group protocol, leading to a significant increase in survival rates (Voeller and Sondel, 2019).

Metastatic NB that has MYCN amplification involves local radiotherapy, conventional chemotherapy, surgical resection of the tumour tissue, high dose chemotherapy with hematopoietic stem cell transplantation, and retinoic acid therapy (Smith et al., 2018).

Some cases of NB have shown spontaneous regression and autoimmune paraneoplastic manifestations, such as the rare opsoclonus myoclonus syndrome (OMS). OMS is associated with lymphocytic infiltration among tumour cells, antineuronal serum antibodies, and a high survival rate have encouraged immunotherapy efforts to treat neuroblastoma (Meena et al., 2016). Spontaneous tumour regression generally occurs in tumours characterized with near triploid number of chromosomes, non-MYCN amplified, and in the absence of chromosome 1p loss (Board, 2022).

The drugs approved for NB treatment include cyclophosphamide, dinutuximab, doxorubicin hydrochloride, naxitamab-gqgk, and vincristine sulfate. Monoclonal antibody-based immunotherapy approaches increased event-free survival in high-risk NB patients where monoclonal antibodies were targeted against tumour-associated disialoganglioside GD2 that is overexpressed in NB (Yu et al., 2010). Dinutuximab beta is an anti-GD2 monoclonal antibody that binds to GD2 on tumour cells, marking these cells for the removal by the body's own immune system. Dinutuximab beta has been approved for use in high-risk NB patients (Achbergerová et al., 2022). Naxitamab-gqgk also binds to GD2 and it has been the second immunotherapeutic approved by FDA to treat patients with high-risk NB (Sengupta and Zaidi, 2021).

CAR-T cells and antibody-drug conjugates (ADC) were also reported to show preclinical and early clinical efficacy. Neuroblastoma was described as ideal target for immunotherapeutic modalities as NB cells do not represent normal developmental process and continue to express lineage-specific cell surface molecules. Buongervino and colleagues reported that they developed GPC2-targeting ADC that is highly specific to human GPC2 (Glypican 2) antibody conjugated to pyrrolobenzodiazepine (PBD) dimers. However, they encountered technical challenges such as potential therapeutic index remains limited due to PBD dimer payloads in humans (Buongervino et al., 2021).

Although the initial CAR-T clinical trials in NB have proven safe and feasible, some limitations were spotted such as the lack of T cell persistence, difficulty in target antigen selection, and suppressive tumour microenvironment. These challenges might shed light onto the underlying reasons for limited success in CAR-T trials. However, some of these challenges are not only exclusive to NB but also to the whole CAR-T cell field (Richards et al., 2018).

MYCN is considered undruggable due to some of the underlying challenges. MYCN's homology to MYC, intrinsically disordered protein nature of MYC family members in their monomeric form, limited knowledge about MYCN-interacting proteins, the lack of structural information about MYCN protein complexes, and the limitations of small molecules to drug protein-protein or protein-DNA interactions (Wolpaw et al., 2021). Therefore, targeting MYCN is not yet possible in standard of care for MYCN amplified neuroblastoma. However, the first direct inhibitor of MYC (OMO-103) has recently entered human clinical trial and shown early signs of safety with antitumour activity in patients with advanced solid cancers, but it is still very early to know more about the mechanism of action and target engagement (Llombart and Mansour, 2022).

Growing evidence from a wide range of genome wide association studies (GWAS), whole exome, and whole genome sequencing studies showed that ALK might be a promising target as a validated driver of the disease in animal models. However, *ALK* mutations occur in only a small subset of the patient population and initial studies against targeting ALK in these patients have been disappointing (Carpenter and Mosse, 2012, NCT02780128). More recently lorlatinib, which is a third-generation inhibitor of ALK and ROS1 entered in phase 1 trial as monotherapy and in combination with chemotherapy in NB (Trigg and Turner, 2018; NIH, 2017).

1.2. Protein Arginine Methyl Transferase 5 (PRMT5) and cancer

Arginine methylation acts as a key regulator of cellular mechanisms such as epigenetic regulation, mRNA splicing, DNA damage response, cell signalling, and cell fate decision (Jarrold and Davies, 2019; Blanc and Richard, 2017).

Protein arginine methylation is widespread post-translational modifications where a methyl group is added onto the arginine residues (Raposo and Piller, 2018). Arginine methylation occurs in three forms as monomethylation, asymmetric dimethylation, and symmetric dimethylation that are carried out by three different types of protein arginine methyltransferases (PRMTs) (Figure 1.1) (Wu et al., 2016).

So far, nine different mammalian PRMTs have been characterized into three categories based on their ability to transfer one or two methyl groups to the nitrogen atoms of the guanidinium side chains of arginine residues with the use of S-adenosylmethionine (SAM) as the methyl donor. Type I PRMTs (PRMT1, 2, 3, 4, 6, and 8) generate monomethylarginine (MMA) and asymmetric dimethylarginine, Type II PRMTs (PRMT5 and 9) produce MMA and symmetric dimethylarginine, and Type III PRMT (PRMT7) produces only MMA (Figure 1.1) (Hwang et al., 2021).

The guanidinium groups in arginine remain protonated and have a relatively high pKa range of 12.5-14.0 compared to other amino acids at physiological pH. This allows arginine to form salt bridges and serve as a donor. The methylation of arginine does not affect the functionality of guanidinium, but its shape and charge distribution is altered. This increases its hydrophobicity and limits its ability to form H-bonds by one per methylation event (Lorton and Shechter, 2019).

All PRMTs have four conserved sequence motifs (I, post-I, II, and III) and a THW loop where S-adenosyl-L-methionine (AdoMet) binds in the tertiary structure (Figure 1.1) (Hwang et al., 2021).

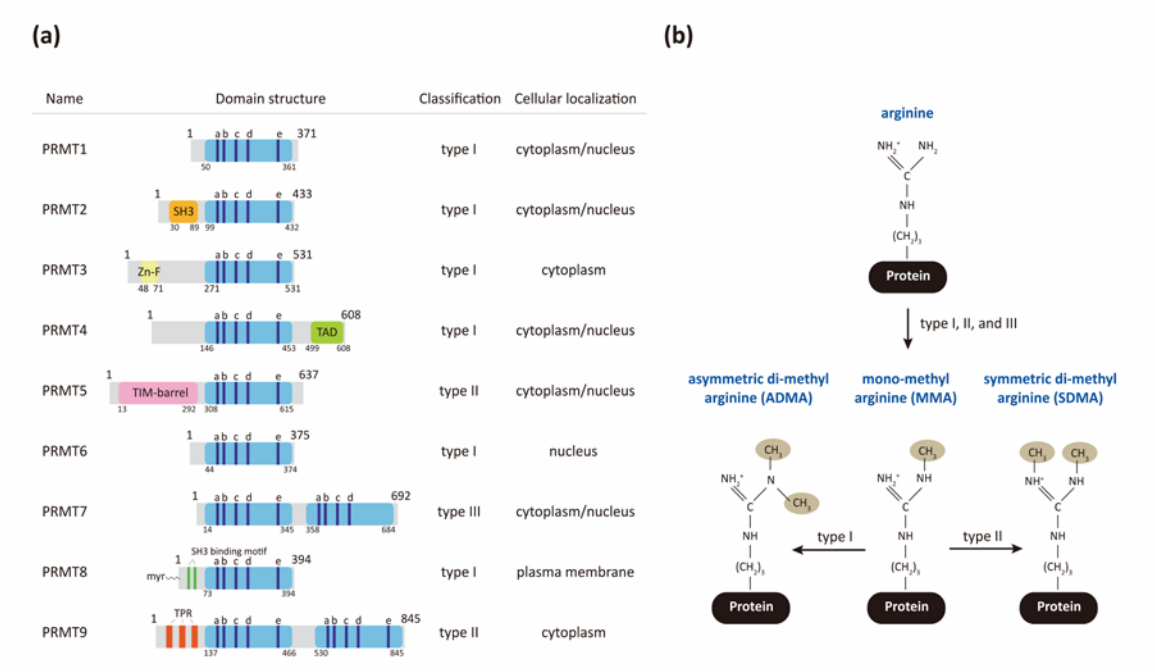

Figure 1.1. The protein arginine methyltransferases (PRMTs) a) PRMT enzyme family. b) Types of arginine methylation. Asymmetric dimethylarginine (ADMA), Symmetric dimethylarginine (SDMA) or Monomethylarginine (MMA) (Hwang et al., 2021).

PRMT1 and PRMT5 are the most common type I and II arginine methyltransferases. Their ability to methylate both histone and nonhistone molecules enable them to regulate several biological processes. Arginine and glycine rich motifs (RGG/RG) have substrate specificity for PRMT1 and PRMT5. PRMT5 methylates histones H2AR3, H3R2, H3R8, and H4R3 and therefore affect transcriptional regulation. PRMT5 also methylates non-histone proteins like RNA binding Sm proteins, ribosomal proteins, and E2F1 transcriptional factor (Al-Hamashi et al., 2010).

1.2.1. PRMT5

PRMT5 is responsible for arginine methylation, which has a major influence on the splicing patterns of RNA-binding proteins and splicing machinery. This process of methylation is responsible for the regulation of both constitutive and alternative splicing (Bezzi et al., 2013).

PRMT5 is involved in methylating nuclear and cytoplasmic substrates including histone and non-histone proteins (Ratovitski et al., 2015). An increasing number of non-histone proteins have been identified as PRMT5 substrates (Scaglione et al., 2018). Tumour suppressor p53 is methylated by PRMT5 upon DNA damage and this methylation has an important consequence on the p53 response (Li and Diehl, 2015). Our group has previously showed that p53 undergoes arginine methylation and that can influence the outcome of the p53 response. PRMT5 is a co-factor in a complex that interacts with p53 and is responsible for methylating p53. PRTM5 depletion causes p53-dependent apoptosis; therefore, methylation of arginine residues is a key process for controlling the p53 response (Jansson et al., 2008).

PRMT5 plays a regulatory role in cancer progression by promoting the proliferation, invasion, and migration of cancer cells (Xiao et al., 2019). PRMT5 is also involved in the maturation of small nuclear ribonucleoproteins (snRNPs) and maintenance of splicing fidelity. PRMT5 inhibition induces intron retention with weak 5’ splice sites and exon skipping (Guccione and Richard, 2019). PRMT5 methylates RGG/RG motif containing proteins, which are the modulators of mRNA functional states (Lorton et al., 2019). PRMT5 depletion leads to mis-splicing of genes that regulate cell proliferation and signalling. Studies have shown that the lack of symmetrical dimethylation of Sm proteins due to PRMT5 depletion promotes expression of the MDM4 short isoform, which contains a premature stop codon that suppresses the p53 pathway. This has been shown in numerous cancers, such as melanoma and haematological malignancies. PRMT5 inactivation results in the mis-splicing of MYC-regulated transcripts in B-cell lymphoma, resulting in apoptosis of the transformed cells (Guccione and Richard, 2019).

Sachamitr and colleagues found that PRMT5 inhibition led to dramatic changes in mRNA splicing and increased splicing events that disrupts cell cycle relevant transcript levels in 46 different patient derived glioblastoma cell lines (Sachamitr et al., 2021). PRMT5 has profound effects on regulating key cell cycle, DNA damage response, and repair mechanisms. PRMT5 inhibition induces aberrant splicing of downstream molecules that leads to R-loop formation. DNA-RNA hybrids can cause DNA damage due to collision between RNA transcription and DNA replication machinery (Kalev et al., 2021).

PRMT5 has dual role in normal development as well. PRMT5 knockout mice are lethal and conditional knockout mice show alterations in hematopoiesis suggesting the role of PRMT5 in development and hematopoiesis. PRMT5 overexpression has been associated with a poor prognosis in ovarian, lung, multiple myeloma, breast, glioblastoma, and prostate tumours (Lattouf et al., 2019).

1.2.2. PRMT5, E2F1, and alternative splicing

1.2.2.1. Alternative splicing in cancer

Alternative RNA splicing is the main step of post-transcriptional gene expression regulation. Alternative splicing has been evolutionarily conserved and enables a single gene to generate different mRNA isoforms thereby enhancing the proteomic and functional genomic diversity.

Cancer cells alter the splicing process to produce isoforms in favour of cell growth, migration, and to avoid cell death. Mutations in splicing-regulatory components of specific cancer genes lead to defective alternative splicing. Transcriptional and post-transcriptional regulation of splicing factors is differentially regulated in tumour cells (Urbanski, 2018). Alternative splicing plays an essential role in cell differentiation, tissue identity, and organ development. Mutations in pre-mRNA elements, splicing

factors or other components of the spliceosome complex can cause a variety of human diseases (Baralle and Giudice, 2017).

Alternative splicing can generate several different types of mRNA isoforms, depending on the type and location of splicing events. The most common types of alternative splicing mechanism have been described as exon skipping, intron retention, mutually exclusive exons, and alternative 5' or 3' splice site selection (Fackenthal and Godley, 2008) (Figure 1.2).

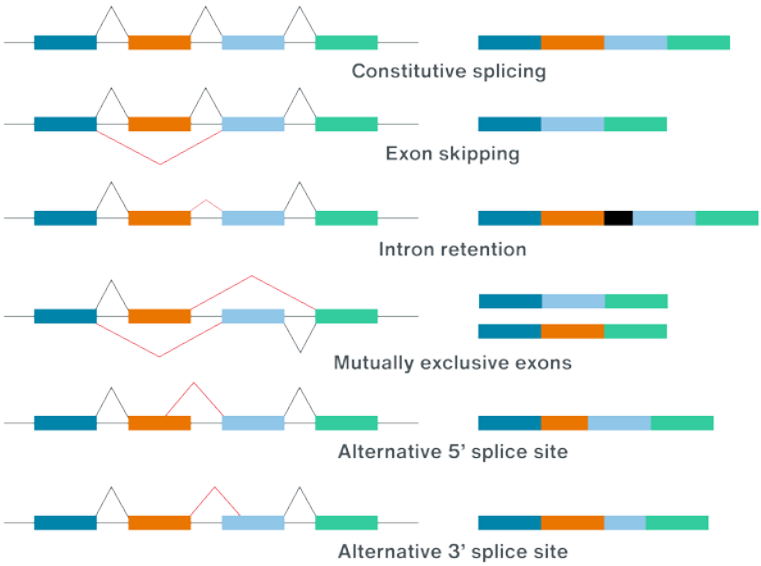

Figure 1.2. Different types of alternative splicing. Alternative splicing could be divided into groups of constitutive splicing, exon skipping, intron retention, mutually exclusive exons, alternative 5'splice site, and alternative 3'splice site.

Exon skipping is the removal of certain exons during the splicing process where introns are removed from mRNA in order to form mature mRNA. Splicing is strictly regulated to avoid errors, but alternative splicing takes place in more than 90% of human genes, diversifying the range of mRNAs and protein products. Notably, exon skipping is the most frequent type of alternative splicing (Matsuo, 2021).

Intron retention (IR) occurs when a complete and unspliced intron remains in mature mRNA. IR has a significant role in many biological activities in health and disease

(Grabski et al., 2021). IR is thought to be the least prevalent form of alternative splicing in animals, whereas it is the most frequent form in plants, fungi, and single-celled eukaryotes. However, there is emerging evidence that IR controls cell type specific and developmental gene expression and therefore globally impacts gene expression in mammalian cells (Braunschweig et al., 2014).

Mutually exclusive exons are characterized by splicing of one out of two exons (or one group out of two exon groups) is retained, while the other one is spliced out as they are mutually exclusive. Unlike the other forms of alternative splicing, mutually exclusive splicing can result in a protein of the same size as the original, if the exchanged sequence is the same length as the original and does not include a premature termination of the protein (Pohl et al., 2013).

Alternative 5' or 3' splice site selection can result in the use of different 5' or 3' splice sites, leading to the inclusion or exclusion of exons. Splice site selection is a fundamental process in alternative splicing in order to avoid exon skipping among all multiple introns containing pre-mRNAs. Splice site selection occurs during the formation of spliceosomes, which are large protein-RNA complexes containing pre-mRNA, 5 snRNPs (U1, U2, U4/U6, and U5 snRNAs), and a large number of proteins (Wu and Maniatis, 1993).

Trans- and cis-acting regulators regulate alternative splicing. Cis-acting regions are exonic and intronic splicing enhancers or silencers, which are targeted by RNA-binding proteins. Trans-acting regulators consist of heterogeneous nuclear ribonucleoproteins (HNRNPs), serine-arginine-rich proteins (SR proteins) like SRSF1, and auxiliary proteins such as SF1 and U2AF. Other influential factors include the location of cis-elements, the pre-mRNA's secondary structure, sequence modifications from RNA editing, and epigenetic alterations (Gallego-Paez et al., 2017).

Defective alternative splicing has been associated with several human diseases. Somatic mutation in splicing machinery components have been found both in solid tumours including bladder, brain, breast, cervix, colon, kidney, liver, lung, oral, ovary, prostate, skin, stomach, thyroid, and haematological malignancies including acute myeloid leukaemia (AML) and myelodysplastic syndrome (MDS) (Zhang et al., 2021).

Although there is a great effort to identify the tumour-specific splicing variants that have clinical significance, only recently genome-wide profiling methods have been used to reveal alternative splicing roles in cancer. Guo and colleagues showed that NB tumours have distinct alternative splicing profiles according to the stage and MYCN amplification status (Guo et al. 2011).

Targeting splicing in MYCN amplified cancers

MYC-driven cancers were shown to be dependent on the spliceosome and targeting splicing factors in MYC-driven neuroblastoma might be an effective treatment strategy. Spliceosome assembly was significantly enriched pathway in high-risk neuroblastoma, where 3,000 most differentially expressed genes were analysed in 498 primary NB samples. DNA replication and cell cycle signatures were the most relevant gene ontology categories (Singh et al., 2021).

Early (stage 1) and late stage (stage 4) NB tumours exerted distinct global alternative splicing patterns in exon array profiling where 47 neuroblastoma tumour samples in stage 1 and stage 4 with normal or amplified MYCN copy number were compared. This distinct profile points out the importance of alternative splicing relevant changes in high stage neuroblastoma (Guo et al., 2011).

Splicing factor expression levels are correlated with poor prognosis in cancer. More than 900 primarily intra-chromosomal fusions containing canonical splicing sites had been identified in 172 RNA-sequenced neuroblastoma tumours (Shi et al., 2021).

MYCN regulates the expression of diverse splicing factors that might be necessary for the symmetrical dimethylation activation of the splicing machinery by PRMT5. Canonical *MYC* gene sets include transcription and RNA processing, chromatin remodelling, and translational processes (Zhang et al., 2016).

In MYC-driven cancers, the oncogenic *MYC* gene leads to increased transcription (gene amplification, translocation, and changes in upstream signalling pathways), overwhelming the splicing machinery and making cells more sensitive to splicing interventions (Koh et al., 2016). Genetic knockdown or pharmacological inhibition of spliceosomes caused retained introns to accumulate, leading to increased apoptosis, reduced tumorigenesis, and metastasis in MYC-driven tumours (Anczuków and Krainer, 2015). In addition to that, mutations in spliceosome genes make cells more sensitive to splicing perturbations as cancer cells have a limited ability to tolerate a partial reduction in normal splicing function (Taylor and Lee, 2019). MYC-driven cells that are undergoing oncogenic transformation must cope with an increased demand for RNA processing. Studies have shown that RNA metabolism and splicing relevant genes are the most differentially expressed in high-risk NB (Singh et al., 2021).

Targeting RNA splicing in cancer treatment could provide benefits. Splicing modulation can be achieved via modifying the splicing regulators, thereby affecting their downstream splicing network, or by precisely targeting a single spliced isoform expressed in cancer cells (Urbanski et al., 2018).

1.2.2.2. E2F1 and alternative splicing

The E2F transcription factors consist of 8 genes that can be divided into 3 groups depending on their functions during the cell cycle: activators (E2F1, E2F2, and E2F3), canonical repressors (E2F4, E2F5, and E2F6), and non-canonical repressors (E2F7 and E2F8) (Kent et al., 2017). In mammalian cells, physiological E2F forms heterodimer

complexes with dimerization partner (DP). To date, eight E2F and two DP subunits have been characterized and these heterodimeric transcription factors are involved in cell cycle control (Milton et al., 2006; La Thangue, 1994). E2Fs (E2F1-E2F6) require forming heterodimers with binding partners (DP-1 or DP-2) in order to bind to DNA. However, E2F7 and E2F8 can bind to DNA without binding to DPs and act as transcriptional repressors in a growth-inhibitory manner (Rowland and Bernards, 2006).

E2Fs regulate gene expressions that are involved in various biological functions (Meng and Ghosh, 2014). The complexity of the E2F family arises from differential promoter usage and splicing, thereby leading to multiple E2F isoforms (Dimova and Dyson, 2005). E2F activators and repressors were found to regulate cell cycle-dependent gene expression by sequential binding to target promoters.

E2Fs can regulate the expression of genes involved in G1-S phase transition positively and negatively as well as other cell-cycle progression molecules like cyclins, cyclin-dependent kinases (CDKs), transcription factors, and CDK inhibitors (Denechaud et al., 2017).

The RB/E2F regulatory pathway is one of the most frequent targets of genetic alterations in human cancer, which controls the cell cycle progression through the G1 restriction point. Any alterations in this pathway results in the deregulated expression of the transcription factor E2F, one of the key mediators of cell cycle progression (Stanelle et al., 2012).

E2F1 is the first identified protein amongst the other E2F members and remains as the best characterized. The E2F1 transcription factor is involved in the regulation of the cell cycle, in health, and disease (Swiss and Casaccia, 2010).

The activity of E2F1 is regulated via its binding partners, which include dimerization proteins and the RB family proteins. RB regulates the cell cycle by binding to E2F1 and inhibiting the transcriptional activity. Rapid MYC protein accumulation and cyclin D induction leads to the inactivation of the RB tumour suppressor (Vélez-Cruz et al., 2017). RB-mediated repression leads to E2F transcription factors release that initiates DNA replication and cell cycle progression and was identified as a key step in regulation of cell cycle entry in mammalian cells (Shats et al., 2017). CDKs regulates RB and E2F1 interaction through phosphorylation of RB. Unphosphorylated RB binds and inactivates E2F1, whereas phosphorylated RB cannot interact with E2F1. Mitogens increase RB phosphorylation via the upregulation of CDK. The transcription factor E2F1 regulates cell cycle progression through the G1/S transition as well as proteins important in DNA repair and apoptosis (Roworth et al., 2019).

Diverse roles include autophagy, DNA repair, and resistance to chemotherapeutic agents underlines the importance and complexity of the E2F1 biology (Figure 1.3) (Carr et al., 2015; Roworth et al., 2015). E2F1 has distinct roles that are not shared by the other E2F family members due to its ability to bind specific promoters that regulates gene transcription (Broeker and Andrechek, 2021). E2Fs have promoter regions in many genes involved in DNA replication and cell cycle control (Polager et al., 2002). E2F1, E2F2, and E2F3 triple knockout in mouse embryonic fibroblasts disrupted colony formation ability and prevents cells from proliferating (Kent and Leone, 2019).

E2F1 protein also plays roles in determining cell fate, higher levels of E2F1 triggers apoptosis, whereas lower expression favours cell cycle progression. In a single-cell quantitative analysis low levels of E2F1 were found to induce several cell cycle relevant genes. Moderate levels induce growth arrest genes like *p18*, *p19,* and *p27*, whereas

higher levels were linked the initiation of the apoptotic E2F1 targets such as *APAF1*, *PUMA*, *HRK*, and *BIM* (Figure 1.3) (Shats et al., 2017).

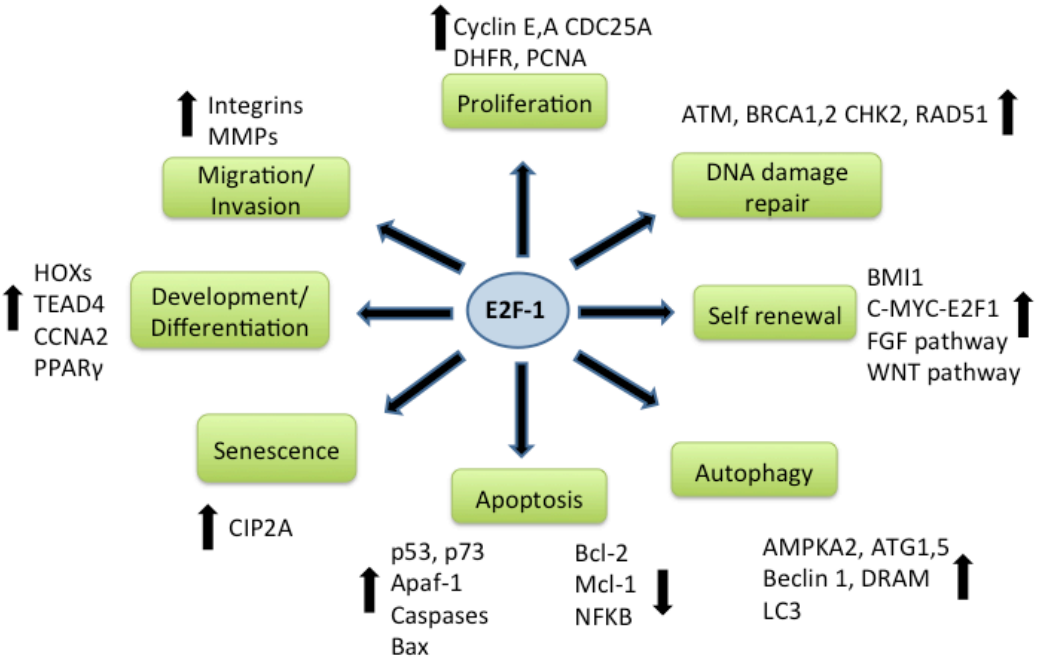

Figure 1.3. The transcription factor E2F1, a key regulator in different cellular processes (Edited from Meng and Ghosh, 2014).

Cell cycle regulation and apoptosis are well-established canonical roles of E2F1. However, our current understanding of how E2F1 regulates cell fate remains limited, as E2F1 is simultaneously able to upregulate both proapoptotic genes such as *p73*, *CASP3*, *CASP7*, *BOK*, *BIM*, *PMAIP1*, *APAF1*, *PUMA*, and antiapoptotic genes like *BCL-2* (Figure 1.3) (Hallstrom and Nevins, 2009).

E2F1 is overexpressed in several types of cancers. Increased expression of E2F1 and E2F3 target genes were found in patients with amplification of E2F1 and this increase in E2F target gene expression was also correlated with poor survival of HCC (hepatocellular carcinoma) patients in TCGA database (Kent et al., 2017). Depletion or pharmacological blockade of E2F1 activity resulted in cell death and senescence in vitro and in vivo due to p53 and p27 activation in melanoma cells (Rouaud et al., 2018).

Kaplan-Meier survival plots based on pan-cancer data reveals that higher E2F1 expression correlates with poor survival for several cancer types including kidney renal clear cell carcinoma (KIRC), kidney renal papillary cell carcinoma (KIRP), liver hepatocellular carcinoma (LIHC), lung adenocarcinoma (LUAD), pancreatic ductal adenocarcinoma (PDAC), and sarcoma (SARC) (Nagy et al., 2021) (Figure 1.4).

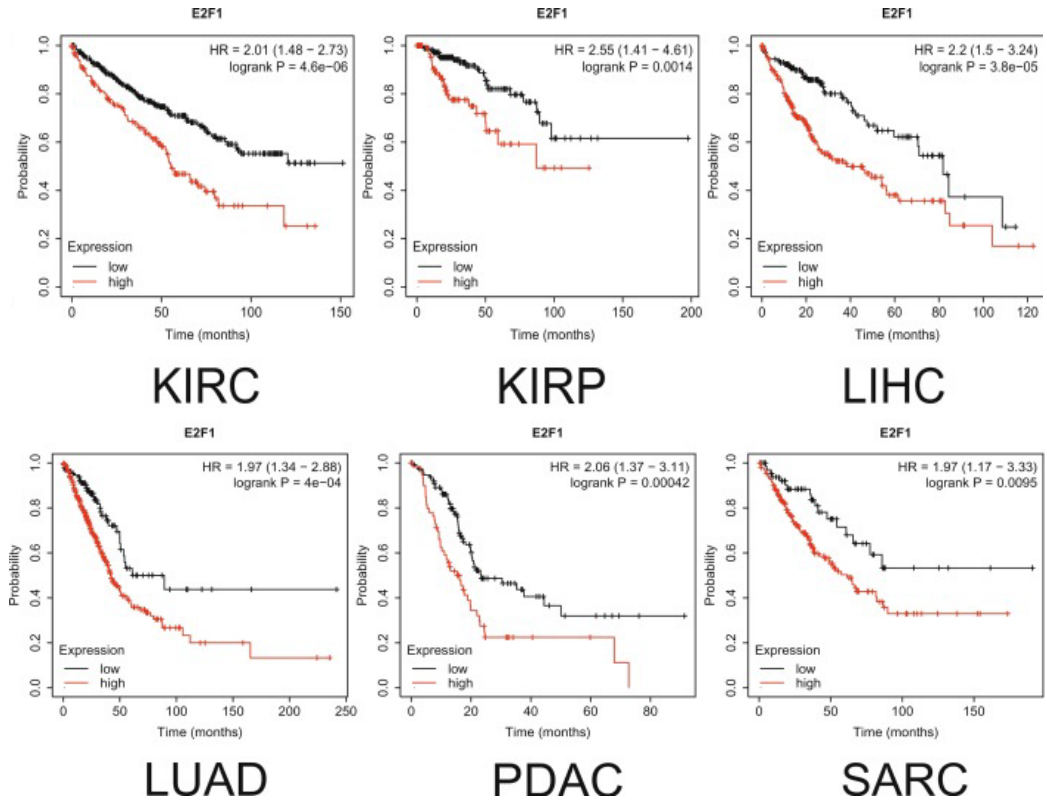

Figure 1.4. Kaplan-Meier plots for E2F1 expression in several carcinomas; kidney renal clear cell carcinoma (KIRC); kidney renal papillary cell carcinoma (KIRP); liver hepatocellular carcinoma (LIHC); lung adenocarcinoma (LUAD); pancreatic ductal adenocarcinoma (PDAC); sarcoma (SARC) (Nagy et al., 2021).

E2F1 proteins regulate MYCN transcription and are required for the full activity of the MYCN promoter in NB (Strieder and Lutz, 2003). MYCN on the other hand regulates the expression of diverse splicing factors for controlling global splicing program in addition to its well-known function in the transcription program (Zhang et al., 2016).

E2F transcription factors are involved in control of early events in cell cycle control, some of those genes are also regulated by transcription factor MYC. MYC target genes include CDKs, cyclins and E2F transcription factors. Therefore, MYC-E2F axis remains important as coordinating the expression of targets genes implicated in cell cycle control, DNA replication, and apoptosis (Bretones et al., 2015).

Beyond the canonical roles of E2F1 in cell cycle progression, our group has recently identified that E2F1 confers genome wide effects in the regulation of splicing (Roworth et al., 2019). E2F1 mediates the alternative splicing of apoptotic genes via direct upregulation of the serine/arginine-rich (SR) family of splicing factors.

The SR protein family consists of a variety of proteins that are evolutionarily conserved and a structure that contains a domain rich in arginine and serine residues known as the RS domain. These proteins have a major role in pre-mRNA splicing and also serve as the key regulators of alternative splicing (Long and Caceres, 2009). SR proteins are a family of RNA-binding phosphoproteins that control both constitutive and alternative pre-mRNA splicing events (Howard and Sanford, 2015). SR proteins have been linked to various activities beyond their roles in constitutive and alternative splicing, such as the export of mRNA, the stabilization of RNA, and the promotion of nonsense-mediated decay (NMD) and translation (Richardson et al., 2011).

Studies have shown that E2F1 has the ability to affect the RNA dynamics. E2F1 controls pre-mRNA processing of specific genes by regulating the expression of the splicing factor, serine and arginine rich splicing factor 2 (*SRSF2*) (Merdzhanova et al., 2008). SRSF2 had been identified as a new transcriptional target of E2F1 and their interaction led to apoptosis in non-small cell lung carcinoma (Edmond et al., 2013). E2F1 and SRSF2 interplay regulates splicing in apoptotic genes *c-FLIP*, *Caspase 8*, *Caspase 9*, and *Bcl-x* (Merdzhanova et al., 2008).

1.2.2.3. PRMT5's role in E2F1 regulation

PRMTs were shown to methylate crucial cell cycle proteins suggesting that protein arginine methylation is an important regulator of the cell cycle (Raposo and Piller, 2018). Our group previously identified that PRMT5 methylates E2F1 transcription factor and the methylation of arginine plays a role in regulating its biochemical and functional characteristics, which affects E2F1-dependent growth control. This methylation has an effect on the stability of E2F1 protein. If E2F1 is methylated in tumour cells, decreased methylation occurs under DNA damage conditions, allowing the stabilization of E2F1, which results in apoptosis. Therefore, arginine methylation control of E2F1's biological activity might contribute to tumorigenesis by influencing the E2F pathway (Cho et al, 2012). Pastore and colleagues also showed that PRMT5 inhibition alters the post-translational methylation of E2F1 that leads to altered expression of E2F1 downstream targets in cell cycle and DNA damage repair pathway relevant genes (Pastore et al., 2020).

PRMT5 mediated modulation of cell growth occurs in part via a small R-rich motif located on the E2F1 that is a target for symmetric methylation. This R-rich domain on E2F1 is first recognized and read by the p100/TSN (Roworth et al., 2019). This process might enable the recruitment of splicing factor to the spliceosome driving splicing events on genes regulating cell growth and survival. Therefore, this reader and writer relationship between PRMT5 and p100/TSN might be used in targeting cell-cycle machinery in cancer.

1.2.3. Inhibitors of PRMT5 in clinical trials

Deregulated PRMT5 expression has been observed across a variety of cancers and previous research has proposed that PRMT5 could be a potential therapeutic target for

spliceosome interventions (Pastore et al., 2020). PRMT5 inhibitors are currently in clinical trials for wide range of cancers (Table 1.1).

Table 1.1. Inhibitors of PRMT5 in clinical trials.

Compound	Activity	Clinical Trial	Clinical Indication
GSK3235025 (EPZ015666)	IC_{50}: 22 nM in vitro, IC_{50}: 61-904 nM in cells	NCT03245619	Terminated, ventricular tachycardia side effect?
GSK3326595	IC_{50}: 6.2 nM in vitro, EC_{50}: 2-160 nM in cells	Phase I: NCT02783300 Phase II: NCT04676516	Phase I: Solid tumours and non-Hodgkin lymphoma Phase II: Breast cancer
JNJ-64619178	Orally active 10mg/kg IC_{50}: 0.14 nM	Phase I: NCT03573310	Neoplasms, Adult solid tumour, Non-Hodgkin lymphoma, Myelodysplastic syndrome
PF-06939999	-	Phase I: NCT03854227	Advanced solid tumours, Metastatic solid tumours
PRT811	IC_{50}: 3.9 nM in vitro, IC_{50}: 29-134 nM in cells	Phase I: NCT04089449	Advanced solid tumours, Gliomas, Myelofibrosis
PRT543	IC_{50}: 10.8 nM in cells	Phase I: NCT03886831	Relapsed/Refractory advanced solid tumours, Diffuse large B-cell lymphoma, Myelodysplasia, Mantle cell lymphoma, Acute and chronic myeloid leukaemia
AMG 193	-	Phase I/II NCT05094336	Advanced MTAP-null solid tumours
MRTX1719	IC_{50}: 3.6 nM (with MTA)	Phase I/II NCT05245500	MTAP-null Mesothelioma, Non-small cell lung cancer, Malignant peripheral nerve sheath tumours, Solid tumours, Pancreatic adenocarcinoma, Advanced solid tumours
TNG908	IC_{50}: 21.2 nM (with MTA)	Phase I/II NCT05275478	MTAP deleted locally advanced solid tumours

PRMTs as the writers of arginine methylation have recently gained interest as novel drug targets. Several ongoing clinical trials of PRMT inhibitors led to an exciting time for the field of arginine methylation (Guccione et al., 2019). Chan-Penebre and colleagues reported EPZ015666 (GSK3235025) as the first potent (IC_{50} 22 nM) and orally bioavailable PRMT5 inhibitor that has anti-proliferative effects in both in vitro and in vivo models of mantle cell lymphoma (MCL). Symmetrically dimethylated PRMT5 substrate levels in tumours decreased correlating well with inhibition of SDMA substrates and proliferation in a time- and concentration-dependent manner, suggesting these effects was a direct consequence of PRMT5 inhibition (Chan-Penebre et al., 2015). Then, the improved compound EPZ015938 was licensed to GSK (GSK3326595) and has entered phase I clinical trials for the treatment of solid tumours and non-Hodgkin lymphoma (NHL) (Guccione et al., 2019). Several other PRMT5 inhibitors are now developed as a potential therapy and are currently being tested in clinical trials (Table 1.1).

JNJ-64619178 is being tested in participants with relapsed/refractory B cell, NHL, or advanced solid tumours in Phase I trial (Villar et al., 2020). Phase I trial for the dose escalation, safety, and tolerability study of PF-06939999 in previously treated patients with advanced or metastatic cancer is now terminated due to company strategy (NCT03854227, NIH 2022). PRT811 (NCT04089449) and PRT543 (NCT03886831) are also being tested in subjects with advanced solid tumours, central nervous system lymphoma, high-grade gliomas and/or haematologic malignancies (NIH, 2019).

Synthetic lethality approach for PRMT5 also showed promising results. The PRMT5•MTA complex has recently emerged as a new synthetically lethal drug target for the treatment of methylthioadenosine phosphorylase (MTAP) deleted cancers. As methylthioadenosine (MTA) is a metabolite cleaved by MTAP, MTAP deletions cause

accumulation of MTA, which inhibits PRMT5 enzymatic activity (Kryukov et al., 2016). Therefore, cancer cells with MTAP deletion are highly sensitive to inhibition of PRMT5. MRTX1719 was developed as an MTA-cooperative PRMT5 inhibitor (Smith et al., 2022). MRTX1719 is now being evaluated in a Phase 1/2 study in patients with advanced solid tumours with homozygous deletion of the *MTAP* gene (NCT05245500). Another cooperative PRMT5 inhibitors that are in clinical trial are AMG 193 and TNG 908. AMG 193 is currently in Phase 1/2 trials for safety, tolerability, pharmacokinetics, pharmacodynamics, and efficacy alone and in combination with docetaxel in patients with advanced MTAP-null solid tumours (NCT05094336). TNG 908 is a selective PRMT5 inhibitor that is currently in Phase1/2 trials for dose escalation and dose expansion for confirmed MTAP-deleted tumour types (NCT05275478).

There are also other pre-clinical PRMT5 inhibitors that show promising results *in vitro* and *in vivo*. JBI-778 received orphan drug designation status recently for the treatment of glioblastoma multiforme (GBM) (Sivanandhan et al., 2018).

Park and colleagues showed that PRMT5 expression corresponds with poor prognosis NB and has identified PRMT5 as a critical post-translation regulator of the MYCN oncoprotein. Therefore, inhibiting PRMT5 may provide a novel alternative for the treatment of NB and MYCN-driven cancers (Park et al., 2015).

T1-44, PRMT5 inhibitor, which is used in this study, was developed as selective small molecule inhibitor in order to be used as a chemical biology tool in efforts to explore and validate PRMT5 as a potential target for clinical treatment. Migration and invasion activity was reduced in T1-44 treated colon cancer cells through the regulation of PRMT5-E2F1 axis and cell motility-related proteins (Barczak et al., 2020). Combination treatment of T1-44 with vactosertib, a TGF-β receptor type 1 inhibitor, improved survival and inhibited cell invasion and epithelial-mesenchymal transition

(EMT) via stimulating apoptosis pathway in pancreatic cancer animal model (Hong et al., 2023).

1.3. Research objectives

We hypothesized that PRMT5-E2F1-MYCN pathway has potential prognostic value in neuroblastoma. We used CHP-134 and GI-ME-N cell lines to model the higher and lower levels of both E2F1 and MYCN in NB, respectively. While previous researches have focused more into the MYCN's role in splicing, in this study we aimed to enlighten E2F1's contribution into the regulation of splicing. We also used other neuroblastoma cell lines: N206, SK-N-BE(2), SHEP2, Tet-off SHEP21N, and E2F1 knockout CHP-134 cells to reveal the underlying molecular mechanism of different response to PRMT5 inhibition.

In this context;

- Neuroblastoma cell lines were characterized in terms of sensitivity to the PRMT5 inhibition,
- Transcriptome wide analysis was performed on the CHIP-134 and GI-ME-N cell lines, that are the most and the least sensitive to PRMT5 inhibition, respectively, to understand the mechanism of action that drives sensitivity to PRMT5 inhibition,
- Transcriptome wide analysis was also performed on CRISPR/Cas9 generated E2F1 knockout CHP-134 cell line to overcome concerns about the impact of cell lineage and to understand the impact of E2F1 in sensitivity to PRMT5 inhibition,
- The prognostic value of E2F1-PRMT5-MYCN axis was evaluated in order to see if we can use this information in a translational context as high PRMT5 levels could be more responsive to the drug treatment,
- Potential biomarkers that can be used in stratifying neuroblastoma patients for PRMT5 inhibition treatment were investigated.

CHAPTER 2. Materials and methods

2.1. Materials

All the reagents used in this study were listed below (Table 2.1).

Table 2.1. List of reagents and resources used in this study.

REAGENT or RESOURCE	SOURCE	IDENTIFIER
Antibodies		
TrueBlot® Anti-Mouse IgG, HRP	Rockland Immunochemicals	Cat#18881733
TrueBlot® Anti-Rabbit IgG, HRP	Rockland Immunochemicals	Cat#18881633
Asymmetric Di-Methyl Arginine Motif [adma-R] mAb	Cell Signalling	Cat#13522
β-Actin mAb	Cell Signalling	Cat#3700
Cleaved PARP mAb	Cell Signalling	Cat#5625
E2F1 Antibody	Cell Signalling	Cat#3742
n-Myc/MYCN mAb	Abcam	Ab227822
PRMT5 mAb	Cell Signalling	Cat#79998
SND1, Polyclonal Antibody	Bethyl Laboratories	Cat#A302883AT
Symmetric Di-Methyl Arginine Motif [SDMA-RG]	Cell Signalling	Cat#13222
Chemicals, peptides, and recombinant proteins		
BpiI (BbsI)	Thermo Fisher Scientific	Cat#ER1011
Bradford Assay Reagent	Thermo Fisher Scientific	Cat#23238
ChIP-grade Protein A/G Magnetic Beads	Cell Signalling	Cat#9006
Clarity Western ECL Substrate	Bio-Rad	Cat#1705061
Color Prestained Protein Standard	New England BioLabs	Cat#P7719
DMEM	Thermo Fisher Scientific	Cat#11966025
Dimethyl sulfoxide	Sigma-Aldrich	276855
Doxycycline	Sigma-Aldrich	D9891
Ethanol	Sigma-Aldrich	32205-M
Fetal Bovine Serum	Thermo Fisher Scientific	Cat#16140071
G418	Clontech	Cat#631308
Glycine	Cell Signalling	Cat#7005
Hygromycin B	Clontech	Cat#631309
ITS Liquid Media Supplement	Sigma-Aldrich	I3146
SYBR® FAST qPCR Kit	Kapa Biosystems	KK4603

L-Glutamine Solution	Thermo Fisher Scientific	Cat#A2916801
MTT Reagent	Sigma-Aldrich	CT01-5
PBS	Thermo Fisher Scientific	Cat#10010015
Penicillin G	Sigma-Aldrich	P30332
Penicillin-Streptomycin	Thermo Fisher Scientific	Cat#15140122
Propidium Iodide Staining Solution	Thermo Fisher Scientific	Cat#00-6990-50
Protease Inhibitor Cocktail	Roche	11836170001
Puromycin Dihydrochloride	Thermo Fisher Scientific	Cat#A1113802
PVDF Membrane	Millipore	IPVH00010
RPMI 1640	Thermo Fisher Scientific	Cat#11875093
Oligofectamine™ Transfection Reagent	Thermo Fisher Scientific	Cat#12252011
Opti-MEM™	Thermo Fisher Scientific	Cat#31985062
SDS-PAGE Sample Buffer	Bio-Rad	Cat#161-0737
SYBR® Green QPCR Master Mix	Agilent	Cat#600882
T1-44	Argonaut Therapeutics	N/A
T4 Polynucleotide Kinase	New England BioLabs	Cat#M0201S
RIPA Lysis and Extraction Buffer	Thermo Fisher Scientific	Cat#89901
Tet-System Approved FBS	Thermo Fisher Scientific	Cat#A4736301
10% Tris-Glycine Gels	Thermo Fisher Scientific	Cat#XP00100PK2
Pierce 10X Western Blot Transfer Buffer, Methanol-free	Thermo Fisher Scientific	Cat# 35040
NuPAGE MOPS SDS Running Buffer (20X)	Thermo Fisher Scientific	Cat# NP0001
TRIzol™ Reagent	Thermo Fisher Scientific	Car#15596018
Commercial assays		
NEBNext® Poly(A) mRNA Magnetic Isolation Module	New England BioLabs	Cat#E7490S
NEBNext® Ultra™ Directional RNA Library Prep Kit for Illumina	New England BioLabs	Cat#E7420L
QIAamp® DNA Mini Kit	Qiagen	Cat#51304
QIAquick® PCR Purification Kit	Qiagen	Cat#28104
SuperScript™ III cDNA Synthesis Kit	Thermo Fisher Scientific	Cat#18080200
Experimental models: Cell lines		
CHP-134	ECACC	Cat#06122002
GI-ME-N	Children Oncology Group, St. Jude Children's Research Hospital	N/A

LAN-5	Children Oncology Group, St. Jude Children's Research Hospital	N/A
LAN-6	Children Oncology Group, St. Jude Children's Research Hospital	N/A
LNCaP	Children Oncology Group, St. Jude Children's Research Hospital	N/A
N206	Children Oncology Group, St. Jude Children's Research Hospital	N/A
NB-1643	Children Oncology Group, St. Jude Children's Research Hospital	N/A
NMB	Children Oncology Group, St. Jude Children's Research Hospital	N/A
SHEP2	Children Oncology Group, St. Jude Children's Research Hospital	N/A
SHEP21N (Tet-Off inducible SHEP2)	Laboratory of Prof Karim Malik, University of Bristol	N/A
SH-SY5Y	ECACC	Cat#94030304
SK-N-AS	ECACC	Cat#94092302
SK-N-BE(2)	ECACC	Cat#95011815
SK-N-FI	ECACC	Cat#94092304
SMS-KCNR	Children Oncology Group, St. Jude Children's Research Hospital	N/A
Oligonucleotides		
E2F1 ChIP Primers for *SRSF1*, *SRSF3*, *SRSF4*, *HNRNPA3*, *CPSF3*, *CPSF4*, *CDC6*, see Table 2.3	This paper	N/A

MYCN ChIP Primers for *SRSF1*, *SRSF3*, *SRSF4*, *HNRNPA3*, *CPSF3*, *CPSF4*, *PARP2*, see Table 2.4	This paper	N/A
E2F1 Sanger Primers, Forward: CGTTTTCGCCACAGGTGAAG, Reverse: CCCGACAAGCCAGACGTTAG	This paper	N/A
qRT-PCR Primers for the RNA sequencing validations, see Table 2.7	This paper	N/A
sgRNA, Forward: 5'CACCGGAAACTGACCATCAGT ACC3, Reverse: 5'AAACGGTACTGATGGTCAGTT TCC	This paper	N/A
Recombinant DNA		
Plasmid: pSpCas9(BB)-2A-Puro (PX459)	Addgene	#62988
Software and algorithms		
CFlow Plus software	BD Biosciences	N/A
CRISP-ID v.1.1	Dehairs et al., 2016	http://crispid.gbiomed.kuleuven.be/
DAVID 6.7	Huang et al., 2009a; Huang et al., 2009b	https://david.ncifcrf.gov/
DESeq2 R Bioconductor package v.1.25.17	Love et al., 2014	https://bioconductor.org/packages/release/bioc/html/DESeq2.html
FunRich v.3.1.4	Pathan et al., 2015	http://funrich.org/index.html
GSEA v.4.2.3	Subramanian et al., 2005	https://www.gsea-msigdb.org/gsea/index.jsp
Prism Software version 9	GraphPad	N/A
rMATS v.4.0.2	Shen et al., 2014	https://bioinformaticshome.com/tools/rna-seq/descriptions/rMATS.html

STAR 2.7.10a	Dobin et al., 2013	https://github.com/alexdobin/STAR
TRANSFAC	Matys et. al., 2006	https://genexplain.com/transfac/
TrimGalore (RRID:SCR_011847) v.0.4.3	Babraham Bioinformatics	https://www.bioinformatics.babraham.ac.uk/projects/trim_galore/

2.2. Methods

2.2.1. Cell culture

All neuroblastoma (NB) cell lines were grown in RPMI 1640 medium supplemented with 10% fetal bovine serum, 1% penicillin, 4 mM L-Glutamine, 1X ITS (5 µg/mL insulin, 5 µg/ml transferrin, 5 ng/ml selenous acid) at 37 °C, 5% CO_2. Neuroblastoma cell lines were obtained from Children Oncology Group, St. Jude Children's Research Hospital. MYCN inducible Tet-off SHEP2 (SHEP21N) cell line was kindly provided from Prof. Karim Malik, University of Bristol. Tet-off inducible cells were maintained in DMEM supplemented with 5% tetracycline negative FBS, 1% penicillin-streptomycin 100 µg/ml G418, and 150 µg/ml hygromycin. 1 µg/ml doxycycline was added for 24 h to induce expression MYCN in the Tet-off cell system. PRMT5 inhibitor T1-44 was obtained from Argonaut Therapeutics, Oxford, UK. The compound was dissolved in DMSO to 1 mM concentration. All the cell lines used in this study are presented in Table 3.1.

2.2.2. Cellular toxicity assay

3-(4,5-dimethylthiazol-2-yl)- 2,5-diphenyltetrazolium bromide (MTT) assay was used to evaluate the cytotoxic effect of T1-44 compound. Cells were seeded into 96 well plates and cultured overnight. Neuroblastoma cells were treated with T1-44 for 6 days. MTT solution (5 mg/ml in PBS) was added to the each well at the end of the treatment and the plate was incubated for 4 h at 37 °C. DMSO was added to the each well in order to solubilize the formazan crystals and the plate was incubated at 37 °C for 30 minutes. Absorbance was measured by using microplate reader (Tecan, Switzerland) at 570 nm.

2.2.3. Flow cytometry

Neuroblastoma cells were harvested and centrifuged for 5 minutes at 1500 rpm. Cell pellets were fixed with 1 ml 70% ice-cold ethanol and incubated at -20 °C overnight.

Cells were washed in 6 ml PBS and stained for 30 minutes with 10 mg/ml propidium iodide solution and RNAse A (10 mg/ml) was added. Data was acquired on an Accuri C6 Flow Cytometer (BD Biosciences) and analysed using BD Accuri C6 software.

2.2.4. Immunoblotting

After the treatment of NB cells for 6 days with 8 nM-1 µM concentration of T1-44, the cells were washed with PBS and scraped into the 1X RIPA lysis buffer and protease inhibitor cocktail (Roche). Samples were left at 4 °C for 30 minutes and centrifuged for 15 minutes at 13500 rpm at 4 °C and the supernatant was collected. Proteins were quantified by using the Bradford reagent. Normalized samples were mixed with SDS sample buffer (Bio-Rad) and denatured at 95 °C for 5 minutes. Samples were loaded into a 10% Tris-Glycine gels (Thermo Fisher Scientific). Color Prestained Protein Standard was used to estimate molecular weight. The proteins were transferred to PVDF membrane at 400 mA for 1 h. Membranes were blocked with 5% non-fat milk powder in 1X TBS-T for 1 h at room temperature and incubated overnight at 4 °C with the primary antibody at 1:1000 dilution. The membranes were washed three times in 1X TBS-Tween (TBS-T). After 1 h incubation with the appropriate secondary antibody, membranes were washed 3 times for 5 minutes with TBS-T and Clarity^{TM} ECL Western Blotting Solution was added. Signals were captured by exposing X-ray films (Kodak) to the membranes and developed on developer (AGFA CP1000).

2.2.5. Chromatin immunoprecipitation (ChIP)

Cells were seeded into 150 cm^2 dishes and harvested. Formaldehyde was added to a final concentration of 1% (v/v) and incubated at room temperature with gentle shaking for 10 minutes. Glycine was added to a concentration of 125 mM and incubated 5 minutes to neutralize the cross-linking activity. Then, cells were collected into 5 ml ice cold PBS and centrifuged at 1500 rpm for 10 minutes and supernatant was removed.

The pellets were resuspended in 500 µl 1X SDS lysis buffer and sonicated on ice for 10 minutes in order to shear chromatin into 200-1000 bp length fragments and stored at -80 °C until the next steps. Chromatin lysates were thawed and pre-cleared with 60 µl of protein A/G beads then rotated for 1 h at 4 °C. Samples were spun down and supernatant was transferred to 15 ml falcon tubes and topped up with 2500 µl 1X dilution buffer. 100 µl was used as ChIP input control and stored at -20 °C. Remaining supernatant was incubated with 1-10 µg of control or specific antibodies on rotating wheel at 4 °C overnight.

On the following day, 60 µl of protein A/G beads were added and samples were incubated for 1 h then spun down at 3000 rpm for 1 minute and supernatant was discarded. Beads were washed with 2 times low salt buffer, 4 times LiCl buffer and 2 times TE buffer. ChIP buffer details were presented at Table 2.2. Samples were eluted with 500 µl 1X elution buffer and left on 65 °C hot block for 25 minutes. Samples were treated with 1 µl RNAse (10 µg/ml) at 55 °C for 2 h and left for reverse cross-linking overnight at 65 °C. DNA was isolated by using the QIAquick® PCR purification kit according to the manufacturer's instructions. The purified DNA was prepared for quantitative real time PCR (qPCR) using SYBR® FAST qPCR Kit. Experiment was performed in triplicates in AriaMx Real-Time PCR System (Agilent Technologies). The primer sequences used in qPCR are given at Table 2.3 and Table 2.4.

Table 2.2. Buffers used for in this study.

Buffer	
ChIP Dilution Buffer	50 µl 10% SDS 300 µl 200 mM EDTA 835 µl 1M Tris pH 8 1.67 ml 5 M NaCl 550 µL 100% Triton X-100 dH_2O added to 50 ml
Low Salt Wash Buffer (ChIP)	2 ml 1M Tris pH 8 3 ml 5 M NaCl 1 ml 200 mM EDTA 1 ml 10% SDS 100% Triton X-100 dH_2O added to 100 ml
LiCl Wash Buffer (ChIP)	1 ml 1M Tris pH 1.06 gr LiCL 500 µL 200 mM EDTA 2 ml 100% Igepal® 2 g Na-deoxycholate dH_2O added to 100 ml
Lysis Buffer II (ChIP)	10 mM Tris pH 8 200 mM NaCl 1 mM EDTA 0.5 mM EGTA
Lysis Buffer III (ChIP)	10 mM Tris pH 8 100 mM NaCl 1 mM EDTA 0.5 mM EGTA 0.1% Na-deoxycholate 0.5% Na-deoxycholate
Elution Buffer (ChIP)	1 ml 10% SDS 1 M $NaHCO_3$ dH_2O added to 10 ml
TBS-T	8.65 gr NaCl 6.86 gr Tris base 2 ml Tween-20 dH_2O added to 1000 ml
TE	0.2 ml 0.5M EDTA pH 8 1 ml 1M Tris-Cl pH 8 dH_2O added to 100 ml

Table 2.3. List of primers used for E2F1 ChIP qPCR.

ChIP Primer	Forward primer sequence 5'-3'	Reverse primer sequence 5'-3'
SRSF1	CGGGTATCTTCGTAGGGTGC	TTCTGACGAGAAGGCGGAAC
SRSF3	TCTCGGTAAGAGACCAGCGA	TGAACGTCACAAAATGGCGG
SRSF4	ACCGGGTGTGGTTTGGATTT	AGGTCACGGGTACACAATCG
CDC6	GGCCTCACAGCGACTCTAAGA	CTCGGACTCACCACAAGC

Table 2.4. List of primers used for MYCN ChIP qPCR.

ChIP Primer	Forward primer sequence 5'-3'	Reverse primer sequence 5'-3'
SRSF1	ACAGCGATTCGATCCCAACA	GCACCCTACGAAGATACCCG
SRSF3	TCTCGGTAAGAGACCAGCGA	GGCCGTGACCTGGAATACAA
SRSF4	GGAAGGTAACCGGAGAGAGC	AAGCTCCAGCTCCGAAATCC
PARP2 P2SB2	TCAGGGAGAGCCCTGTTAGG	CGGAGGGAAGCTCATCAGTG

2.2.6. Generation of CRISPR/Cas9 knockout cell lines

Forward Guide RNA (sgRNA): 5'CACCGGAAACTGACCATCAGTACC, and reverse sgRNA: 5'AAACGGTACTGATGGTCAGTTTCC were used, and the protocol described in Ran et al. (2013) was followed. Cells were transfected with sgRNA containing plasmid (pSpCas9(BB)-2A-Puro) and after 24 h 2 µg puromycin was used for the colony selection. After 48 h puromycin selection, remaining cells were seeded into 96 well plates in order to have single cell colonies. When cells become confluent, clones were isolated and grown up before identifying E2F1 knockout colonies. Then, colonies were screened via immunoblotting. E2F1 knocked out colonies' genomic DNA was extracted using QIAamp® DNA Mini Kit and sent for Sanger sequencing after PCR amplification of the target region with the primers given in Table 2.5.

Table 2.5. List of primers for Sanger sequencing.

Gene	Forward primer sequence 5'-3'	Reverse primer sequence 5'-3'
E2F1	CGTTTTCGCCACAGGTGAAG	CCCGACAAGCCAGACGTTAG

2.2.7. Drug treatments

T1-44 was dissolved in DMSO and used at a concentration range for 8 nM to 1 µM for 72 h. 1 µg/ml doxycycline was added for 24 h to induce expression of Tet-responsive MYCN in the Tet-off cell system in SHEP2 cell lines.

2.2.8. RNA sequencing

RNA was extracted from NB cells by using Trizol® extraction method according to the manufacturer's instruction. The RNA quality and quantity for each sample was analysed by Nanodrop (ensuring a 260/230 ratio of >2.0 and a 260/280 ratio >1.8-2.0). To ensure the samples from each biological replicate were in good quality for further library preparation and sequencing, an aliquot of RNA was taken for cDNA synthesis and qRT-PCR analysis of target genes were analysed to ensure that the cells behaved as expected.

Then, the samples were shipped to BGI Hong Kong for the bulk RNA sequencing at 30 million reads coverage. mRNA was enriched using the NEBNext® Poly(A) mRNA Magnetic Isolation Module. cDNA libraries were made using the NEBNext® Ultra™ Directional RNA Library Prep Kit for Illumina. Sequencing was carried out on an Illumina NextSeq platform by BGI.

2.2.9. Bioinformatic analysis of differentially expressed and spliced genes

All the bioinformatics analysis was performed by Prof. Anastasia Samsonova from the Saint-Petersburg State University, Computational Systems Biology Group. FASTQ files for CHP-134 and GI-ME-N (DMSO vs. T1-44 treatment) were generated in three biological replicates. These were trimmed to remove adapters and low-quality bases with TrimGalore v.0.4.3. The trimmed reads were aligned to the human reference genomes build hg19 with STAR aligner v.2.7 with two mismatches allowed. Differential gene expression analysis was done with DESeq2 R Bioconductor package (v.1.25.17) using read counts data provided by the aligner. Genes were considered differentially expressed if the adjusted p-value, calculated using the Benjamini-Hochberg method to minimize the false discovery rate, was less than 0.01. We further filtered significantly differentially expressed gene sets using 2-fold change in absolute expression level. Blue and red heat-maps were used for the differentially expressed genes that correspond to statistically significant differentially expressed genes. Blue colour represents the lowest difference, and red colour represents the highest ($padj<0.01$).

The RNA Sequencing data was further filtered to identify those genes differentially regulated with a fold change of 2 or greater. The TRANSFAC database release 2015.3 was used to identify E2F1 binding motif consensus and promoter sequences. Gene set enrichment analysis was done by GSEA v.4.2.3 with an FDR of 25%, those with a

q<0.05 were considered significant. Additional GO analysis was done using DAVID 6.7 with BP_GO_FAT terms.

Canberra heat-maps were used to represent absolute values of ΔΨ (percent spliced in) for cell lines, corresponding to statistically significant alternative splicing event changes to E2F1 target genes (as previously determined from the ENCODE data) derived by analysing the RNA-seq data with rMATS algorithm. Yellow colour represents the lowest difference and blue colour represents the highest (FDR >0.01). For the differentially spliced genes, delta psi scores were used as following: delta psi <0.1 insignificant; 0.1-0.3 low weak; 0.3-0.5 moderate; >0.5 strong.

2.2.10. Quantitative PCR (qRT-PCR)

RNA samples were obtained by using Trizol® isolation method. 200 ng total RNA was reverse transcribed by Superscript III cDNA Synthesis Kit. Target genes were selected according to the p-values and log2 (fold changes) from the RNA-seq analysis for the qPCR validation. qPCR reaction mix and PCR conditions were provided in Table 2.6. qPCR was performed on the AriaMx Real-Time PCR (Agilent Technologies). All primer sequences were provided in Table 2.7.

Analysis was performed using the ΔΔCT method where raw CT values were normalized to the input (for ChIP) or the control treatment (RT-PCR) followed by normalization to *IgG* (for ChIP) or the *GAPDH* (RT-PCR). Then, these values were converted into fold enrichment according to the equation:

$$\Delta CT = CT \text{ (treatment or specific IP)} - CT \text{ (control or input)}$$

$$\Delta\Delta CT = \Delta CT \text{ (target gene or specific IP)} - \Delta CT \text{ (control gene or IgG IP)}$$

$$\text{Fold enrichment} = 2^{-\Delta\Delta CT}$$

Table 2.6. qPCR protocol.

Buffer	**Components**			
qPCR reaction mix	SYBR® FAST qPCR master mix	5 µl		
	Forward primer	0.25 µl		
	Reverse primer	0.25 µl		
	cDNA	2 µl		
	RNAse free H_2O	2.5 µl		
PCR conditions	Cycling step	Temperature	Time	# of Cycles
	Enzyme activation	95 °C	5 min	1
	Denaturation	95 °C	20 sec	50
	Annealing/Extension	60 °C	20 sec	
	Melting	95 °C	1 min	1
		55 °C	30 sec	1
		55-95 °C (in 0.5 °C inc.)	30 sec / step	1

Table 2.7. List of RT-PCR primers.

RT-PCR Primer	Forward primer sequence 5'-3'	Reverse primer sequence 5'-3'
E2F1	ATGAGACCTCACTGAATCTGACCACC	AGTCACAGTCGAAGAGGTCTCTG
GAPDH	CCATCAATGACCCCTTCATTGACC	GAAGGCCATGCCAGTGAGCTTCC
PLK2	TGCACAGAGATCTCAAACTAGGG	TGGGGTACCACATATCGTTCT
CDC6	GCCACAGCTGTTGAACTTCC	ATAGCTCTCCTGCAAACATCCA
LIF	AGAAGCTGGGCTGTCAACTC	CCCACATCTGGACCCAACTC
CSF1	GGAGACCTCGTGCCAAATTA	TATCTCTGAAGCGCATGGTG
PHLDA3	GCTGAGGTCAAGGCAGCTT	GGCTCGTCCATTCCTTCAG
METTL7A	GAACCAGGAGCGGATTCTCC	GCTCTCTCTGGTCAGGTTGC
TIGAR	ATCCTGAAAGAAGCGGATCAAAA	AACTAAGACACTGGCTGCTAATC
AHNAK	GTGCCAAGGGCAACAAACAC	AGTCCCAAACCTAAGCCCAC
TSN	AGACGATTCACCTGTCCAGC	GGAATGTCATACAGGGGACG
SDHA	CTGATGAGACAAGATGTGGTG	CAATCTCCCTTCAATGTACTCC
DNAJB1	GGCCTGATGGGTCTTATCTATGG	TTAGATGGAAGCTGGCTCAAGAG
C1QL1	GCAACATTCCCGGCACCTAC	TTGCTGGCGTAGTCGTAGTTC
PAGE1	TGATACCAAGAGGGTGTGCC	TCACCTCCTCTGGATTTGGC
IGFBP5	AACGAAAAGAGCTACCGCGA	CCGACAAACTTGGACTGGGT
CRYZ	TTTTGGGCACTGCTGGTACT	TCCTTTCTCACCAACATACTTCT
CDK10	CAGATCTGGAGTGCGAGCAG	TTCCGGAGGCACCGTGAAG
CDK10 intron 8	GGAGAGGAGCCGGCTGTATT	ACATGTCGATGCTGGTGGTCT
CDK10 exon 8-9	GGTGGTCACTCTCTGGTACCGA	ACATGTCGATGCTGGTGGTCT
CDK10 negative control	GAAGGGGAATTAAGGCGGGA	GTCAGAAGCATCTGGCCTGT
BCL2L11 SE2	CCACTATCTCAGTGCAATGG	TCAATGCATTCTCCACACCAG
BCL2L11 SE2-2	TAGAGAAATAGAGGAAGTTGTC	TCAATGCATTCTCCACACCAG

2.2.11. Designing primers for differentially spliced genes

Once we received clean and filtered RNA-seq data from our bioinformatician collaborators (Prof. Samsonova), we have a full list of differentially spliced genes, splicing types (exon skipping, intron retention, mutually exclusive exons, and alternative 5' or 3' splice site selection), percent of spliced in scores (psi), FDR rates, and the exact coordinates of the splicing event in the genome. Then, we design our primers depending on the splicing event type (Table 2.7). For skipped exons, inclusion to exclusion ratio of a skipped exon is measured by qPCR (Roworth et al., 2019).

2.2.12. Statistical analysis

All experiments were performed independently with at least three biological and technical replicates, reported as mean (M) ± standard deviation (SD). Differences between the control and treatment groups were analysed by using student's t-test, one-way or two-way ANOVA that was included in the figure legends. GraphPad Prism 9.0© software was used to illustrate graphical results as well as to perform t-test. A significance value of 0.05 was used to determine significance between groups.

Chapter 3. MYCN-E2F1-PRMT5 interaction in neuroblastoma

3.1. Introduction

We aimed to enlighten E2F1-MYCN-PRMT5 axis contribution to the pathogenicity of neuroblastoma as higher expression levels of MYCN, E2F1, and PRMT5 coincide with lower overall survival rates in NB patients. Therefore, we used MYCN amplified and non-MYCN amplified cell line model systems to identify any role for the E2F1-PRMT5 axis in the pathogenicity of neuroblastoma. We used CHP-134, GI-ME-N, N206, SK-N-BE(2), and SHEP2 cells as cell lines. CHP-134 cell line was used as our main model system for MYCN amplification, whereas GI-ME-N cell line was used as a model system for non-MYCN amplification in NB cells. In order to rule out cell line specific effects, N206 and SHEP2 cell lines were also used as representatives of the MYCN amplified and non-MYCN amplified cell line model, respectively. Then, we further characterized cell lines for deeper investigation in terms of sensitivity to the PRMT5 inhibition.

3.2. MYCN amplified NB cells are more sensitive to PRMT5 inhibition

We performed cellular cytotoxicity assay (MTT) in order to test sensitivity to PRMT5 inhibition in MYCN and non-MYCN amplified cells. Compound T1-44 was used for the biochemical inhibition of PRMT5 (Figure 3.1).

Formula Structure	Molecular weight
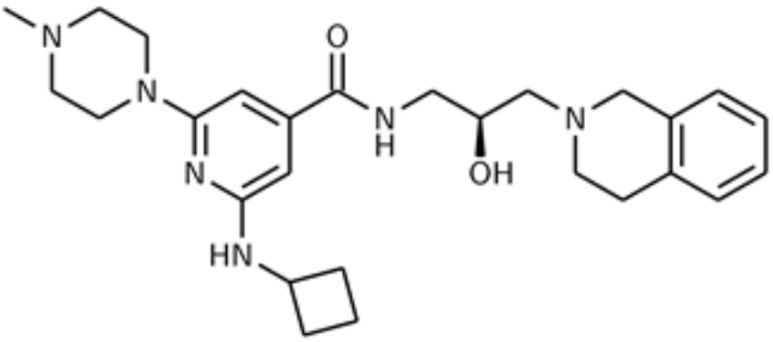	478.63

Figure 3.1. PRMT5 inhibitor compound T1-44's chemical structure.

We performed the MTT assay for 6 days of treatment with T1-44 in 14 NB cell lines. Characteristics of the cell lines used in this study were shown at Table 3.1. As the compound was dissolved in DMSO, which was used as a vehicle control, IC_{50} values were normalized to DMSO treated samples. We found that the MYCN amplified cells were significantly more sensitive to PRMT5 inhibition than non-MYCN amplified cells. As calculated by GraphPad Prism, IC_{50} levels for MYCN amplified NB cells were significantly lower than the non-MYCN amplified cells (Figure 3.2). While the most sensitive neuroblastoma cell line was CHP-134 (IC_{50}=0.005 μM), the most resistant cell line was SK-N-AS (IC_{50}=30 μM). Non-neuroblastoma cell line was also used as a control and non-MYCN amplified prostate cancer cell line LNCaP had higher IC_{50} levels (IC_{50}=42.5 μM). We found significant correlation with IC_{50} levels and MYCN status of the cells ($p<0.0062$) (Figure 3.2).

We found that lower IC_{50} values for PRMT5 inhibition in MYCN amplified cells was also accompanied by the higher E2F1 expression levels as compared to non-MYCN amplified cells which express lower E2F1 levels (Figure 3.2). Then, we were further interested in identifying the underlying sensitivity to the PRMT5 inhibition in MYCN amplified neuroblastoma cells.

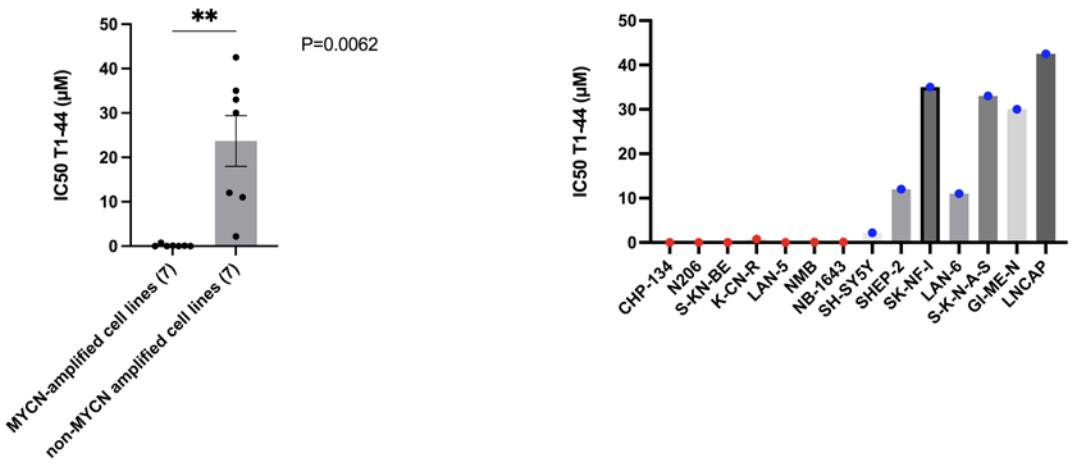

Figure 3.2. IC_{50} level comparisons for MYCN amplified versus non-MYCN amplified NB cell lines. MYCN amplified cell lines: CHP-134, N206, SK-N-BE(2), LAN-5, SMS-KCNR, NMB, NB-1643; non-MYCN amplified cell lines: SH-SY5Y, LAN-6, SHEP2, GI-ME-N, SK-N-AS, SK-N-FI, LNCaP. Cell lines were compared by using two-tailed unpaired t-test with Welch's correction and p=0.0062 (Data was kindly provided from Dr. Laurel Bate-Eya).

Table 3.1. Characteristics of the cell lines used in this study.

Cell line	Sample type	MYCN	TMM	Sequence variations
CHP-134	Adrenal gland	A		
N206	Autonomic ganglia	A	TERT+	ALK: p.Phe1174Leu (c.3522C>A)
SK-N-BE(2)	Bone marrow	A	TERT+	TP53: p.Cys135Phe (c.404G>T)
LAN-5	Bone marrow	A	TERT +	ALK: p.Arg1275Gln (c.3824G>A)
SMS-KCNR	Bone marrow	A	TERT+	ALK: p.Phe1174Leu (c.3522C>A)
NMB	Bone marrow	A		TP53: P.G245S (c.733G>A)
NB-1643	Retroperitoneal mass	A	TERT+	ALK: p.Arg1275Gln (c.3824G>A)
SH-SY5Y	Bone marrow	N		ALK: p.Phe1174Leu (c.3522C>A)
LAN-6	Bone marrow	N	EST	ALK: p.Asp1091Asn c.3271G>A
SHEP2	Bone marrow	N		ALK: p.Phe1174Leu (c.3522C>A) NRAS: p.Gln61Lys (c.181C>A
GI-ME-N	Bone marrow	N	TERT+	NF1; Unexplicit; Microdeletion
SK-N-AS	Bone marrow	N	TERT+	TP53: p.His168Arg (c.503A>G) NRAS: p.Gln61Lys (c.181C>A)
SK-N-FI	Bone marrow	N		TP53: p.Met246Arg (c.737T>G) NF1: Unexplicit; Partial deletion
LNCaP (Prostate carcinoma)	Supraclavicular lymph node	N	TERT+	AR: p.Thr878Ala (c.2632A>G) MEN1: p.Tyr318Ter (c.954T>G), p.Tyr313Ter, (c.939T>A) PIK3R1: p.Arg639Ter (c.1915C>T) PTEN: p.Lys6Argfs*4 (c.17_18delAA)
SHEP21N (Tet-off MYCN inducible)	Bone marrow	C		ALK; Simple; p.Phe1174Leu (c.3522C>A) NRAS; Simple; p.Gln61Lys (c.181C>A)

A: MYCN amplified, C: Conditional, N: MYCN non-amplified, TMM: Telomere maintenance mechanism, TERT+: Telomerase positive, EST: Ever shorter telomeres, i.e. telomerase and ALT negative.

3.3. Generation and characterization of the model cell lines

We evaluated the effects of PRMT5 inhibitor on cells over a range of drug concentrations to investigate the cellular mechanisms at protein expression level. We treated CHP-134, GI-ME-N, N206, SK-N-BE(2), and SHEP2 cells with 8 nM-1 µM concentrations of compound T1-44 for 6 days. Later on, we compared the protein expression levels of E2F1, PRMT5, MYCN, SDMA (symmetric dimethylarginine), ADMA (asymmetric dimethylarginine), β-Actin in MYCN amplified CHP-134 and non-MYCN amplified GI-ME-N cell lines. CHP-134 cell line had higher levels of E2F1 protein expression, whereas GI-ME-N had lower levels of E2F1 (Figure 3.3). To further confirm that GI-ME-N cell line has lower E2F1 expression, we compared *E2F1* mRNA expression level differences between CHP-134 and GI-ME-N cell lines by qPCR where we found *E2F1* expression were significantly different in these two cell lines (Figure 3.4).

Symmetric dimethylarginine motif antibody was used as a pharmacodynamic measure to show that the PRMT5 inhibitor had worked as PRMT5 causes symmetrical dimethylation. After 6 days of compound treatment with concentrations of 8 nM-1 µM, we found that SDMA levels decreased significantly even at low concentrations such as 8 nM. The PRMT5 inhibition sensitivity was mirrored by dose-dependent reduction of symmetric dimethylarginine mark (Figure 3.3). Asymmetric dimethylarginine motif antibody was used as a control to indicate that PRMT5 inhibition did not affect the asymmetric arginine methylation (Figure 3.3). Other cell lines including N206 and SHEP2 were also assessed for the aforementioned protein expression levels (Appendix A, Figure 1).

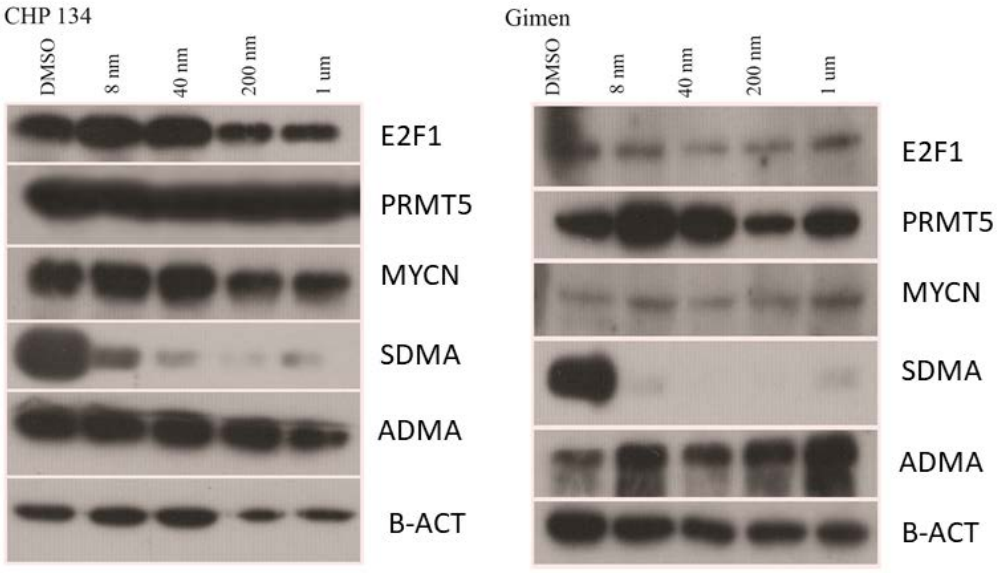

Figure 3.3. MYCN amplified CHP-134 and non-MYCN amplified GI-ME-N cell lines were treated with 8 nM-1 µM concentrations of T1-44 compound treatment for 6 days. Representative image of western blots for 3 different biological replicates was presented. 20 µg total protein was loaded onto the gels. β-actin was used as a loading control.

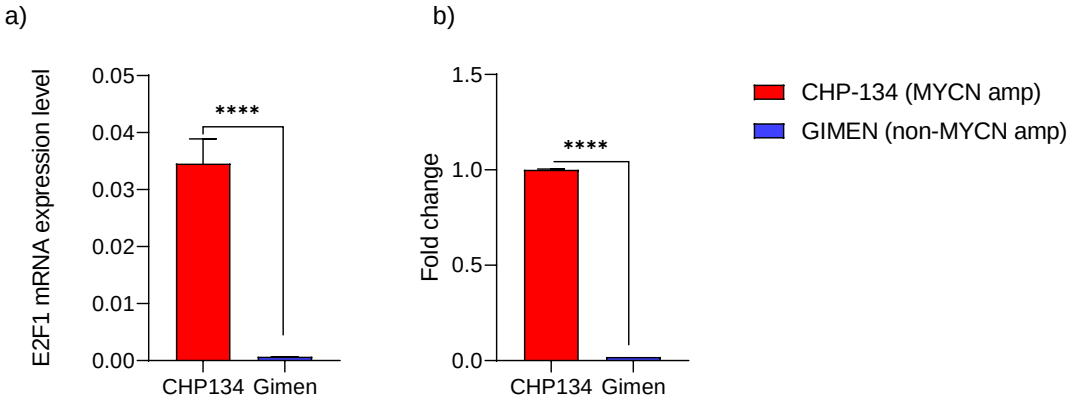

Figure 3.4. a) Relative mRNA expression levels of E2F1 in CHP-134 (MYCN amplified) and GI-ME-N (non-MYCN amplified) cell lines. b) Fold changes were calculated as mean of n=3 biological replicates. Data was presented as mean ± SD. Statistical analyses were performed using the two-tailed, unpaired student's t-test. The p-values <0.05 were considered as significant and are indicated as ****p < 0.0001.

The cell cycle distribution differences between MYCN amplified CHP-134 and non-MYCN amplified GI-ME-N cell lines were assessed by PI staining and cells were analysed by flow cytometer after 8 nM-5 µM concentrations of T1-44 compound treatment for 6 days. We found that T1-44 induced the number of SubG1 phase cells significantly (Figure 3.5). More details about the SubG1 differences in CHP-134 and GI-ME-N cells were presented at Appendix A, Figure 3.

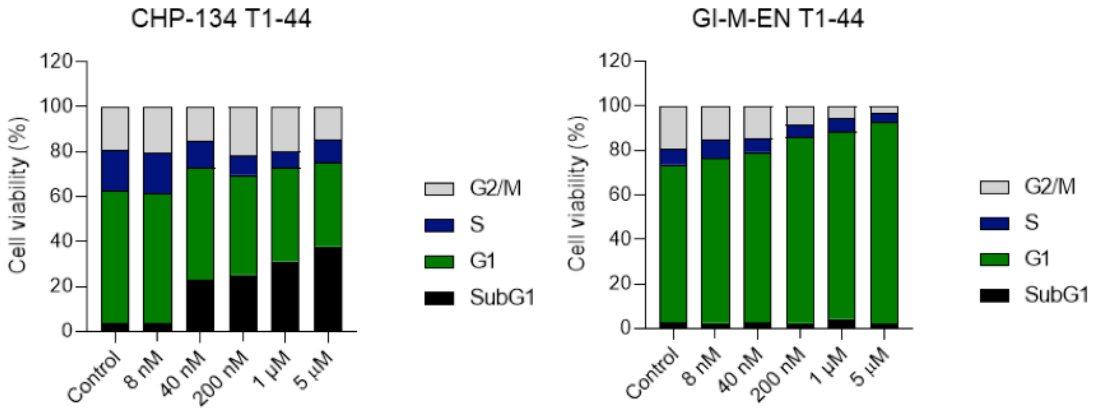

Figure 3.5. MYCN amplified CHP-134 and non-MYCN amplified GI-ME-N cell lines were treated with 8 nM-5 µM concentrations of T1-44 compound treatment for 6 days and cell cycle distribution was analysed by flow cytometer. Results shown are average of three independent experiments (Data was kindly provided from Dr. Laurel Bate-Eya).

3.4. MYCN inducible SHEP2 cell line

We also needed an isogenic cell system so that we can investigate MYCN's role in the sensitivity to PRMT5 inhibition. We used SHEP21N MYCN inducible Tet-off system for this purpose. The Tet-off system (tTA) activates gene expression in the absence of its ligand doxycycline. Upon addition of doxycycline, transcription of the gene of interest is silenced (Figure 3.6) (Palais et al., 2009). PRMT5 was previously identified as an important regulator of MYCN in neuroblastoma cells by using this isogenic cell line model (Park et al., 2015). Once we received the cells from Prof. Malik's lab, we measured MYCN, E2F1, PRMT5, and p100/TSN protein expression levels. In the absence of doxycycline MYCN is overexpressed, when doxycycline is added to the cell media MYCN expression is suppressed as doxycycline inhibits the transcription (Figure 3.7). PRMT5 levels remained unchained upon MYCN overexpression, while there was an increase in E2F1 protein levels. This increase indicates co-expression of E2F1 and MYCN *in vitro*. p100/TSN protein expression level remained unchanged upon doxycycline treatment (Figure 3.7).

To rule out the cell lineage specific effect, we also included a TET-off MYCN inducible SHEP21N cell line as another comparison model to the PRMT5 inhibition sensitivity. We found that MYCN induced SHEP21N cells were more sensitive to T1-44 (IC_{50}= 3 µM), whereas doxycycline treated cells were more resistant to T1-44 (IC_{50}= 47 µM) highlighting the role of MYCN in sensitivity to the PRMT5 inhibition (Figure 3.8).

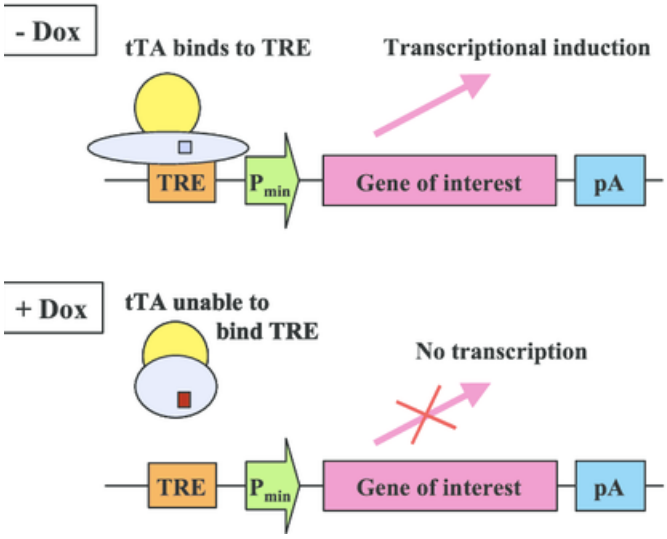

Figure 3.6. Schematic representation of Tet-off inducible expression system. The Tet-off system (tTA) activates gene expression in the absence of its ligand doxycycline. Upon addition of doxycycline, transcription of the gene of interest is silenced (Palais et al., 2009).

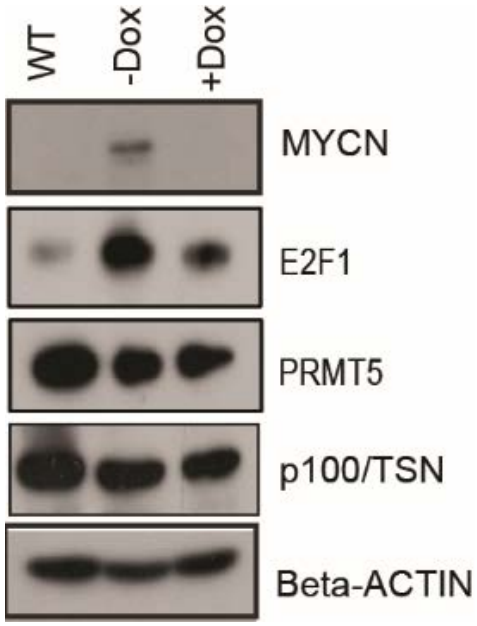

Figure 3.7. MYCN, E2F1, PRMT5, and p100/TSN protein expression levels in SHEP21N MYCN inducible cell line. 20 µg total protein was loaded onto the gels and β-actin was used as a loading control. WT: SHEP21N without any treatment, –DOX: without antibiotic doxycycline, +DOX: doxycycline treated cells.

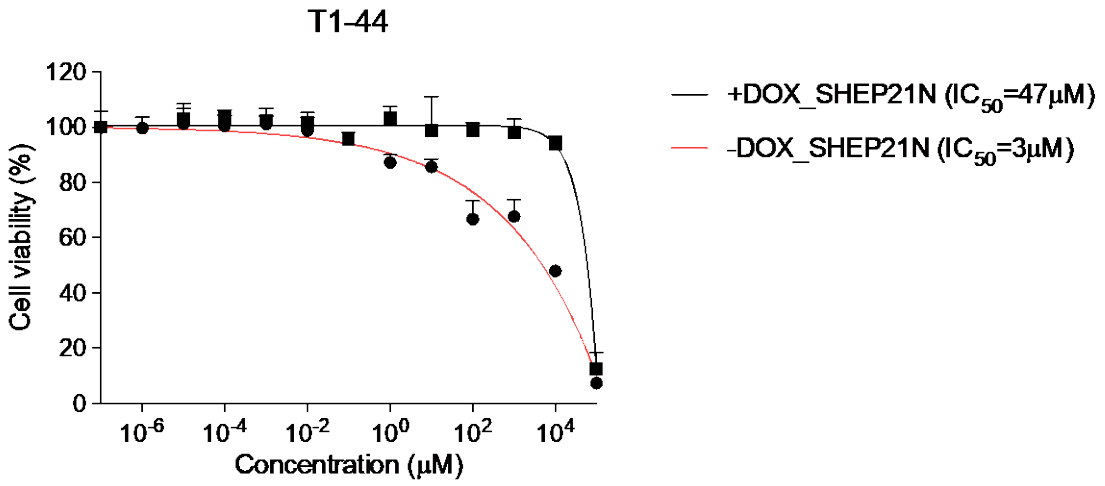

Figure 3.8. Differences in sensitivity to T1-44 between SHEP21N – and + DOX. We found that SHEP21N MYCN induced cells were more sensitive to T1-44 (IC_{50}= 3µM), whereas doxycycline treated cells were more resistant to T1-44 (IC_{50}= 47µM). Results shown are average of three independent experiments with standard error of mean shown, IC_{50} values were calculated by nonlinear regression analysis (curve fit) (Data was kindly provided from Dr. Laurel Bate-Eya).

3.5. Higher MYCN-PRMT5-E2F1 levels are poor prognostic factors for overall survival in NB patients

As we found that MYCN amplified cells are more sensitive to PRMT5 inhibition experimentally (Figure 3.2), our further interest was to understand the prognostic value of MYCN-PRMT5-E2F1 axis. Therefore, we checked the gene expression levels of *MYCN*, *PRMT5*, and *E2F1* by Kaplan-Meier survival plots in real disease setting. We also checked the expression levels of *p100/TSN*, as it is reader for the arginine methylation of E2F1 (Zheng et al., 2013). Kaplan-Meier survival curves for all four genes were compared in terms of overall survival in neuroblastoma. We found that patients with high *PRMT5* (n=98), *E2F1* (n=135), and *MYCN* (n=68) mRNA had significantly (*PRMT5*, $p=7.6e^{-28}$, *E2F1*, $p=4.2e^{2}$, and *MYCN*, $p=6.5e^{-34}$) lower overall survival rates compared to patients with low *PRMT5* (n=378), *E2F1* (n=341), and *MYCN* (n=408) expression, while *p100/TSN* expression did not reveal a prognostic significance for neuroblastoma patients with high or low expression of *p100/TSN* (Figure 3.9). Higher *PRMT5* and *E2F1* expression levels were found in MYCN amplified tumours (n=66) when compared to non-MYCN amplified tumours (n=405) (*PRMT5* $p=1.90e^{-33}$ and *E2F1*, $p=9.73e^{-20}$) (Figure 3.10).

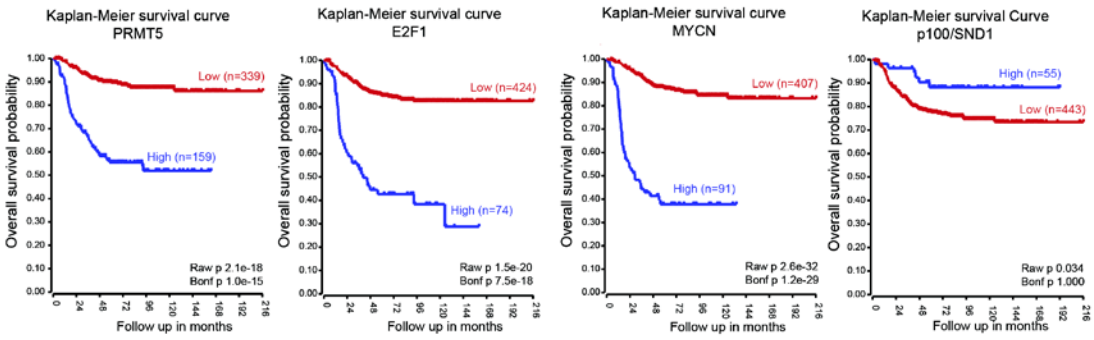

Figure 3.9. Overall survival rate comparison in higher versus lower expression of *PRMT5*, *E2F1*, *MYCN*, and *p100/TSN* in 649 neuroblastoma tumours. Patients with low gene expression are shown in red, while patients with high expression are shown in blue colour. Patients with high *PRMT5* (n=98), *E2F1* (n=135), and *MYCN* (n=68) mRNA expression had significantly lower overall survival compared to patients with low *PRMT5* (n=378), *E2F1* (n=341), and *MYCN* (n=408) expression (*PRMT5*, $p=7.6e^{-28}$; *E2F1*, p=4.2e-^{21} and *MYCN*, $p=6.5e^{-34}$). The overall survival in patients with a low mRNA expression of *p100/TSN* (n=74) was lower than patients with high mRNA expression and this was not statistically significant (Kocak Data set was retrieved from the R2 Genomics Analysis and Visualization Platform, Amsterdam University Medical Centers, University of Amsterdam and kindly provided by Dr. Laurel Bate-Eya).

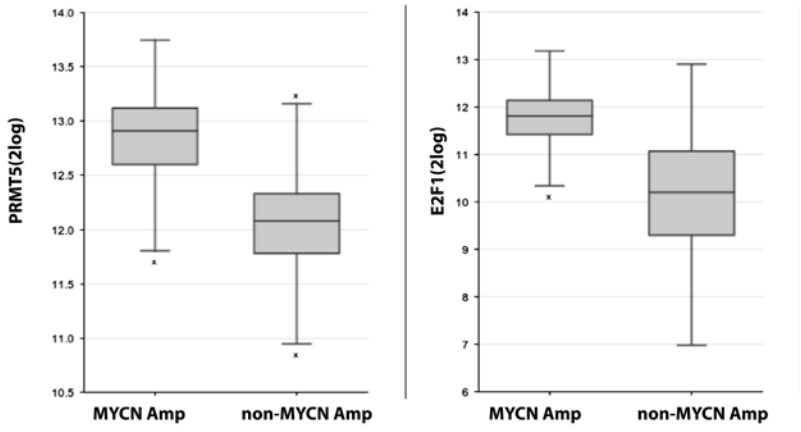

Figure 3.10. Higher PRMT5 and E2F1 levels were found in MYCN amplified tumours (n=66) when compared to non-MYCN amplified tumours (n=405). Statistical significancy was autocalculated by ANOVA (PRMT5 $p=1.90e^{-33}$ and E2F1, $p=9.73e^{-20}$) (Kocak Data set was retrieved from the R2 Genomics Analysis and Visualization Platform, Amsterdam University Medical Centers, University of Amsterdam).

3.6. Higher MYCN mRNA expression levels coincide with higher E2F1 and PRMT5 at both mRNA and protein expression levels in different cell lines

We then checked the mRNA expression levels of *E2F1*, *MYCN*, *PRMT5*, and *SND1/p100* (*TSN*) in silico to see whether the cell lines represent the real disease setting. MYCN amplified cell lines were represented as "sensitive" and non-MYCN amplified cell lines were represented as "insensitive" to the PRMT5 inhibitor T1-44 (Table 3.1). Amongst this cell line panel, non-MYCN amplified, non-neuroblastoma, prostate cancer cell line LNCaP was also included as another level of comparison to question whether MYCN amplification status and PRMT5 inhibition sensitivity are replicable in non-neuroblastoma cell lines.

We found that *PRMT5*, *E2F1*, and *MYCN* were significantly expressed higher at mRNA expression levels in MYCN amplified (PRMT5 sensitive) cell lines, whereas *SND1/p100* (*TSN*) mRNA expression levels were not correlated with the MYCN amplification status significantly. We also wanted to confirm this result in house where we grew 12 of the cell lines and checked their mRNA expression level by qPCR. Our results were mostly aligned with the in-silico data. However, E2F1 and PRMT5 correlations were not statistically significant due to some outlier cell lines (Figure 3.11, Figure 3.12).

Then, we checked the protein expression levels of E2F1, MYCN, PRMT5, and TSN in 12 cell lines. We also confirmed that the protein expression levels were parallel with the mRNA expression levels in vitro but PRMT5 and E2F1 protein levels were not found statistically significant like mRNA expression levels (Figure 3.13, Figure 3.14).

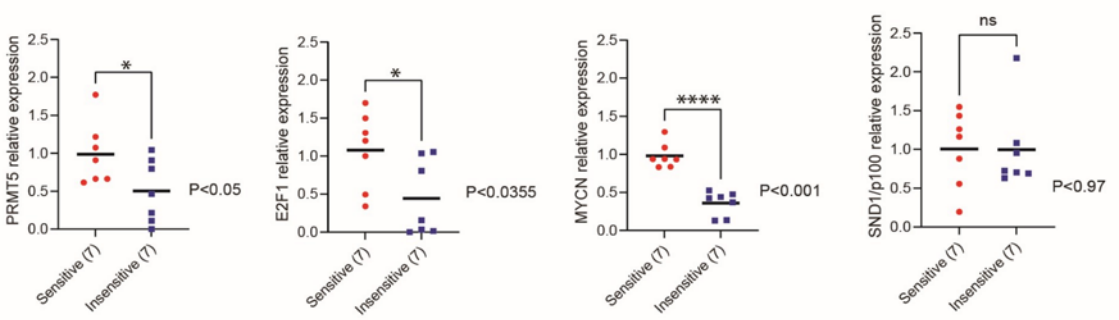

Figure 3.11. *PRMT5*, *E2F1*, *MYCN*, and *SND1/p100* mRNA expression levels across 14 cell lines. Term "Sensitive" refers to the MYCN amplified cell lines and "Insensitive" refers to the non-MYCN amplified cell lines in terms of PRMT5 inhibition. Cell lines were compared by using student's t-test. ns: $p>0.05$, * $p<0.05$, **** $p<0.0001$ (The data was retrieved from the R2 Genomics Analysis and Visualization Platform, University of Amsterdam).

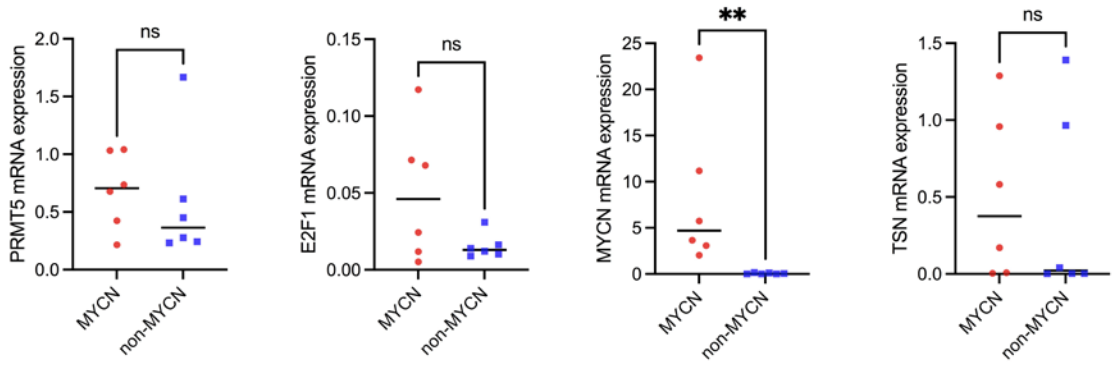

Figure 3.12. *PRMT5*, *E2F1*, *MYCN*, and *p100/TSN* mRNA expression levels across 12 cell lines by RT-PCR performed in-house. MYCN amplified (Sensitive), non-MYCN amplified (Insensitive). Statistical analyses were performed using the two-tailed, unpaired student's t-test. ns: $p>0.05$, ** $p<0.01$.

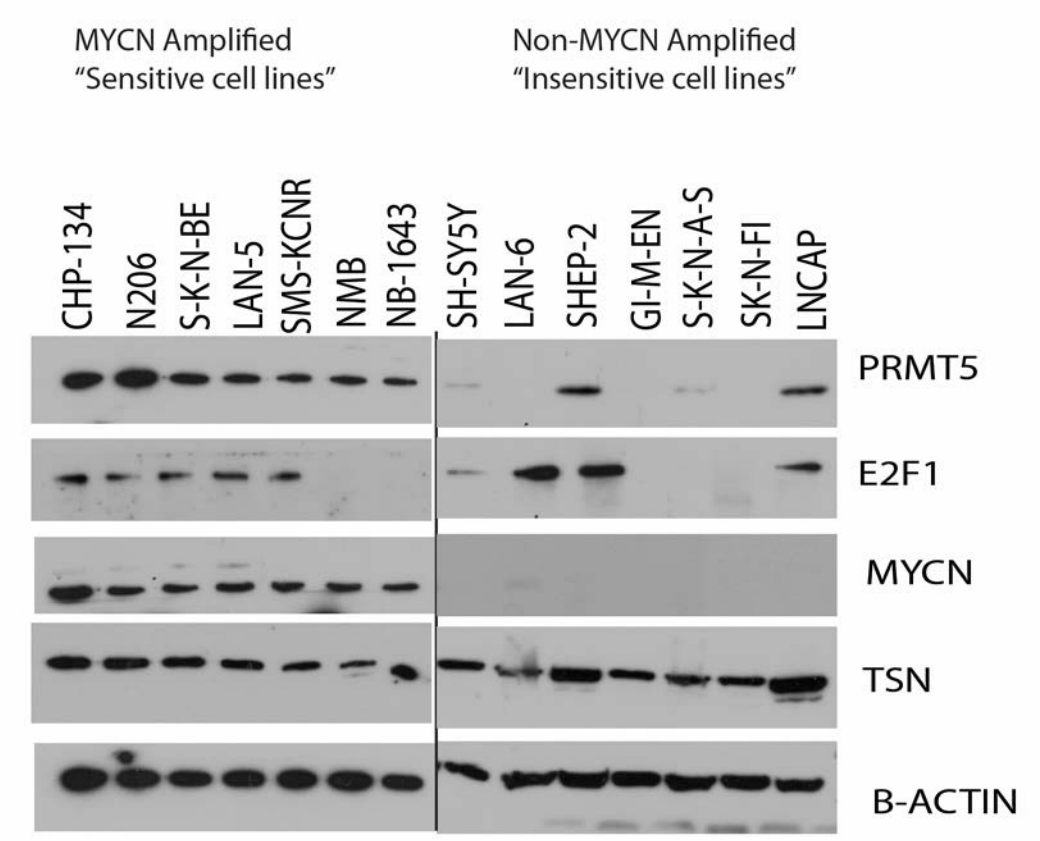

Figure 3.13. PRMT5, E2F1, MYC, and TSN (SND1/p100) protein expression levels across 12 different cell lines. 20 µg total protein was loaded onto the gels and β-actin was used as a loading control and representative western blot images from three independent experiments were presented.

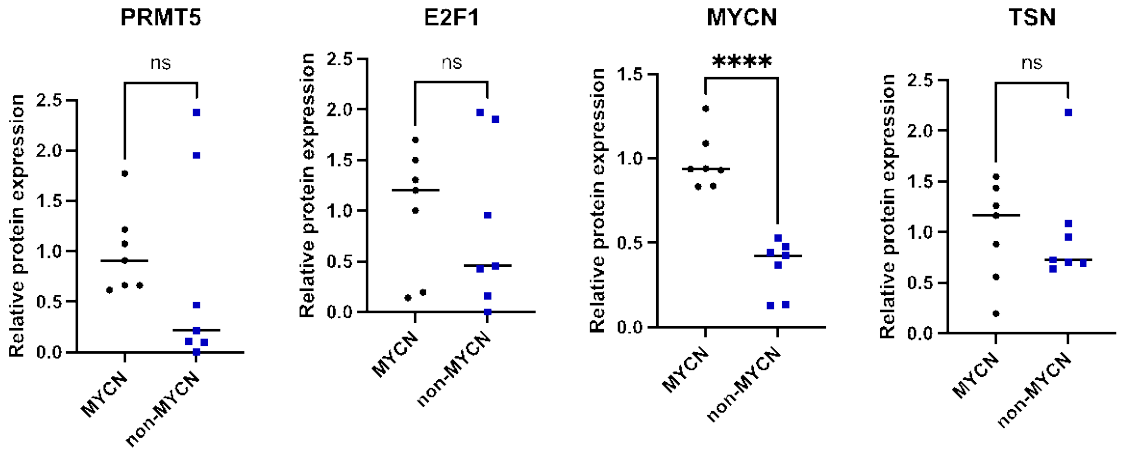

Figure 3.14. PRMT5, E2F1, MYCN, and TSN (SND1/p100) protein expression levels were quantified by ImageJ across 12 cell lines. Statistical analyses were performed using the two-tailed, unpaired student's t-test. ns: $p>0.05$, **** $p<0.0001$.

3.7. Chapter conclusions

We found that higher MYCN levels coincide with the higher E2F1 levels when we analysed high number of neuroblastoma tumour tissue samples in publicly available data sets. Then, we revealed that higher PRMT5, MYCN, and E2F1 levels are poor prognostic factor in neuroblastoma according to their Kaplan-Meier survival plots (Figure 3.9). We also found out that MYCN-E2F1-PRMT5 axis is an indicator of poor prognosis.

We checked the *E2F1*, *PRMT5,* and *TSN* mRNA expression levels of MYCN amplified cell lines in 14 cell line panel in-silico. We found that E2F1 and PRMT5 levels correlate with MYCN amplification status of the cells. Then, we presented in-house mRNA and protein expression levels and we found that some cell lines deviated from the correlation.

Once we validated the importance of MYCN-E2F1-PRMT5 axis in neuroblastoma and its potential translational importance, we aimed to drug this network via PRMT5 inhibition. We found that MYCN amplified NB cancer cells were significantly more sensitive to the PRMT5 inhibition.

We aimed to enlighten the underlying molecular mechanisms to the PRMT5 inhibition sensitivity. Therefore, we compared different cell line models to test our hypothesis. Our first model was comparing two of the cell lines that were at the distant edges of spectrum in terms of the sensitivity to the PRMT5 inhibitor (T1-44) *in vitro*. CHP-134 was used as a MYCN amplified “sensitive” cell line, whereas GI-ME-N was used as non-MYCN amplified “insensitive” cell line model. To rule out the cell lineage specific effect, we also included a TET-off MYCN inducible SHEP21N cell lines as another comparison model to the PRMT5 inhibition sensitivity. We found that MYCN induced SHEP21N cells were more sensitive to T1-44 (IC_{50}= 3 µM), whereas doxycycline

treated (MYCN inactivated) cells were more resistant to T1-44 (IC_{50}= 47 µM) highlighting the role of MYCN in sensitivity to the PRMT5 inhibition (Fig 3.8).

CHAPTER 4. Differences in response to PRMT5 inhibition in MYCN amplified CHP-134 versus non-MYCN amplified GI-ME-N cell lines

4.1. Introduction

In order to understand the mechanism of action that drives sensitivity to PRMT5 inhibition in higher E2F1/MYCN expressing cell lines versus lower E2F1/MYCN expressing cell lines, we performed transcriptome wide analysis of the most sensitive neuroblastoma cell line (CHP-134) and the least sensitive cell line (GI-ME-N) by RNA sequencing (RNA-seq) as RNA-seq is great tool for transcriptome-wide analysis of differential gene expression and differential splicing of mRNAs (Stark et al., 2019).

4.2. PRMT5 inhibition led to higher number of differentially expressed genes in MYCN amplified cell line

To further understand the underlying mechanism in sensitivity to PRMT5 inhibition, we performed RNA-seq analysis of one of the most sensitive cell line MYCN amplified CHP-134 versus resistant non-MYCN amplified cell line GI-ME-N. We treated CHP-134 and GI-ME-N cells with 200 nM T1-44 and DMSO for 72 hours.

We then looked at the gene enrichment terms upon drug treatment in CHP-134 cells. We used Metascape tool to identify biological pathways that were impacted under different conditions in the RNA-seq data. Gene set enrichment analysis uses gene ontology terms to categorize gene functions based on the number of significantly altered genes. Figure 4.1 and Figure 4.2 shows those pathways that are significantly (gene expression fold change cut-off >2 with an adjusted p-value ≤0.01) enriched in each comparison (Zhou et al., 2019). P53 mediated cell signalling, MAPK cascade, positive regulation of programmed cell death, G1 DNA damage signalling, regulation of apoptotic signalling pathway, and negative regulation of intracellular signal transduction were amongst up-regulated gene expression pathways in CHP-134 cell line after 200 nM T1-44 treatment for 72 hours (Figure 4.1).

Cell cycle, RB pathway, DNA replication, cell morphogenesis, RTK (receptor tyrosine kinase) pathway, DNA repair pathways, and cell surface receptor signalling pathway were amongst down-regulated gene expression pathways in CHP-134 cell line after 200 nM T1-44 treatment for 72 hours (Figure 4.2).

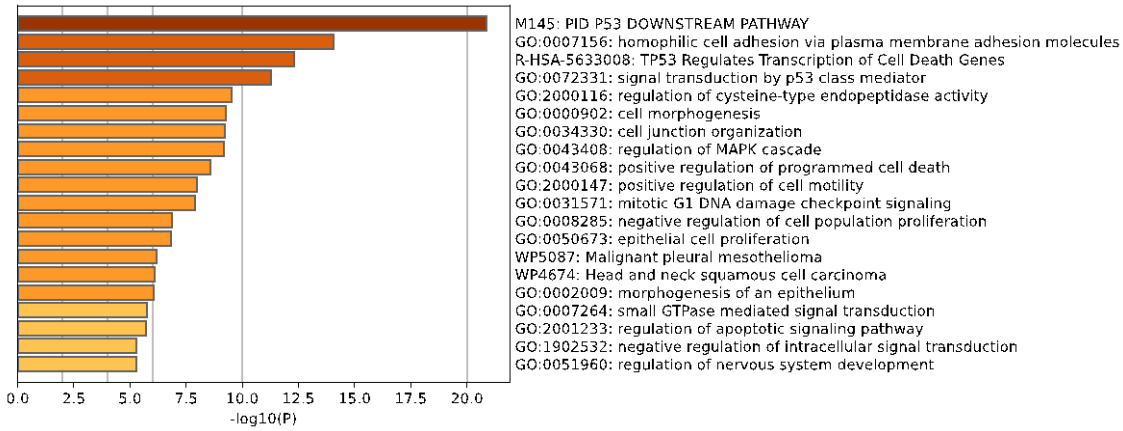

Figure 4.1. Gene ontology analysis for the up-regulated genes in MYCN amplified CHP-134 cell line that was treated with T1-44 for 72 hours (gene expression fold change cut-off >2 with an adjusted p-value ≤0.01). The analysis was performed by using Metascape.

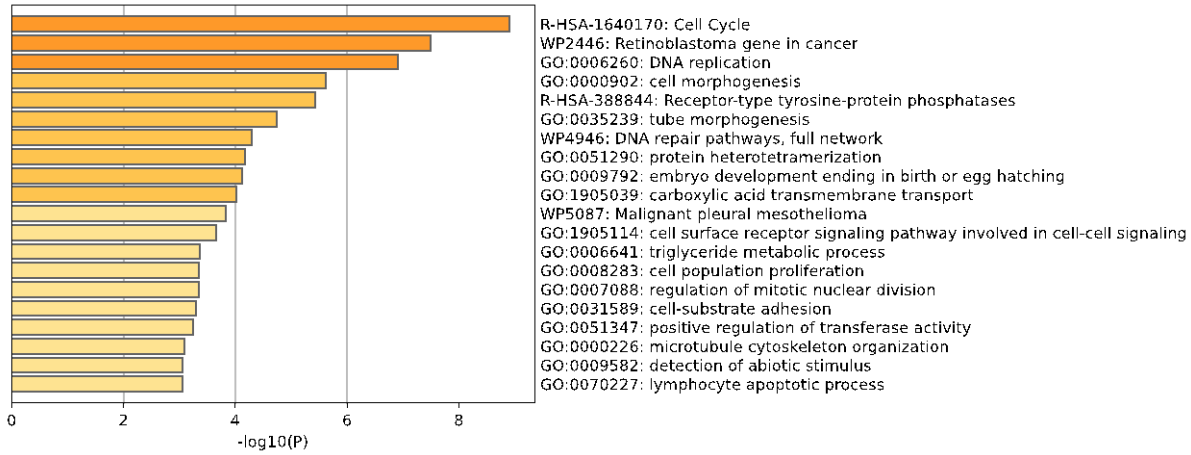

Figure 4.2. Gene ontology analysis for the down-regulated genes in MYCN amplified CHP-134 cell line that was treated with T1-44 for 72 hours (gene expression fold change cut-off >2 with an adjusted p-value ≤0.01). The analysis was performed by using Metascape.

One very striking finding from the RNA-seq data was the number of differentially expressed genes was significantly higher in CHP-134 cell line. We previously confirmed T1-44's engagement in both cell lines by checking SDMA marks in western blot before sending the samples for the RNA-seq. After adjusted p-value ≤0.01 cut-off was applied, there were so few genes that were differentially expressed in GI-ME-N cell line. Therefore, gene set enrichment analysis was not presented here. The top differentially expressed gene lists were provided in Appendix B, Table 2. That finding was also reflected in heat-map analysis in CHP-134 and GI-ME-N cell lines, suggesting that base line gene expression differences were significant (Figure 4.3).

The most differentially and significantly expressed genes (up-regulated or down regulated) from RNA-seq data were validated at total mRNA transcript level by RT-PCR in MYCN amplified [CHP-134, N206, SK-N-BE(2)] and non-MYCN amplified (GI-ME-N, SHEP2) cell lines in order to check if RNA-seq data is aligned with qPCR data. *LIF*, *PHLDA3*, *PLK2*, *CSF1*, *CDKN1A*, *TIGAR*, *METTL7A*, and *AHNAK* genes were validated by qPCR. Various selection criteria were used while selecting the genes for further qPCR validation. These criteria include log2 fold expression difference (>1), targets that have higher base mean in the RNA-seq data, genes that are targets of E2F1 and/or MYCN as we were interested in them for instance; *CSF1* (E2F1 target), *LIF1* (E2F1 and MYCN target), *PLK2* (E2F1 and MYCN target), *P21* (MYCN target).

The list of validated DEGs (differentially expressed genes) and their log2 (fold changes) in RNA sequencing experiment were represented in Table 4.1. Top 100 differentially expressed gene list was provided at Appendix B, Table 1. qPCR validation results of these genes can be found in Figure 4.4-Figure 4.7. These validated targets revealed similar trends in mRNA expression levels between MYCN amplified and non-MYCN amplified cell lines (Figure 4.4-Figure 4.7).

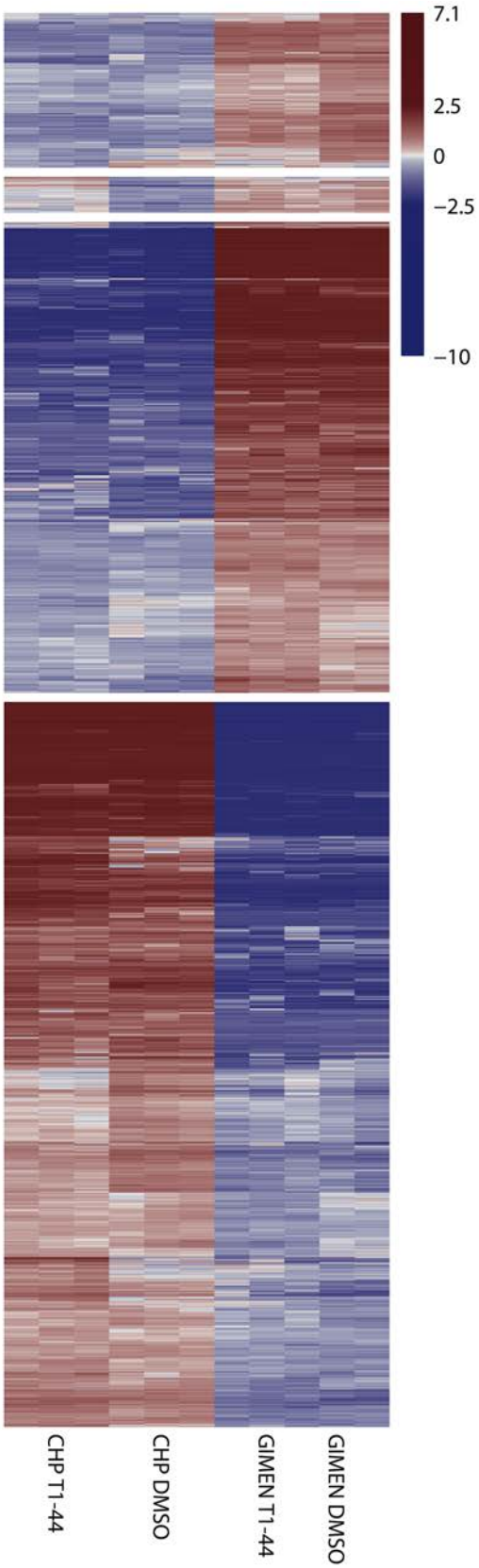

Figure 4.3. Heat-map analysis of the differentially expressed genes in CHP-134 and GI-ME-N cell lines after 200 nM T1-44 treatment for 72 hours. Adjusted p-value ≤0.01.

Table 4.1. List of qPCR validated differentially expressed genes (DEGs) and their log2 (fold changes) after 200 nM T1-44 treatment for 72 hours in RNA sequencing.*

Gene	RNA-Seq (T1-44 vs DMSO in CHP-134) Log2 (fold change)
AHNAK	1.316026
P21	2.998828
PLK2	2.636602
CSF1	2.460153
PHLDA3	2.847747
MTTL7A	3.49309
LIF	5.017673
TIGAR	1.738898

*Genes were considered differentially expressed if the adjusted p-value, calculated using the Benjamini-Hochberg method to minimize the false discovery rate, was less than 0.01. We further filtered significantly differentially expressed gene sets using 2-fold change in absolute expression level.

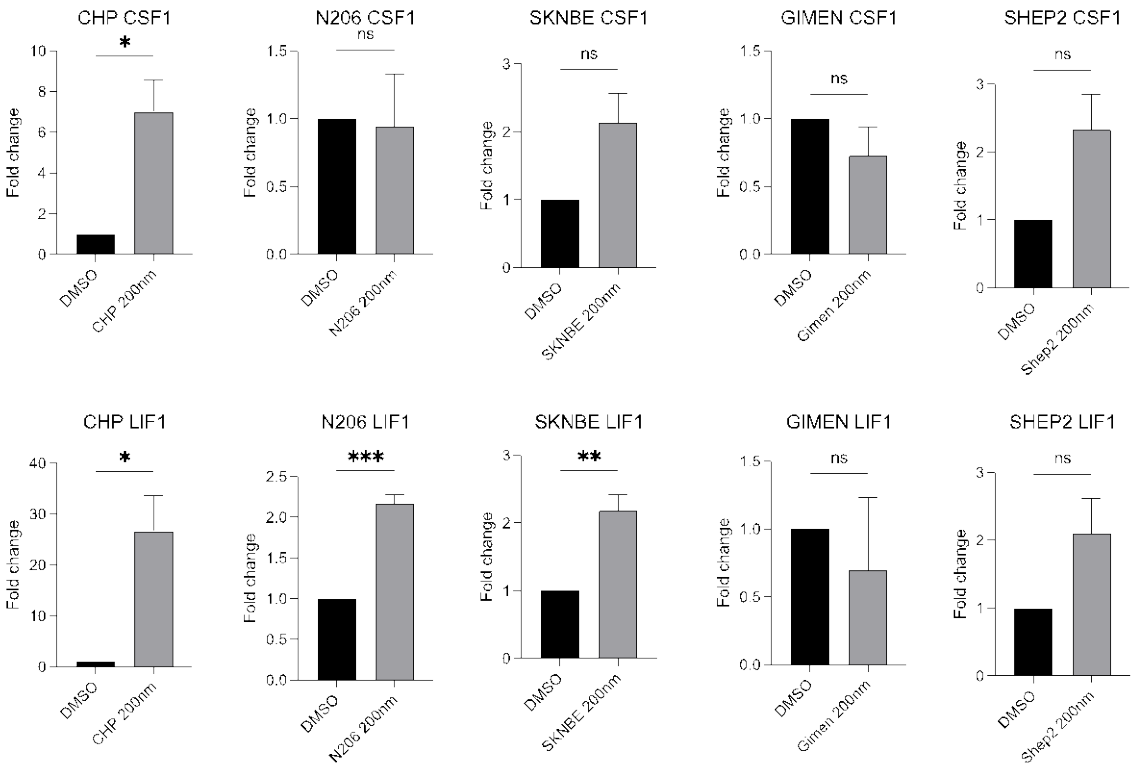

Figure 4.4. qPCR validation of total *CSF1* (Colony Stimulating Factor 1) and *LIF1* (Leukemia Inhibitory Factor) mRNA expression levels after 200 nM T1-44 treatment for 72 hours. CHP-134, N206, and SK-N-BE(2) MYCN amplified; GI-ME-N and SHEP2 non-MYCN amplified. Fold changes were calculated as mean of n=3 biological replicates. Data were analysed by unpaired t-test. ns: $p>0.05$, * $p<0.05$, ** $p<0.01$, *** $p<0.001$.

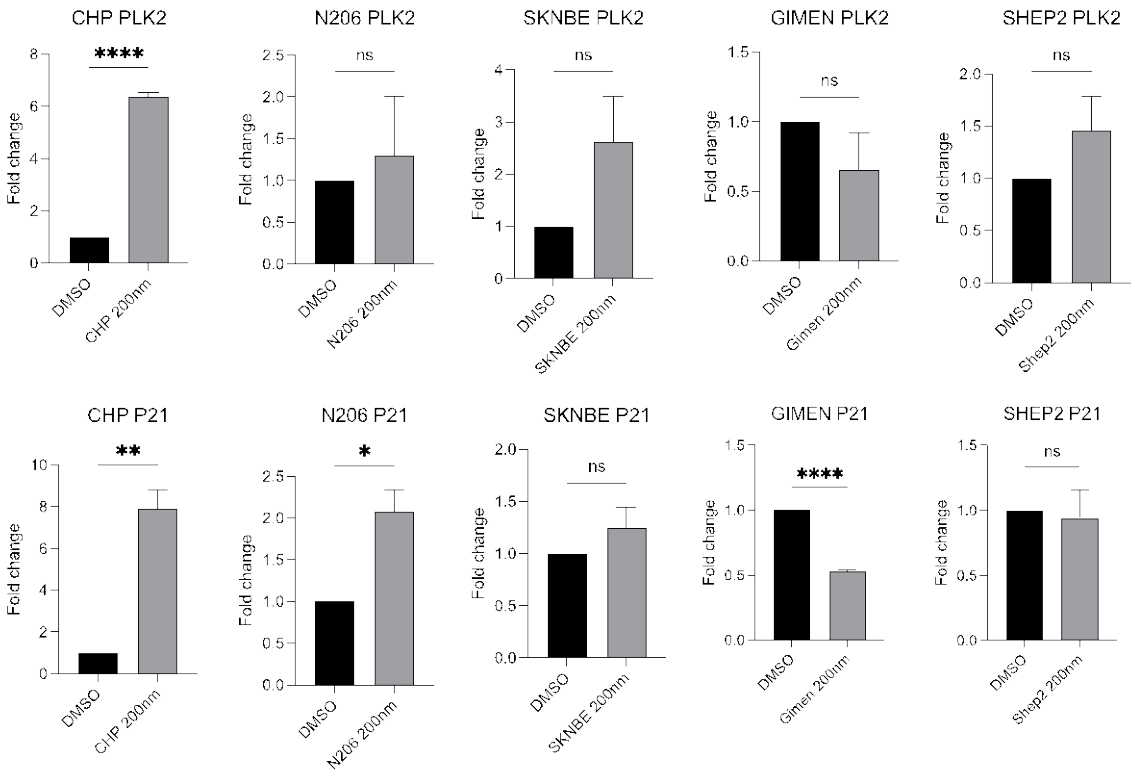

Figure 4.5. qPCR validation of total *PLK2* (Polo Like Kinase 2) and *CDKN1A* (Cyclin Dependent Kinase Inhibitor 1A) mRNA expression levels after 200 nM T1-44 treatment for 72 hours. CHP-134, N206, and SK-N-BE(2) MYCN amplified; GI-ME-N and SHEP2 non-MYCN amplified. Fold changes were calculated as mean of n=3 biological replicates. Data were analysed by unpaired t-test. ns: $p>0.05$, * $p<0.05$, ** $p<0.01$, **** $p<0.0001$.

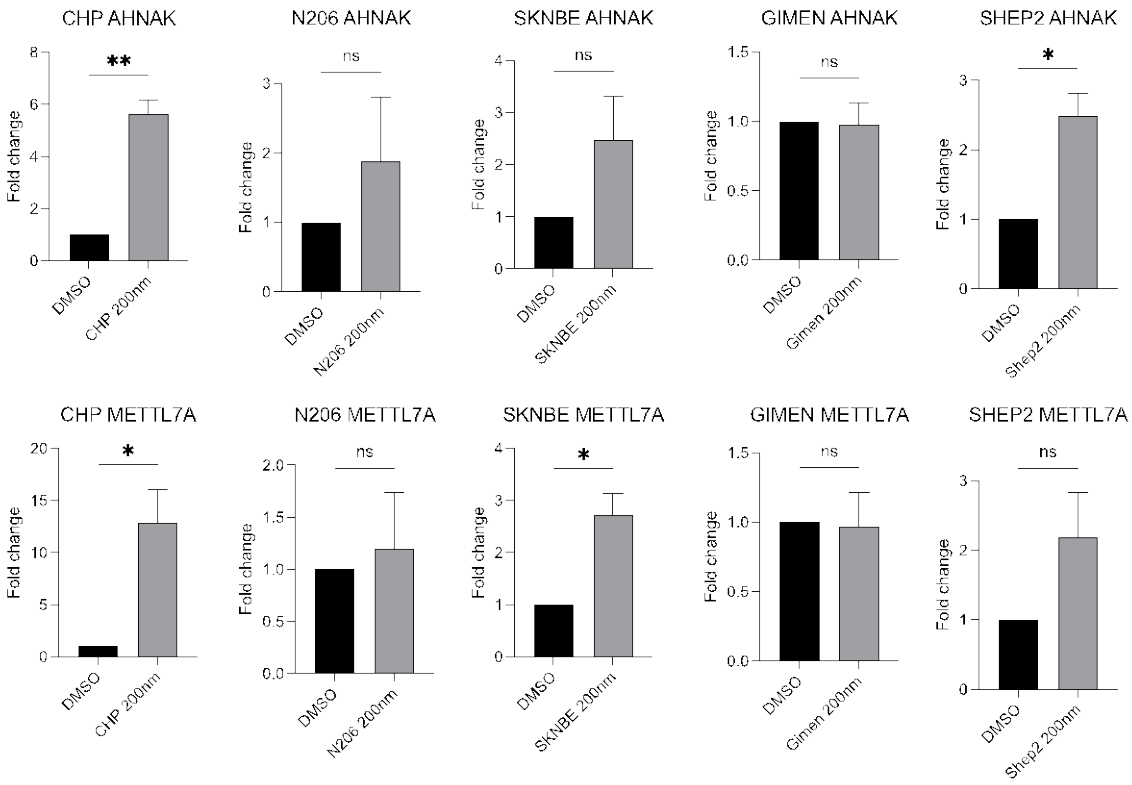

Figure 4.6. qPCR validation of total *AHNAK* (Desmoyokin) and *METTL7A* (Methyltransferase Like 7A) mRNA expression levels after 200 nM T1-44 treatment for 72 hours. CHP-134, N206, and SK-N-BE(2) MYCN amplified; GI-ME-N and SHEP2 non-MYCN amplified. Fold changes were calculated as mean of n=3 biological replicates. Data were analysed by unpaired t-test. ns: $p>0.05$, * $p<0.05$, ** $p<0.01$.

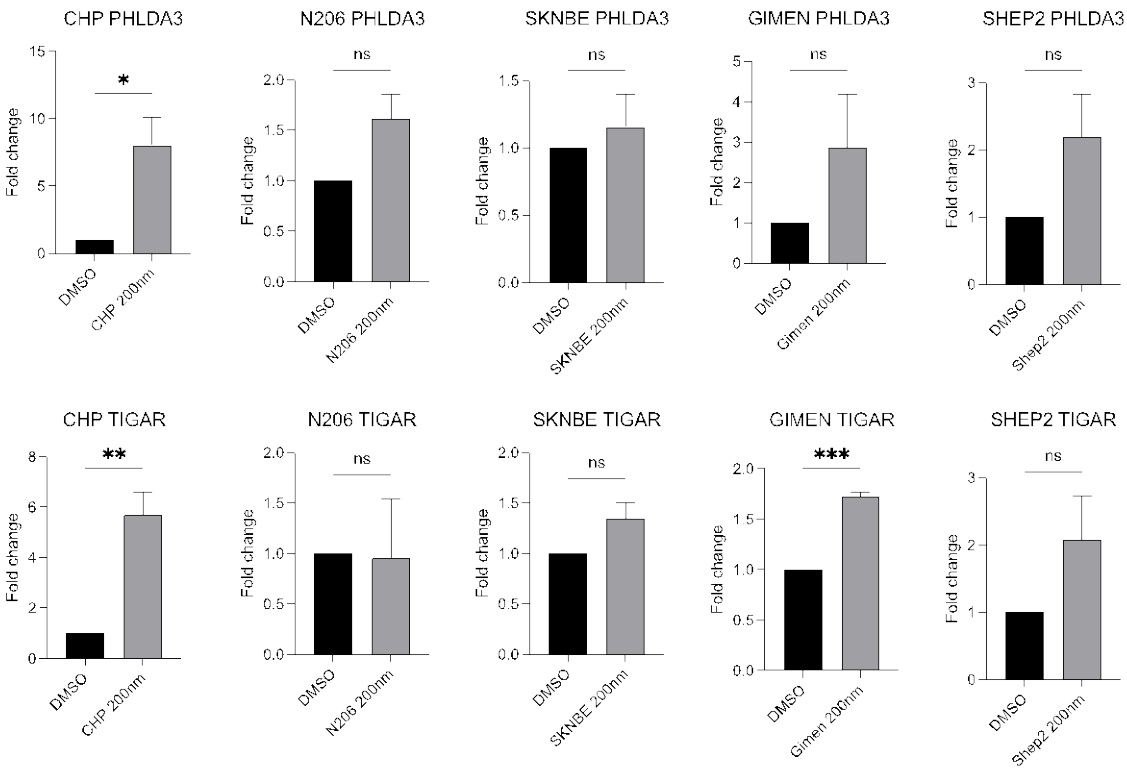

Figure 4.7. qPCR validation of total *PHLDA3* (Pleckstrin Homology Like Domain Family A Member 3) and *TIGAR* (TP53 Induced Glycolysis Regulatory Phosphatase) mRNA expression levels after 200 nM T1-44 treatment for 72 hours. CHP-134, N206, and SK-N-BE(2) MYCN amplified; GI-ME-N and SHEP2 non-MYCN amplified. Fold changes were calculated as mean of n=3 biological replicates. Data were analysed by unpaired t-test. ns: $p>0.05$, * $p<0.05$, ** $p<0.01$, *** $p<0.001$.

4.3. PRMT5 inhibition induced differentially spliced events in CHP-134 and GI-ME-N cells

We were also interested in the differentially spliced gene differences in sensitive cell line CHP-134 compared to the insensitive GI-ME-N cell line, as such differences might be key to understanding the functional mechanism of PRMT5 inhibitor sensitivity. Differentially spliced genes after T1-44 treatment were calculated using the rMATS algorithm (Robust and flexible detection of differential alternative splicing from replicate RNA-seq data) (Shen et al., 2014). rMATS results revealed different number of alternatively spliced genes between CHP-134 and GI-ME-N cell line as it was shown at Figure 4.8.

We found that T1-44 treatment induced higher number of differentially spliced events in the high E2F1/MYCN expressing cell line CHP-134 when compared with the low E2F1/MYCN expressing cell line GI-ME-N. Some of the splicing events were only specific to CHP-134, whereas some of the events were common between these two cell lines. 1812 genes were spliced in T1-44 treated CHP-134 cells, whereas 626 genes were spliced in GI-ME-N cell line in the same treatment conditions. 673 genes were spliced in both cell lines (Figure 4.8, Figure 4.9).

Canberra heat-map analysis showing the differential splicing differences in CHP-134 and GI-ME-N cell lines, each comparison revealed unique set of spliced genes. CHP-134 DMSO versus GI-ME-N DMSO column represents base level differences in splicing between those two cell lines. 200 nM T1-44 treatment for 72 hours induced the splicing of different set of genes (Figure 4.9). These different patterns in splicing again shows the differences between these cell lines.

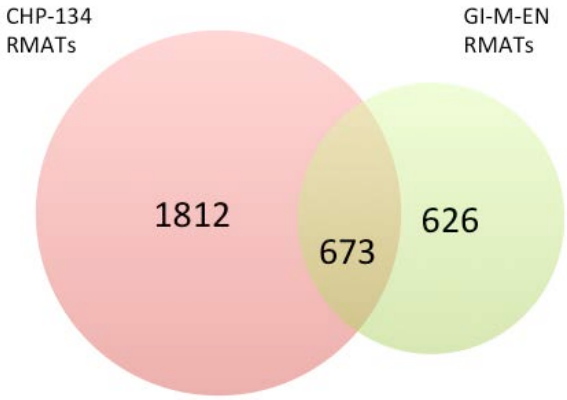

Figure 4.8. The number of differentially spliced genes upon 200 nM T1-44 treatment for 72 hours in CHP-134 (MYCN amplified) and GI-ME-N (non-MYCN amplified) cell lines.

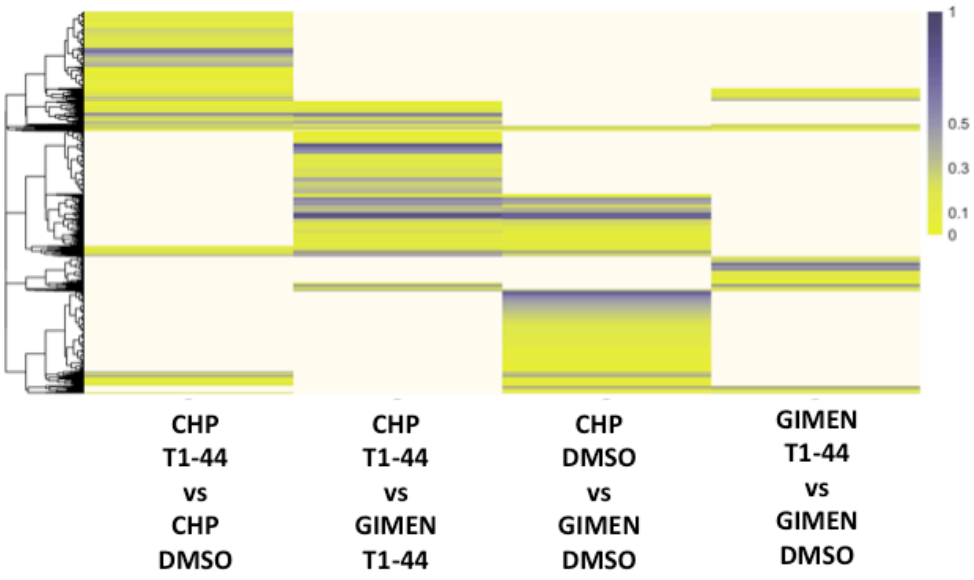

Figure 4.9. Canberra heat-map for statistically significant differential splicing events in MYCN amplified cell line CHP-134 versus non-MYCN amplified cell line GI-ME-N upon 200 nM treatment with T1-44 for 72 hours. This heat-map represents absolute values of ΔΨ (percent spliced in) for cell lines, corresponding to statistically significant alternative splicing event changes to E2F1 target genes (as previously determined from the ENCODE data) derived by analysing the RNA-seq data with rMATS algorithm. Yellow colour represents the lowest difference, and blue colour represents the highest differences (FDR >0.01).

4.4. Splicing factor gene expression differences in MYCN amplified cell lines versus non-MYCN amplified cell lines

Previously, it was shown that splicing factors were enriched in other MYCN amplified, non-neuroblastoma cancer cells (Zhang et al., 2016; Singh et al., 2021). When we analysed the enriched gene sets in our RNA-seq data, a number of shared enriched genes were connected with the splicing factors and these splicing factors were also E2F1 targets. As we were interested in E2F1's role in this sensitivity to the PRMT inhibition in MYCN amplified cells, we further checked the splicing factors hypothesizing that the differences in the expression of these splicing factors might indicate their transcriptional regulation by either E2F1 and/or MYCN. We checked the splicing factor genes in RNA-seq data and *SRSF*1, *SRSF3*, and *SRSF4* were amongst the topmost differentially expressed genes in CHP-134 versus GI-ME-N cell line (Figure 4.10). Therefore, we validated the expression levels of splicing factors such as *SRSF1*, *SRSF3*, *SRSF4*, *CPSF3*, *CPSF4*, and *HNRNPA3* which were expressed higher in E2F1-high/MYCN-amplified cell line CHP-134 versus E2F1-low/MYCN-non-amplified cell line GI-ME-N. Then, we found that these splicing factor genes were expressed higher levels in MYCN amplified CHP-134 cell line when compared with non-MYCN amplified GI-ME-N cell line at base levels without any drug treatment (Figure 4.11).

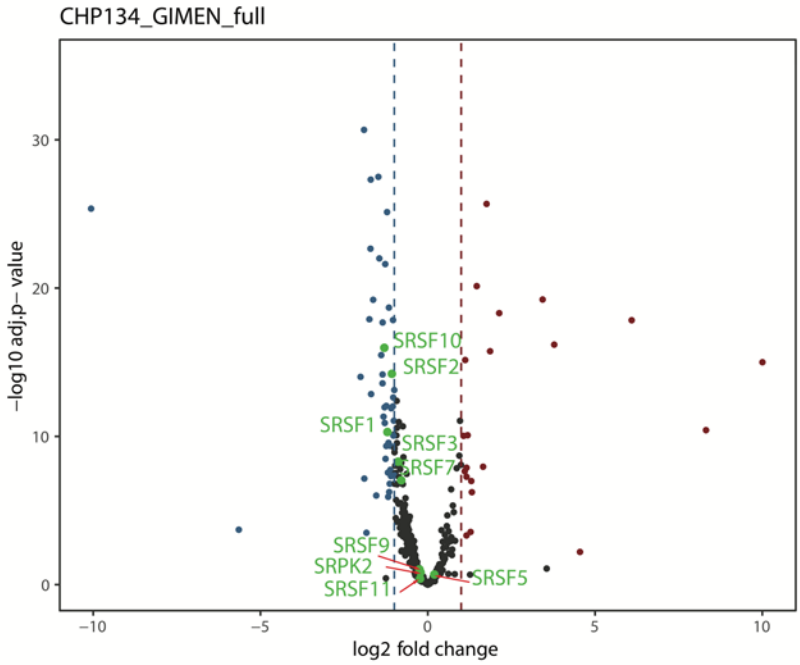

Figure 4.10. Scatter plot of differentially expression of splicing factors in CHP-134 cell line upon 200 nM T1-44 treatment for 72 hours. Data is presented as log2 fold change and $p<0.05$.

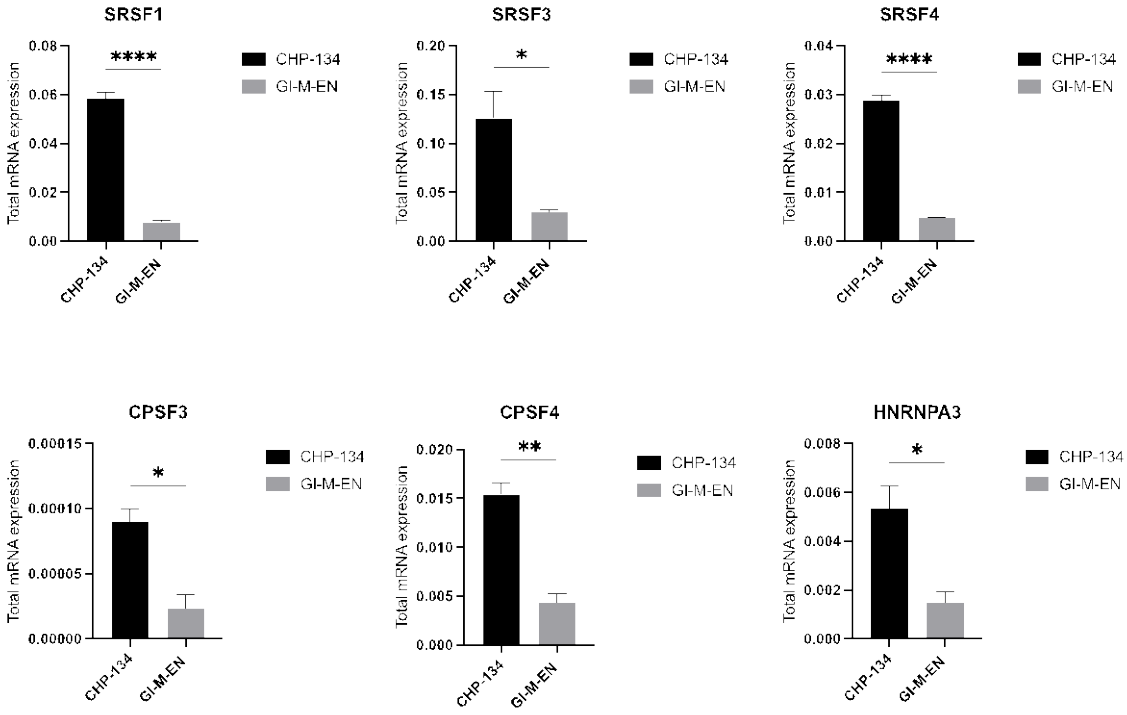

Figure 4.11. Splicing factor gene mRNA expressions in MYCN amplified CHP-134 cells versus non-MYCN amplified GI-ME-N cells. Results shown are average of three independent experiments with standard error of mean, analysed by unpaired t-test. * $p<0.05$, ** $p<0.01$, **** $p<0.0001$.

We also checked the mRNA expression levels for the splicing factors *SRSF1,* S*RSF3,* and S*RSF4* in 6 MYCN amplified and 6 non-MYCN amplified cell lines after confirming their MYCN mRNA expression levels (Figure 4.12). We found that higher levels of *SRSF1* and *SRSF3* were coincided with the higher levels of *E2F1* mRNA expression levels across 12 different cell lines, whereas *SRSF4* mRNA expression levels were more heterogenous in the same cell line panel (Figure 4.13-Figure 4.15).

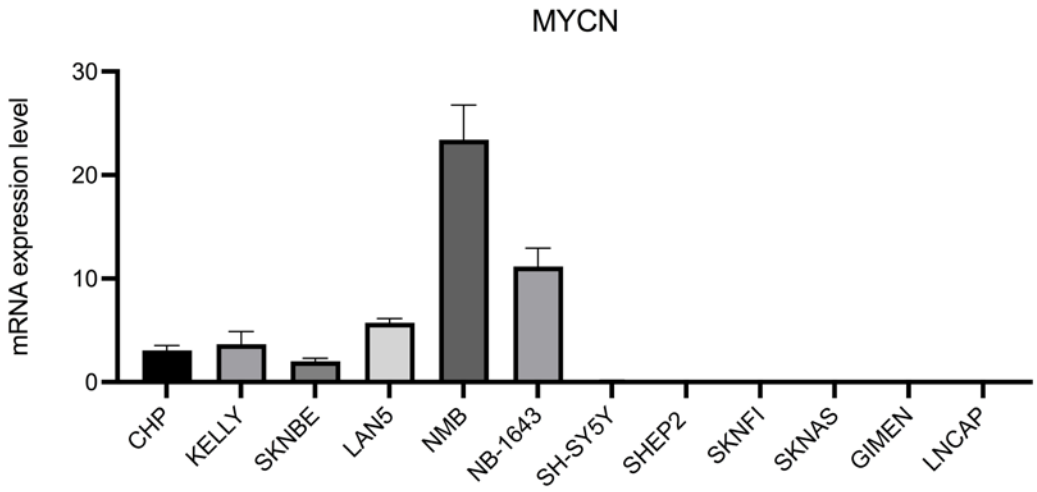

Figure 4.12. *MYCN* mRNA expression levels across 12 MYCN amplified and non-MYCN amplified cell lines (Left to right: 1-6 MYCN amplified cell lines, 7-12 non-MYCN amplified cell lines).

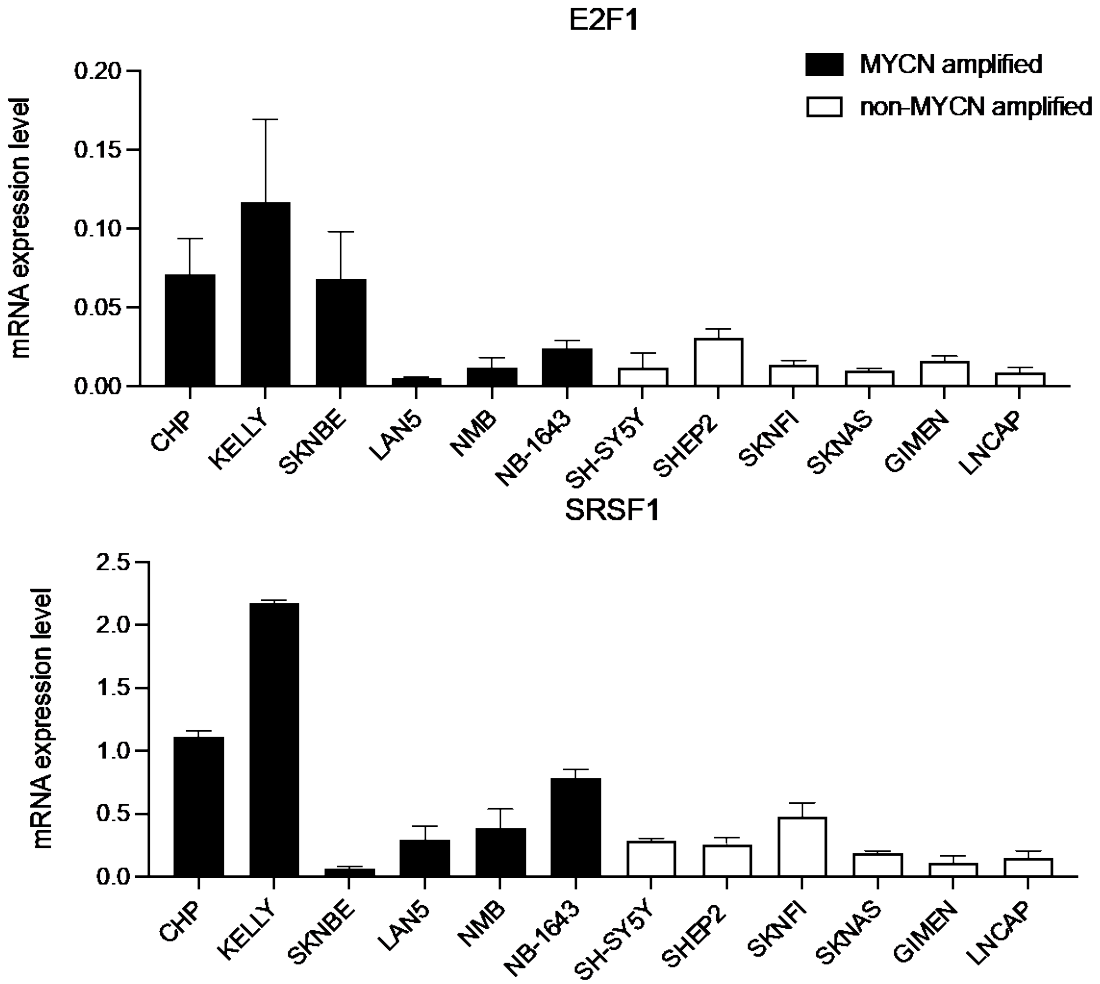

Figure 4.13. *E2F1* and *SRSF1* mRNA expression levels across 12 MYCN amplified and non-MYCN amplified cell lines (Left to right: 1-6 MYCN amplified cell lines, 7-12 non-MYCN amplified cell lines).

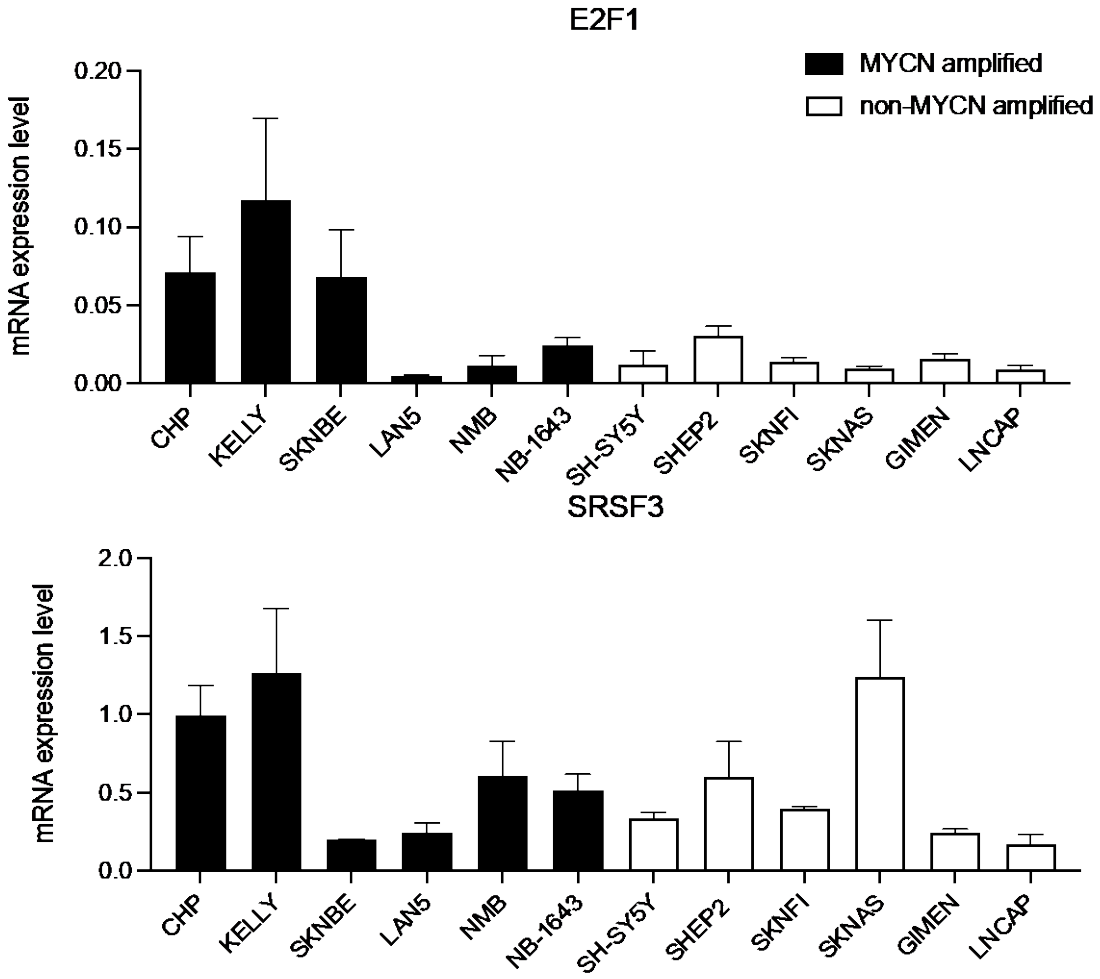

Figure 4.14. *E2F1* and *SRSF3* mRNA expression levels across 12 MYCN amplified and non-MYCN amplified cell lines (Left to right: 1-6 MYCN amplified cell lines, 7-12 non-MYCN amplified cell lines).

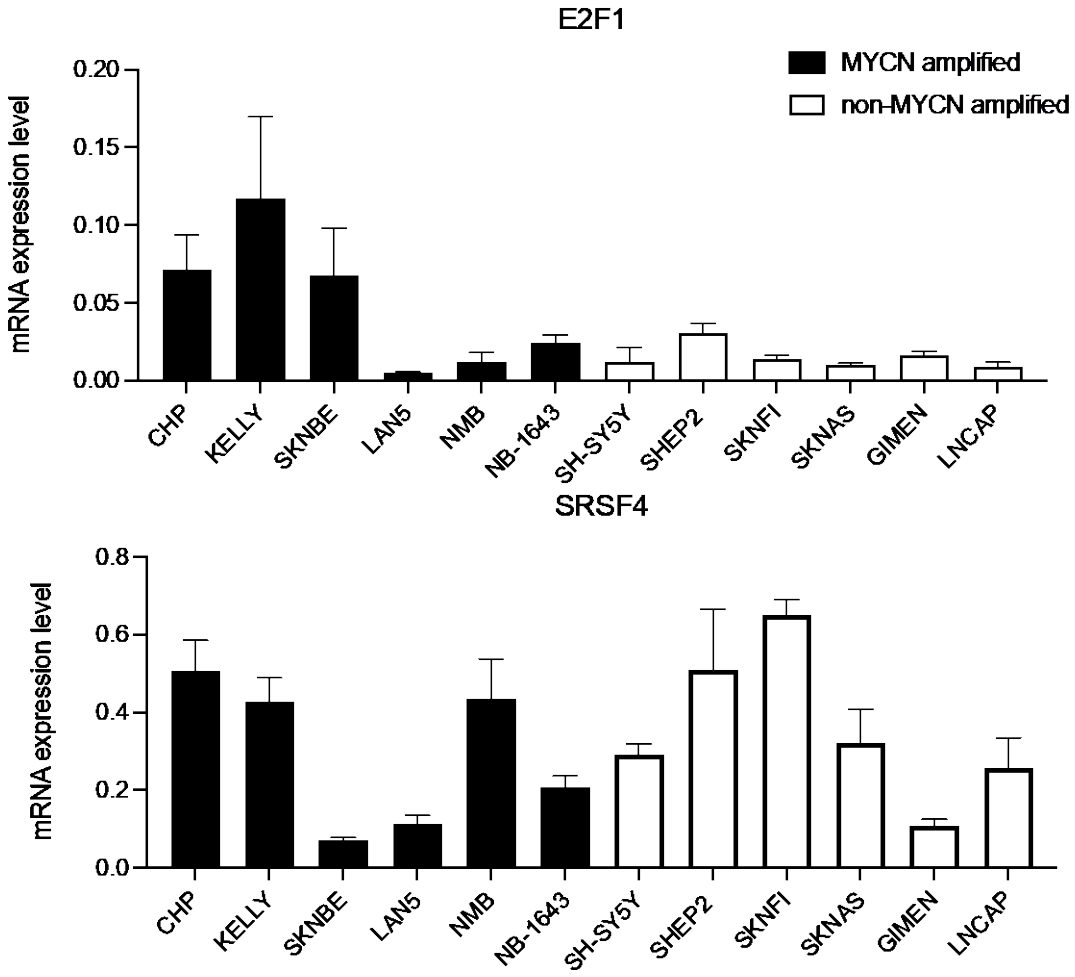

Figure 4.15. *E2F1* and *SRSF4* mRNA expression levels across 12 MYCN amplified and non-MYCN amplified cell lines (Left to right: 1-6 MYCN amplified cell lines, 7-12 non-MYCN amplified cell lines).

In order to further validate RNA sequencing and qPCR results for splicing factors, we performed chromatin immunoprecipitation assays (ChIP) to identify the binding affinity of either E2F1 or MYCN to the promoters of splicing factors *SRSF1*, *SRSF3,* and *SRSF4*. We observed an increased enrichment of MYCN to the promoters of these splicing factor genes in the CHP-134 cell line. *PARP2* gene was used as a positive control for MYCN enrichment to the target genes. As expected, there was a significant decrease in the binding affinity of MYCN to the promoters of the GI-ME-N cell lines for the splicing factors. This was highly expected, as GI-ME-N is non-MYCN amplified cell line (Figure 4.16-Figure 4.18). In order to rule out cell lineage differences, we also used SHEP21N MYCN inducible cell line in order to check the splicing factor gene enrichment in the presence and absence of MYCN. SHEP21N cells MYCN levels were checked prior to ChIP experiment to prove the cell line working as expected. SHEP21N –dox cells (MYCN expressing cells) have higher mRNA expression levels of splicing factors, while +dox cells have lower mRNA expression levels of splicing factors.

We also found that splicing factors were enriched in E2F1 ChIP, showing that *SRSF1*, *SRSF3,* and *SRSF4* were acting as E2F1 targets in MYCN amplified CHP-134 cell line but not in GI-ME-N. These results were expected as GI-ME-N expresses low levels of E2F1 (Figure 4.16-Figure 4.18).

Overall, we observed increased enrichment of the *MYCN* and *E2F1* oncogenes to the promoters of the SR rich splicing factor genes *SRSF1*, *SRSF3,* and *SRSF4* in the CHP-134 cell line but there was no enrichment in GI-ME-N cells possibly due to absence or very low levels of E2F1. The mRNA expression levels of splicing factors were also in parallel with the MYCN induction levels in SHEP21N MYCN inducible cell line (Figure 4.16-Figure 4.18).

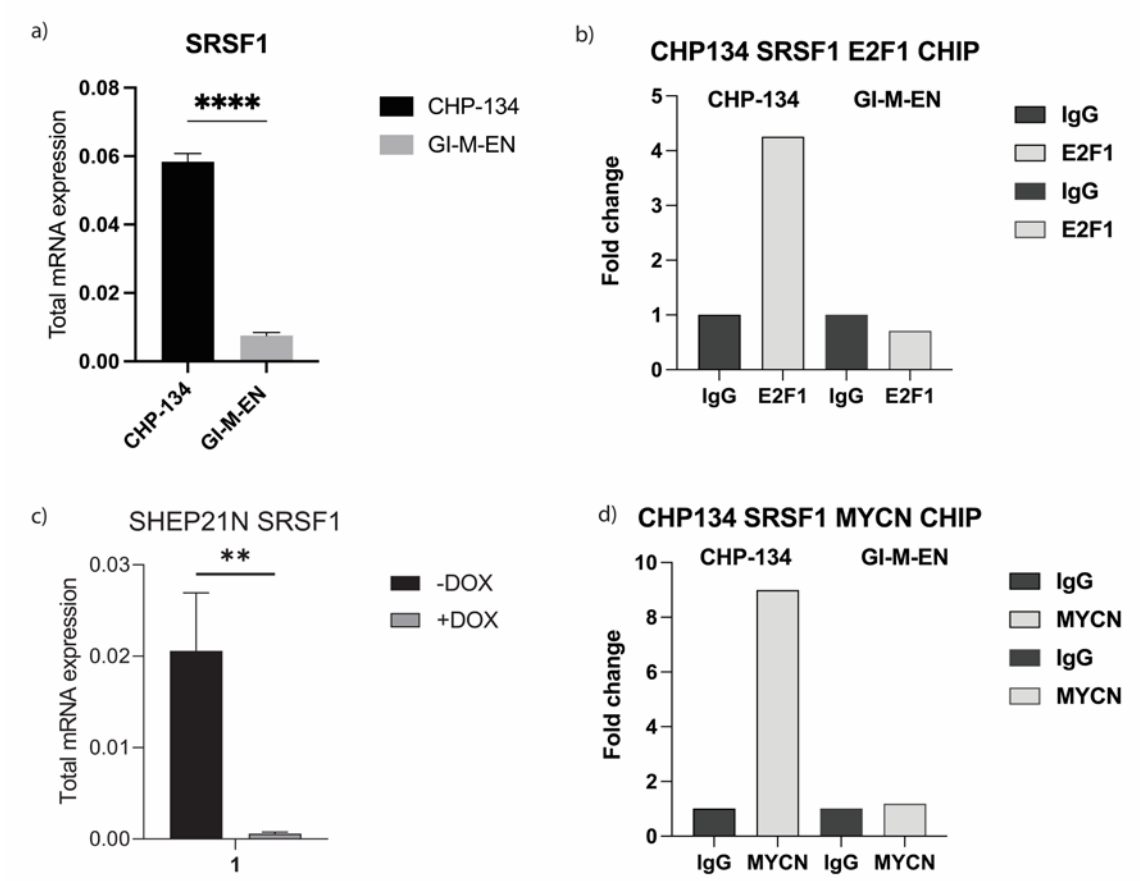

Figure 4.16. E2F1 and MYCN interactions with the *SRSF1* promoter a) *SRSF1* mRNA expressions in MYCN amplified CHP-134 cells versus non-MYCN amplified GI-ME-N cells, b) E2F1 enrichment around E2F1 binding motif at *SRSF1* gene promoter in CHP-134 and GI-ME-N cells, c) *SRSF1* overexpression in MYCN inducible SHEP21N cell line, d) MYCN enrichment around MYCN binding motif in *SRSF1* gene at CHP-134 and GI-ME-N cells. Experiments were run in n=3 biological and technical replicates. Mean values were presented. ** $p<0.01$, **** $p<0.0001$.

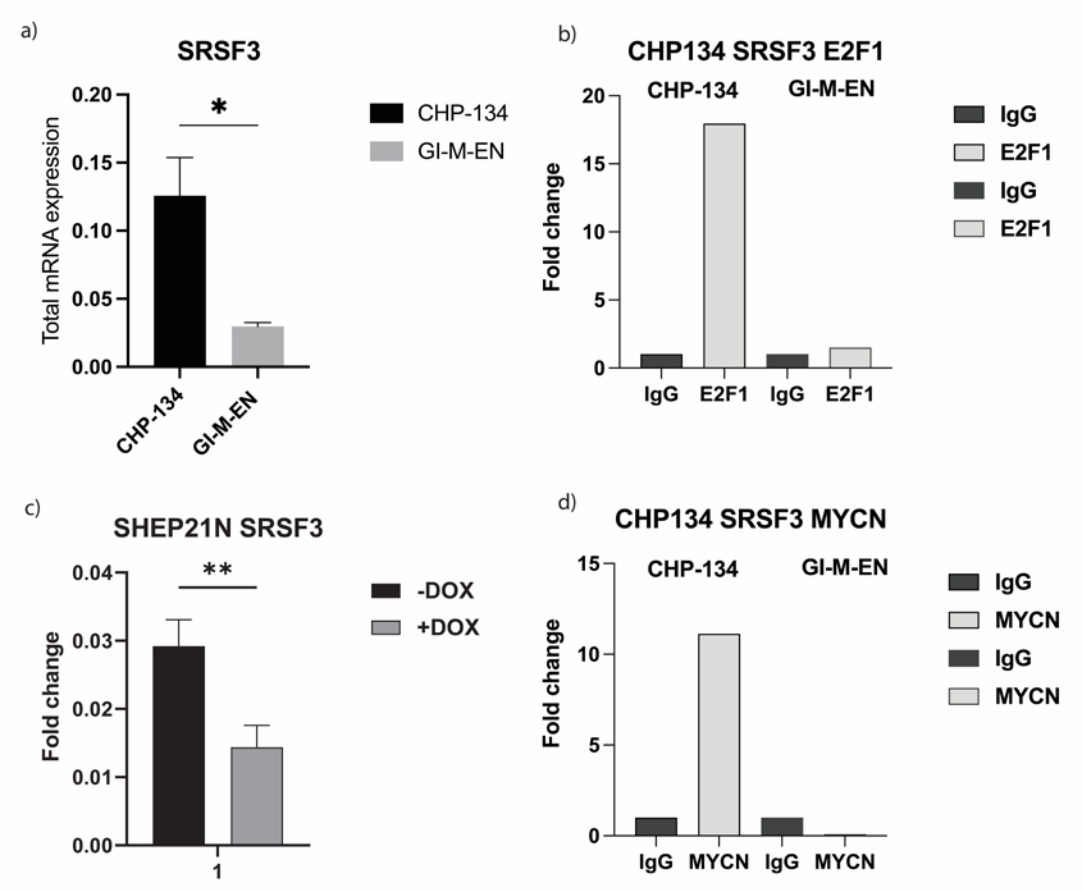

Figure 4.17. E2F1 and MYCN interactions with *SRSF3* promoter a) *SRSF3* mRNA expressions in MYCN amplified CHP-134 cells versus non-MYCN amplified GI-ME-N cells, b) E2F1 enrichment around E2F1 binding motif at *SRSF3* gene in CHP-134 and GI-ME-N cells, c) *SRSF3* overexpression in MYCN inducible SHEP21N cell line, d) MYCN enrichment around MYCN binding motif in *SRSF3* gene at CHP-134 and GI-ME-N cells. Experiments were run in n=3 biological and technical replicates. Mean values were presented. * $p<0.05$, ** $p<0.01$.

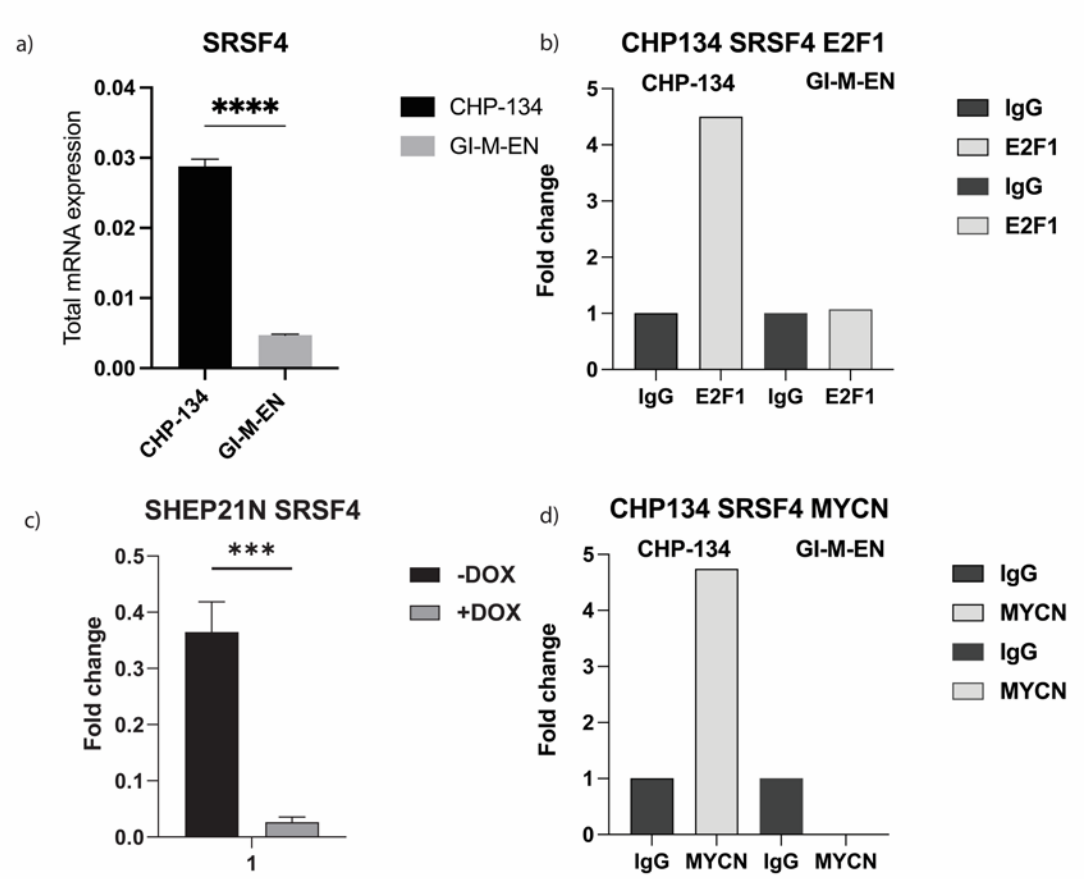

Figure 4.18. E2F1 and MYCN interactions with *SRSF4* promoter a) *SRSF4* mRNA expressions in MYCN amplified CHP-134 cells versus non-MYCN amplified GI-ME-N cells, b) E2F1 enrichment around E2F1 binding motif at *SRSF4* gene in CHP-134 and GI-ME-N cells, c) *SRSF4* overexpression in MYCN inducible SHEP21N cell line, d) MYCN enrichment around MYCN binding motif in *SRSF4* gene at CHP-134 and GI-ME-N cells. Experiments were run in n=3 biological and technical replicates. Mean values were presented. *** $p<0.001$, **** $p<0.0001$.

4.5. Chapter conclusions

To understand the mechanism of action that drives sensitivity to PRMT5 inhibition in higher E2F1/MYCN expressing cell lines versus the lower E2F1/MYCN expressing cell lines, we performed a transcriptome wide analysis of the most sensitive neuroblastoma cell line CHP-134 and the least sensitive cell line GI-ME-N by RNA sequencing. We found that T1-44 treatment induced higher number of differentially expressed and spliced events in the high E2F1/MYCN expressing cell line when compared with the low E2F1/MYCN expressing cell line (Figure 4.8).

When we assessed the differentially expressed gene sets that were present in RNA sequencing, we found that several shared genes enriched were linked with the splicing factors and these splicing factors were also E2F1 targets. Expression levels of splicing factors such *SRSF1, SRSF3,* and *SRSF4* were higher in E2F1-high/MYCN-amplified cell line CHP-134 than E2F1-low/ non MYCN- amplified cell line GI-ME-N. The recruitment of both E2F1 and MYCN to splicing factor gene promoters suggesting that, higher E2F1 and MYCN expressing cells might be more vulnerable to splicing modulations.

Chapter 5. E2F1 knockout reduced the number of genome wide splicing events in CHP-134 cells

5.1. Introduction

Although CHP-134 versus GI-ME-N cell line comparison enabled us to investigate E2F1's role in neuroblastoma cells (CHP-134 has high levels of E2F1, whereas GI-M-EN has low levels of E2F1), we had some concerns about the impact of cell lineage specific effects. At first, we used siRNA to decrease E2F1 activity, but E2F1 mRNA expression levels varied significantly among the different biological replicates. Therefore, we needed a robust E2F1 knockout model in order to understand its function in terms of sensitivity to PRMT5 inhibition. To do so, we generated an E2F1 knockout CHP-134 cell line by using CRISPR/Cas9. Once CHP-134 E2F1 knockout cell lines had been validated, they were ready to be used as a tool to further study the impact of E2F1 in sensitivity to PRMT5 inhibition.

RNA sequencing is a powerful tool that enables a genome-wide analysis of up- or downregulated genes under different conditions. The information can be used in identifying not only potential new target genes of E2F1 but also identifying how genome-wide splicing pattern changes in the absence of E2F1. It may also identify new pathways, which can be impacted by the control of E2F1. As previous work in our lab had looked at known E2F1 target genes that are involved in transcription regulation, we decided to expand this work to identify potential new E2F1 target genes and functions of E2F1 in splicing. We considered that this information could also be used in identifying the PRMT5-E2F1 axis role in neuroblastoma as well.

5.2. Generation of stable E2F1 knockout cell lines by CRISPR/Cas9

sgRNA that targets E2F1 was designed and cloned into the Cas9-puro vector before transfection into CHP-134 cells. Cas9-puro containing no sgRNA inserts were used to obtain the wild-type E2F1$^{+/+}$ control cell lines (*WT)* and a monoclonal line was established from these in parallel with the KO cells. Once the clones reached confluency, genomic DNA was isolated from the cells and sequenced across the predicted cut site in the E2F1 gene. Sanger sequencing results were aligned by BLASTN program, and it was confirmed that the Cas9 site that contains NGG motif resulted in frameshift mutation (Figure 5.1, Figure 5.2). It is known that indel mutations induced by Cas9 are varied and the Sanger sequencing of PCR products from a single mutant genome generates double peaks that begin at the indel sites. We aligned the Sanger sequencing results of the E2F1 KO clones by using CRISP-ID software (Dehairs et al., 2016). The indel sites were beginning from the sgRNA binding sites as expected (Figure 5.3).

Homo sapiens E2F transcription factor 1 (E2F1), RefSeqGene on chromosome 20

Sequence ID: NG_046988.1 **Length:** 17919 **Number of Matches:** 1

Range 1: 10975 to 11094 GenBank Graphics ▼ Next Match ▲ Previous M

Score	Expect	Identities	Gaps	Strand
222 bits(120)	4e-54	120/120(100%)	0/120(0%)	Plus/Minus

```
Query  1      AAGCTCCATAGGTACCTTTTCCTGGATGGCGGCCTCTGCCCCGAGCTGGCCCACTGCTCT  60
              ||||||||||||||||||||||||||||||||||||||||||||||||||||||||||||
Sbjct  11094  AAGCTCCATAGGTACCTTTTCCTGGATGGCGGCCTCTGCCCCGAGCTGGCCCACTGCTCT  11035

Query  61     CGGCCAGGTACTGATGGTCAGTTTCCAGGTCCAGCCTCCGCTTCACCTGTGGCGAAAACG  120
              ||||||||||||||||||||||||||||||||||||||||||||||||||||||||||||
Sbjct  11034  CGGCCAGGTACTGATGGTCAGTTTCCAGGTCCAGCCTCCGCTTCACCTGTGGCGAAAACG  10975
```

Figure 5.1. Sequence alignment of the CHP-134 wild type cells.

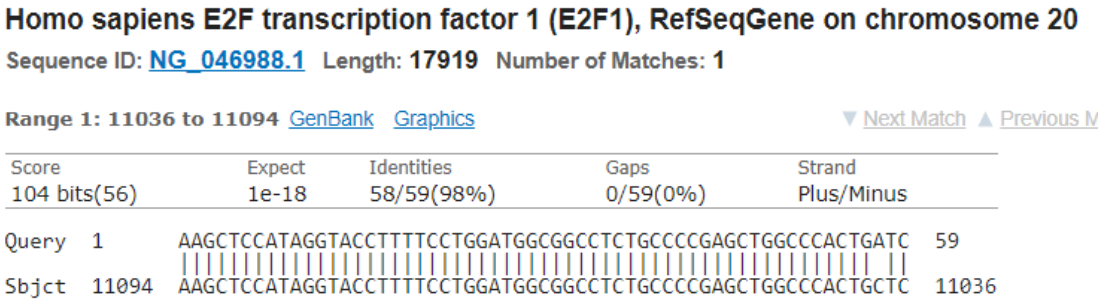

Figure 5.2. Sequence alignment of the CRISPR-Cas9 targeted region after E2F1 knockout in CHP-134 cells. Second sequence led to changes in the E2F1 reference sequence. There was no alignment after 57th nucleotide.

Figure 5.3. Validation of CHP-134 E2F1 knockout cells by Sanger sequencing. CRISPR-Cas9 generated nucleotide deletions and insertions at guide sequence binding sites. CRISP-ID detects CRISPR mediated indels by Sanger sequencing. Sanger sequencing files were uploaded to the CRISP-ID website that allows the detection of the exact indel size and location of a CRISPR-Cas9 targeted region based on direct Sanger sequencing. Yellow arrow indicates indel position in the EF21 KO CHP-134 cells then guide sequence binding sites starts with the region CCAGGTACTGAT where the cut site is expected in the sequence.

5.3. Characterization of E2F1 CRISPR/Cas9 knockout CHP-134 cell line

After completing a series of colony screening experiments by Sanger sequencing, N1 and N2 named clones were picked for further downstream experiments as their Sanger sequencing results were confirming their knockout E2F1 status. Complete KO of E2F1 at the protein level in both clones N1 and N2 were also assessed by immunoblot (Figure 5.4), then we checked the protein expression levels of E2F1, PRMT5, TSN, MYCN, and SDMA after E2F1 KO in CHP-134 cells by western blot in order to see if E2F1 KO had any impact of our genes of interest (Figure 5.4).

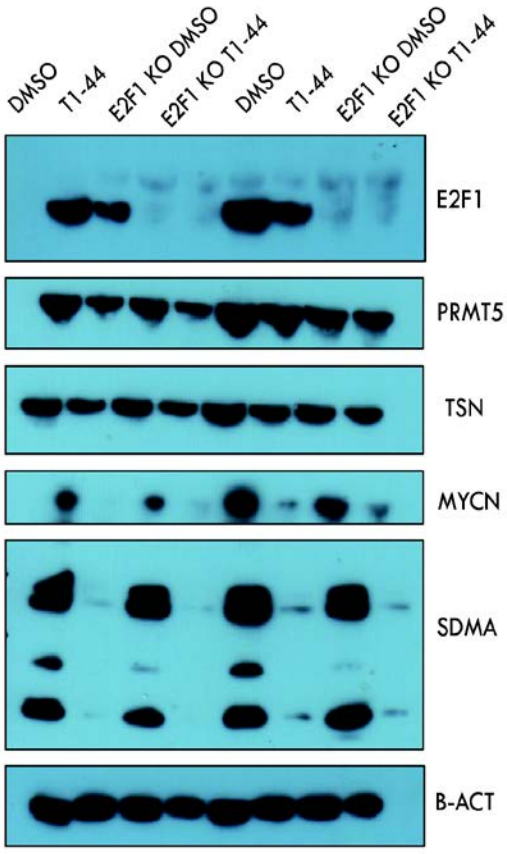

Figure 5.4. Protein expression levels of E2F1, PRMT5, TSN, MYCN, and SDMA after E2F1 KO in CHP-134 cells. β-actin was used as a loading control. Different E2F1 KO clones (first 4 lanes: N1 and the last 4 lanes: N2) were run on the same gel, no significant difference was found in terms of E2F1, PRMT5, TSN, MYCN, and SDMA protein expression levels. As SDMA is a motif antibody, we also showed the range of expression in western blot.

We did not observe significant differences between N1 and N2 E2F1 KO clones in western blots, therefore we further proceeded downstream experiments with the representative E2F1 knockout clone named as N2 (Figure 5.4).

As expected, the mRNA expression level of *E2F1* was significantly lower in knockout cells when compared to the wild-type cells. The canonical E2F1 target gene such as *CDC6* was also quantified at the mRNA expression level to further confirm E2F1 deficiency. Lower expression levels of *CDC6* were observed in the E2F1 KO cell line compared to the wild-type CHP-134 cells (Figure 5.5).

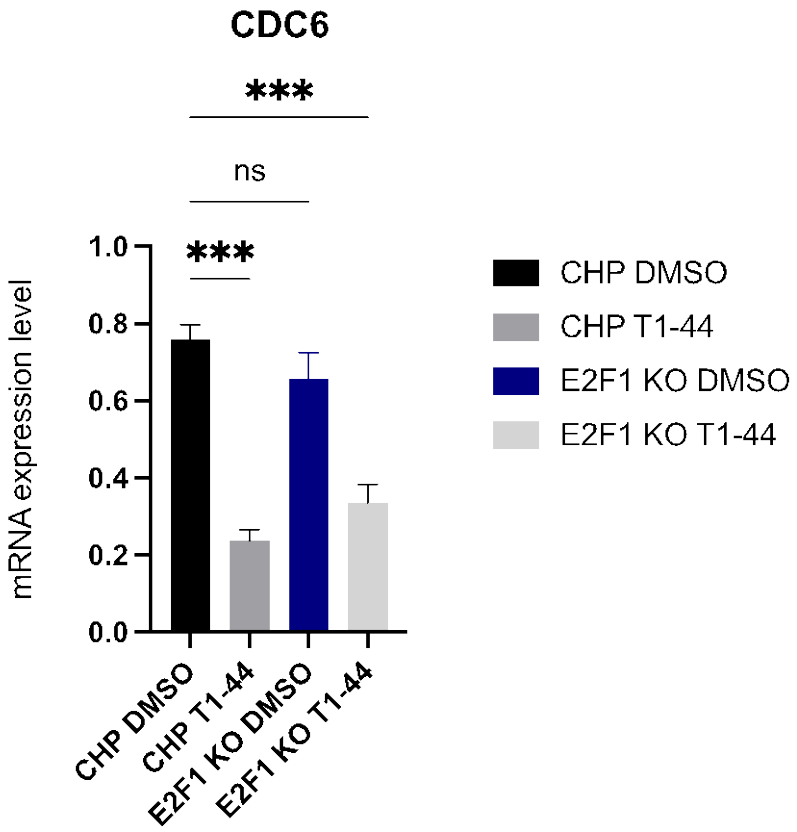

Figure 5.5. *CDC6* mRNA expression levels after E2F1 KO in CHP-134 cells. T1-44 treatment concentration was 200 nM and for 72 hours. Results shown are average of three independent experiments with standard error of mean, analysed by one-way ANOVA. ns: $p>0.05$, *** $p<0.001$.

We also checked our targets *E2F1*, *MYCN*, *PRMT5*, and *TSN* mRNA expression levels by qRT-PCR in the absence of E2F1 in order to observe if there are any significant differences in gene expression. There were no significant gene expression changes in *MYCN*, *PRMT5*, and *TSN* mRNA expression levels (Figure 5.6).

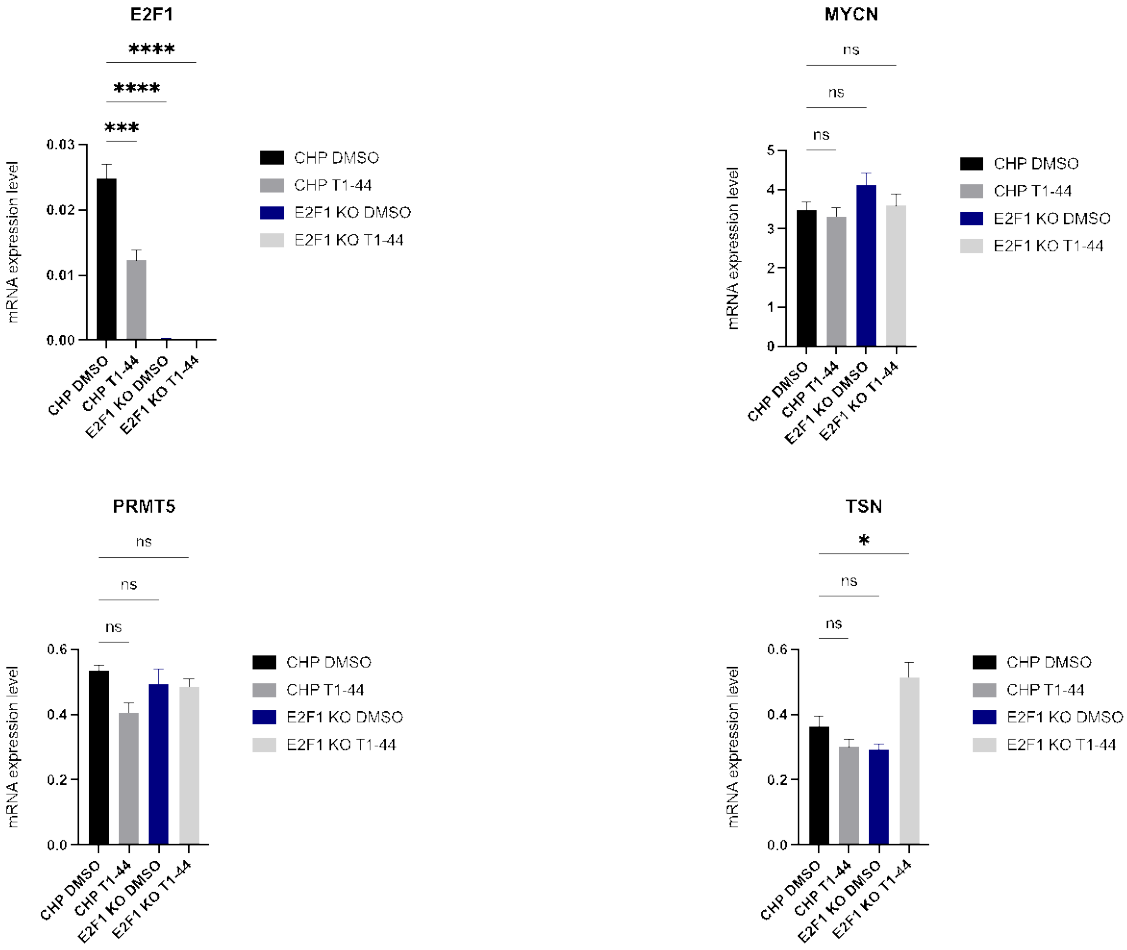

Figure 5.6. *E2F1*, *MYCN*, *PRMT5*, and *TSN* mRNA expression levels after E2F1 KO in CHP-134 cells. Results shown are average of three independent experiments with standard error of mean, analysed by one-way ANOVA. ns: $p>0.05$, * $p<0.05$, *** $p<0.001$, **** $p<0.0001$.

Relative cell viability of CHP-134 wild-type and E2F1 KO CHP-134 cells treated with T1-44 was calculated and the values were normalized to DMSO control in an MTT assay. Samples were prepared in four replicates, averages were calculated, and error bars were represented. We found that CHP-134 wild-type cells had lower IC_{50} (5.1 nM) value than E2F1 knockout counterparts IC_{50} (38 nM) showing that E2F1 knockout cells were more resistant to the PRMT5 inhibition (Figure 5.7).

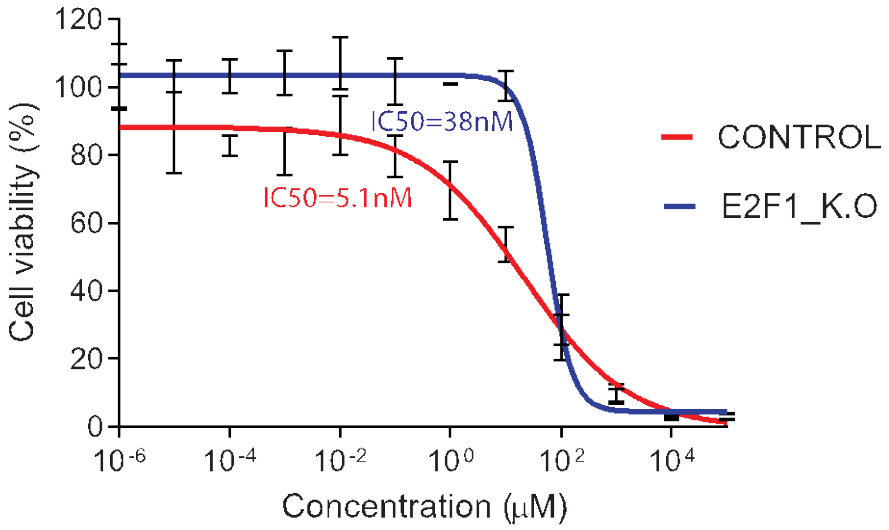

Figure 5.7. Cell viability analysis of PRMT5 inhibition on CHP-134 E2F1 KO cells over wild-type in vitro after 6 days treatment of T1-44 in different concentrations. Data are presented as mean ± SD. Error bars indicate the SD of three independent experiments (Data was kindly provided by Dr.Laurel Bate Eya).

We analysed cell cycle profiles of the wild-type and E2F1 KO CHP-134 cell lines by flow cytometry to identify whether there were any changes in their cell cycle profiles. There were differences in subG1 cycle between wild-type and the E2F1 KO cells. However, these differences were not significant (Figure 5.8).

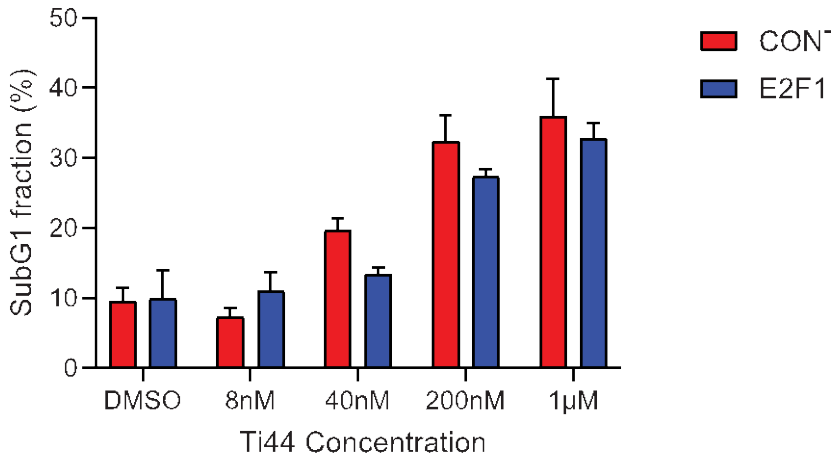

Figure 5.8. Cell-cycle analysis of CHP-134 wild-type (Red) and E2F1 knockout cells (Blue) upon 8 nm-1 μM T1-44 treatment after 6 days (Data was kindly provided by Dr.Laurel Bate Eya).

5.4. RNA sequencing after E2F1 KO in CHP-134 cells

To further understand the underlying mechanism for E2F1's contribution to the sensitivity of PRMT5 inhibition in MYCN amplified CHP-134 cells, we performed RNA sequencing analysis of isogenic E2F1 knockout cells and their wild-type counterparts. We treated CHP-134 wild-type and E2F1 KO cells with 200 nM T1-44 and DMSO for 72 hours in order to make a robust comparison with our first RNA-seq data.

5.4.1. Validation and characterization of differentially expressed genes in CHP-134 WT and E2F1 KO cells

Once we received the RNA sequencing results, we validated genes that were differentially expressed upon PRMT5 inhibition. Various selection criteria were used while selecting the genes for further qPCR validation. These criteria include, log2 fold expression difference (>1), targets that have higher base mean in the RNA-seq data, and targets that are solely dependent to the absence of E2F1 as we were interested in to see E2F1's role in the sensitivity of PRMT5 inhibition.

The list of validated DEGs (differentially expressed genes) and their log2 (fold changes) in RNA sequencing experiment are given below in Table 5.1. Top 100 differentially expressed gene lists were provided at Appendix B, Table 3. *PLK2*, *CDKN1A*, and *PHLDA3* were upregulated after T1-44 treatment. E2F1 KO affected their mRNA expression levels consistently with our RNA-seq data (Figure 5.9-Figure 5.11).

Table 5.1. List of validated genes from the RNA-seq data.

Gene	Function	Differential expression in RNA-seq analysis
PLK2	Tumour suppressor involved in synaptic plasticity, centriole duplication, and G1/S phase transition	Increased in T1-44 treatment compared to DMSO
CDKN1A	Inhibits CDK activity and blocks cell cycle progression	Increased in T1-44 treatment compared to DMSO
PHLDA3	Involved in intrinsic apoptotic signalling pathway in response to DNA damage	Increased in T1-44 treatment compared to DMSO

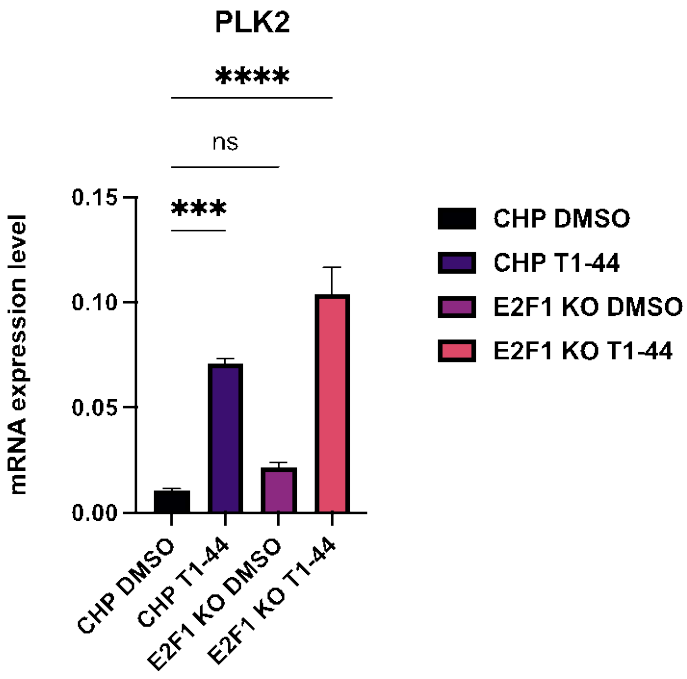

Figure 5.9. *PLK2* mRNA expression level changes upon 200 nM T1-44 treatment after 72 hours. Results shown are average of three independent experiments with standard error of mean, analysed by one-way ANOVA. ns: $p>0.05$, *** $p<0.001$, **** $p<0.0001$.

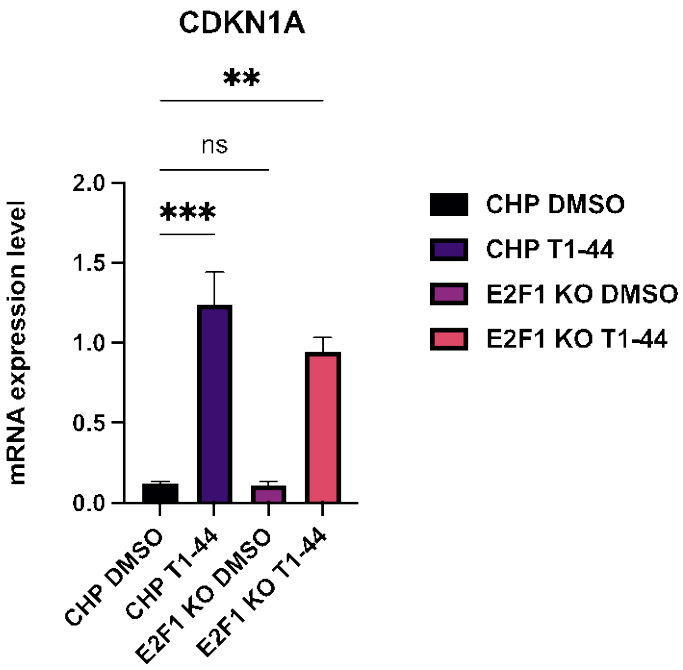

Figure 5.10. *CDKN1A* mRNA expression level changes upon 200 nM T1-44 treatment after 72 hours. Results shown are average of three independent experiments with standard error of mean, analysed by one-way ANOVA. ns: $p>0.05$, ** $p<0.01$, *** $p<0.001$.

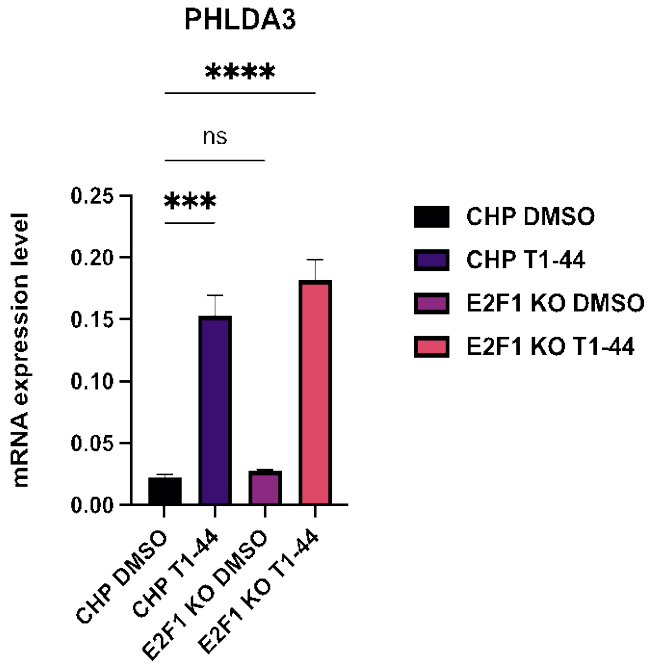

Figure 5.11. *PHLDA3* mRNA expression level changes upon 200 nM T1-44 treatment after 72 hours. Results shown are average of three independent experiments with standard error of mean, analysed by one-way ANOVA. ns: $p>0.05$, *** $p<0.001$, **** $p<0.0001$.

GO maps were generated for gene ontology analysis to identify the enriched pathways upon T1-44 treatment in both CHP-134 wild-type and KO cell lines (Figure 5.12, Figure 5.13). We used Metascape GSEA tool to identify biological pathways that were impacted in the different conditions. GSEA uses gene ontology terms to categorize gene function based on the number of significantly altered genes. Figure 5.13 shows those pathways that are significantly (FDR adjusted $q<0.05$) enriched in CHP-134 wild-type cells upon 200 nM T1-44 treatment.

RNA metabolism, Rho GTPase signalling, nervous system development, VEGFA signalling, transcriptional regulation by p53, cellular response to stress, cell cycle, membrane trafficking, RTK signalling, lipid metabolism, and DNA repair pathways were amongst the most differentially regulated pathways in CHP-134 wild-type cells upon 200 nM T1-44 treatment for 72 hours (Figure 5.12).

In parallel with CHP-134 wild-type cells, RNA metabolism, cell cycle, Rho GTPase signalling, transcriptional regulation by p53, lipid metabolism, regulation of cellular localization, histone modification, mitotic cell cycle process, hemostasis, and protein phosphorylation were amongst the most differentially regulated pathways in CHP-134 E2F1 KO cells upon 200 nM T1-44 treatment for 72 hours (Figure 5.13).

Consistent with the role of E2F1 in post-translational modifications, histone modification and protein phosphorylation gene ontologies were the different gene ontology categories at differentially expressed gene level in wild-type versus E2F1 KO CHP-134 cells (Figure 5.12, Figure 5.13).

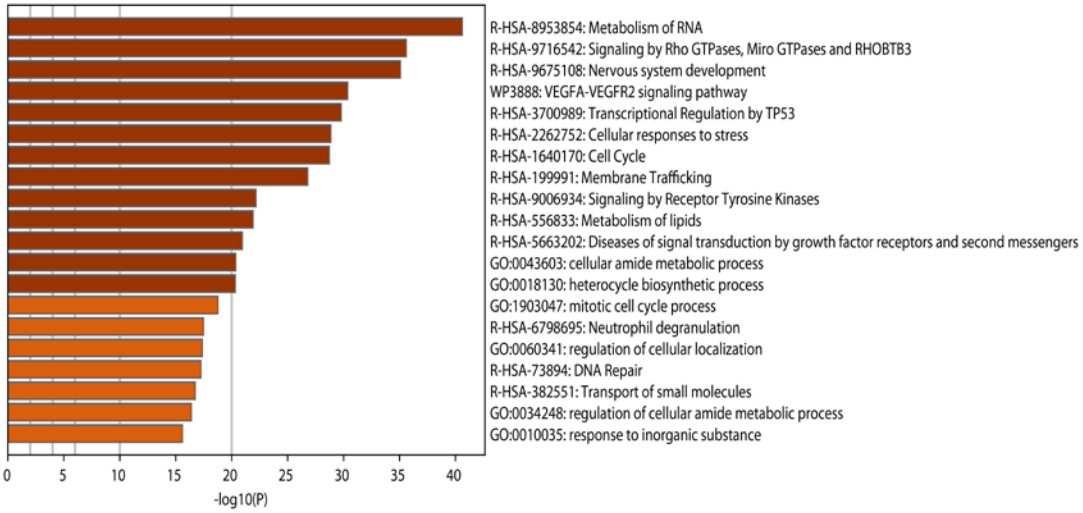

Figure 5.12. Gene ontology analysis for the differentially expressed genes in MYCN amplified CHP-134 cell line that was treated with 200 nM T1-44 for 72 hours (gene expression fold change cut-off >2 with an adjusted p-value ≤0.01). The analysis was performed by using Metascape.

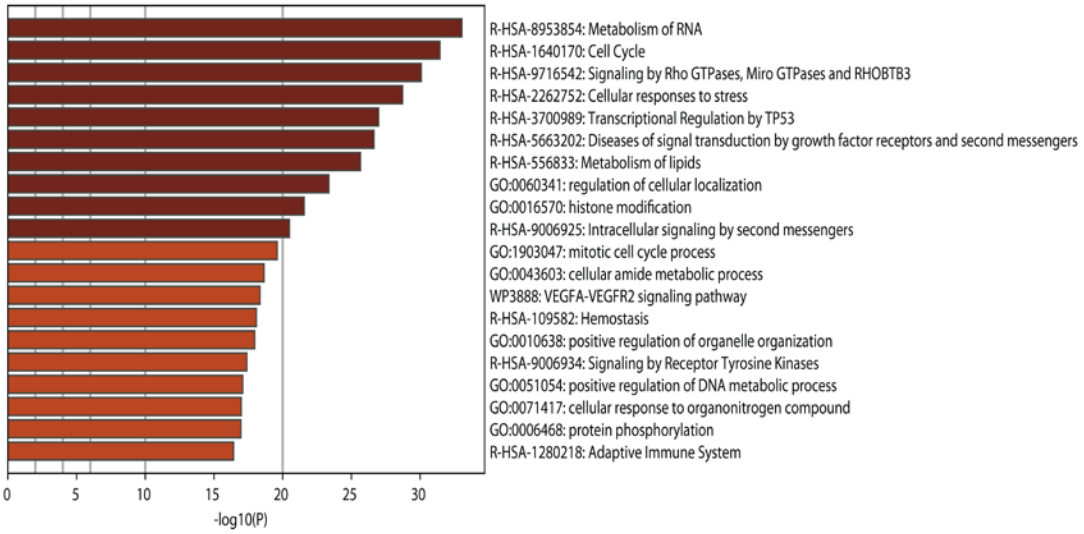

Figure 5.13. Gene ontology analysis for the differentially expressed genes in MYCN amplified CHP-134 E2F1 knockout cell line that was treated with 200 nM T1-44 for 72 hours (gene expression fold change cut-off >2 with an adjusted p-value ≤0.01). The analysis was performed by using Metascape.

5.4.2. E2F1 dependent differentially expressed genes in CHP-134 cells

Heat-map clusters helped us to identify the E2F1 unique differentially expressed genes that could provide hints for identifying non-canonical E2F1 targets. We found that the heat-map clusters of CHP-134 wild-type versus E2F1 KO upon 200 nM T1-44 treatment for 72 hours (padj<0.01) were highly consistent across three biological replicates (Figure 5.14). Two separate heat-map clusters named as Cluster 1 and Cluster 2 (Figure 5.14) were linked with the absence of E2F1, without PRMT5 inhibitor effect in CHP-134 cells. As we were interested in E2F1's role in this sensitive cell line model, we delved deeper into this heat-map clusters to validate and understand their roles in the sensitivity to the drug treatment (Figure 5.15, Figure 5.16).

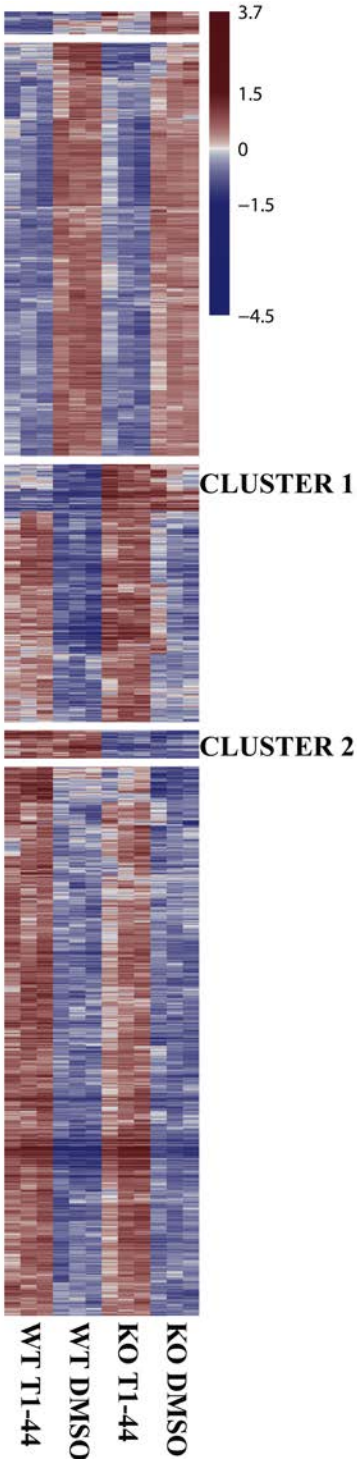

Figure 5.14. Heat-map clusters of differentially expressed genes in CHP-134 wild-type versus E2F1 KO upon 200 nM T1-44 treatment for 72 hours across 3 biological replicates. A heat-map corresponding to statistically significant differentially expressed genes. Blue colour represents the lowest difference and red colour represents the highest (padj<0.01). Two unique sets of genes that are regulated via E2F1 were named as Cluster 1 and Cluster 2. Cluster 1 genes were upregulated, whereas Cluster 2 genes were downregulated in the absence of E2F1.

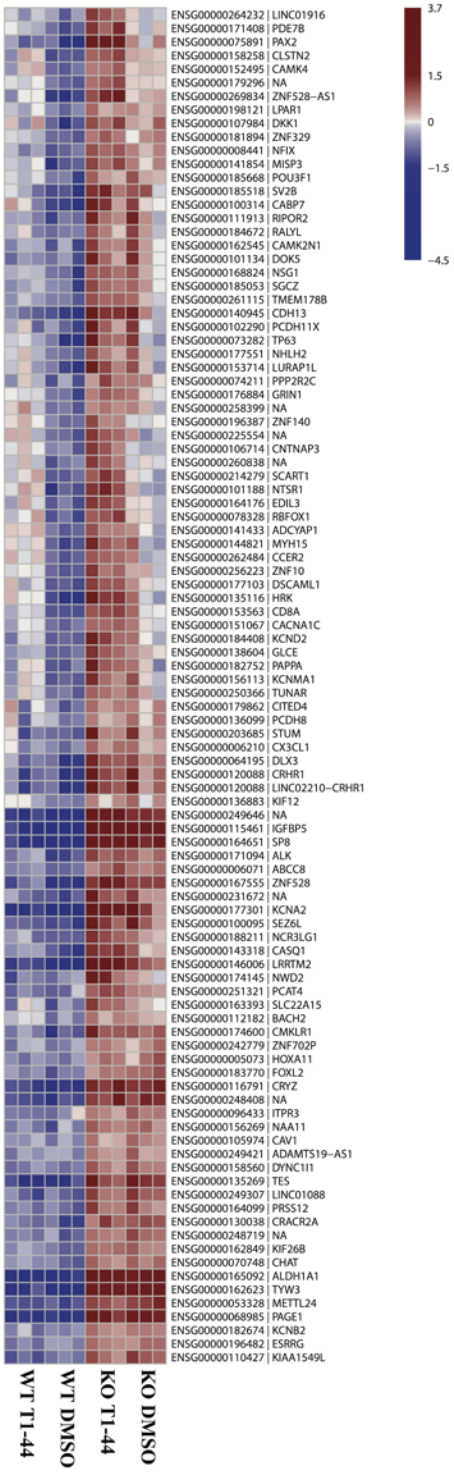

Figure 5.15. Cluster 1 genes heat-map illustrating the differentially expressed genes that were unique to E2F1 in CHP-134 wild-type versus E2F1 KO upon 200 nM T1-44 treatment for 72 hours across 3 biological replicates. A heat-map corresponding to statistically significant differentially expressed genes. Blue colour represents the lowest difference and red colour represents the highest (padj<0.01). Among this cluster *PAGE1*, *IGFBP5*, and *CRYZ* were further validated by qPCR. These set of genes were upregulated in the absence of E2F1 suggesting E2F1's role in repressing these genes.

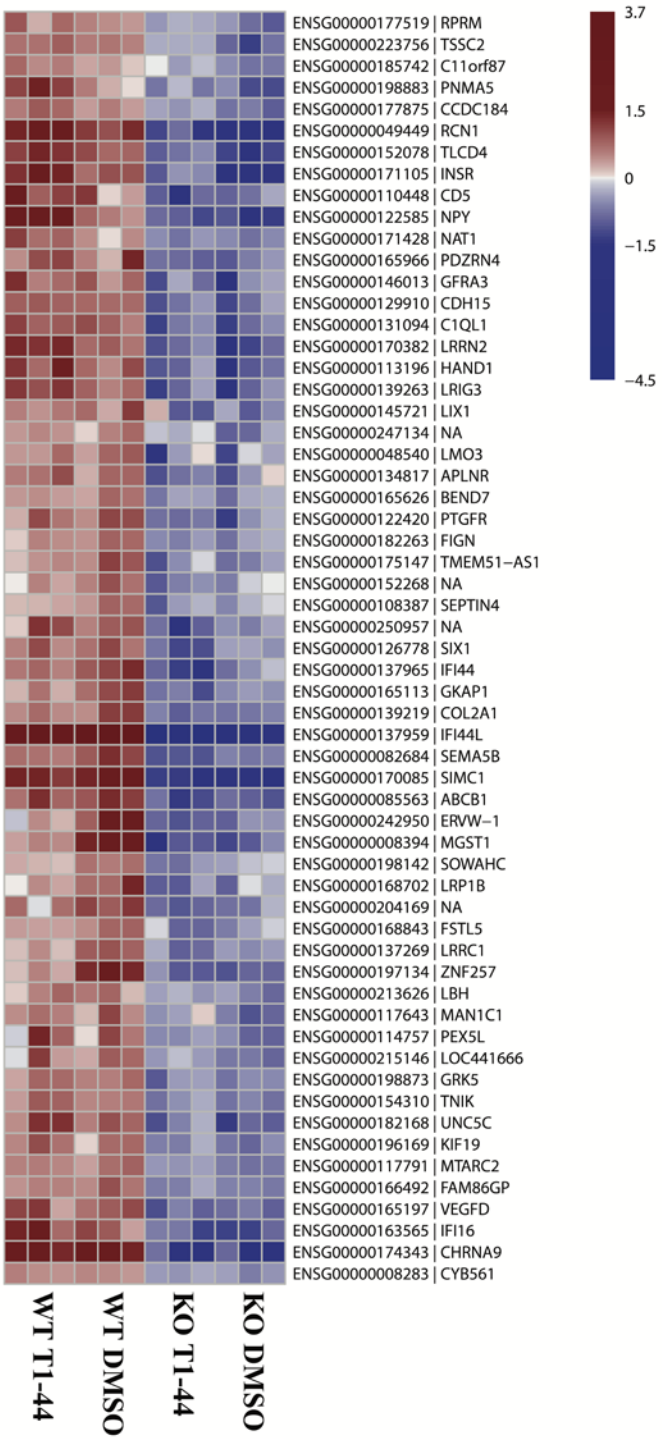

Figure 5.16. Cluster 2 genes heat-map illustrating the differentially expressed genes that were unique to E2F1 in CHP-134 wild-type versus E2F1 KO upon 200 nM T1-44 treatment for 72 hours across 3 biological replicates. A heat-map corresponding to statistically significant differentially expressed genes. Blue colour represents the lowest difference and red colour represents the highest (padj<0.01). Among this cluster *C1QL1* was further validated by qPCR. These set of genes were downregulated in the absence of E2F1 suggesting E2F1's role in activating these genes.

We validated some of the genes that belong to the cluster 1 and cluster 2 from the differentially expressed genes by qPCR. We picked the genes that have significant differential gene expression, log2 fold changes greater than 2, and consistent across three biological replicates. These genes were: *PAGE1*, *IGFBP5*, *CRYZ*, and *C1QL1* (Table 5.2).

Table 5.2. List of E2F1 specific differentially expressed genes and their functions.

Gene	Function
PAGE1	Not identified
IGFBP5	Cellular response to cAMP, regulation of smooth muscle cell migration, and regulation of smooth muscle cell proliferation
CRYZ	Enhances the stability of mRNA coding for BCL2
C1QL1	Predicted to enable signalling receptor binding activity. Predicted to act upstream of or within maintenance of synapse structure, motor learning, and neuron remodelling

We validated the RNA sequencing results of those four genes (*PAGE1*, *IGFBP5*, *CRYZ*, and *C1QL1*) successfully by qPCR. Our results suggest that these genes are regulated in the absence of E2F1 as their expression levels were depending on the presence or absence of E2F1 in E2F1 KO cells and E2F1 KO T1-44 treated cells (Table 5.3) (Figure 5.17). *PAGE1* and *CRYZ* were not previously identified as canonical E2F1 target genes in the literature. More functional experiments are required for further validation of these genes, as existing literature remains very limited in terms of their biological functions.

Table 5.3. List of qPCR validated differentially expressed genes and their log2 (fold changes) after E2F1 KO in RNA sequencing in CHP-134 cells.

Gene	RNA-Seq *Log2 (fold change)
PAGE1	3.898180472
IGFBP5	4.867813948
CRYZ	5.375079461
C1QL1	-1.644767114

*E2F1 KO DMSO treatment versus wild-type DMSO treatment. Genes were considered differentially expressed if the adjusted p-value, calculated using the Benjamini-Hochberg method to minimize the false discovery rate, was less than 0.01. We further filtered significantly differentially expressed gene sets using 2-fold change in absolute expression level.

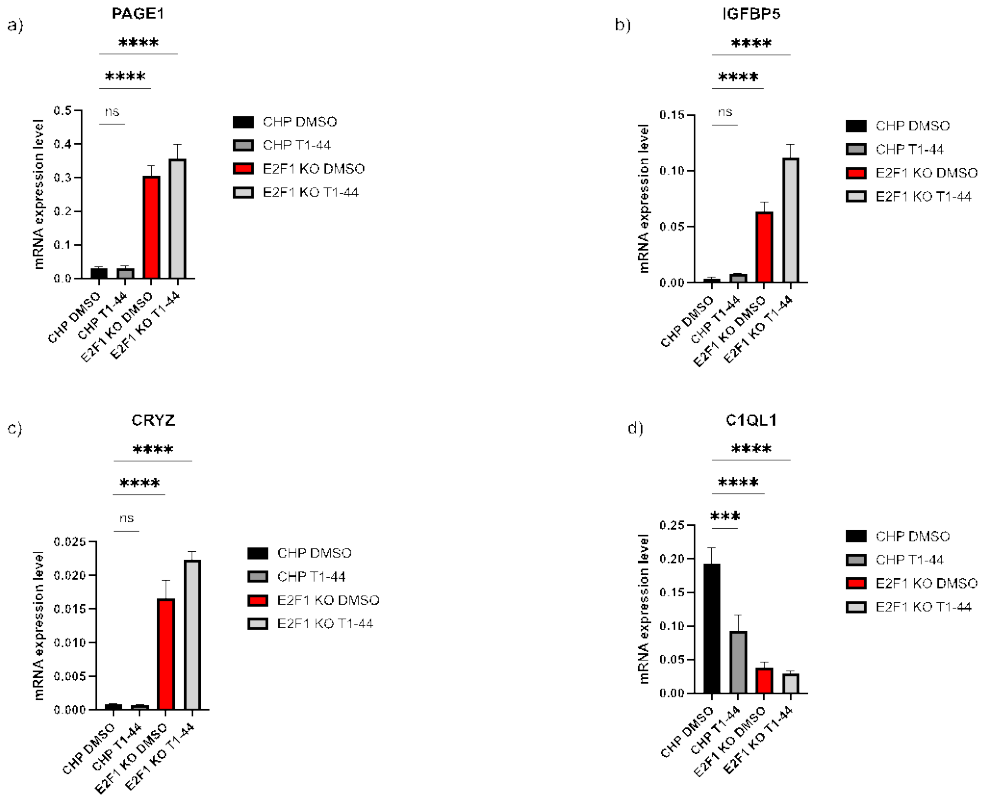

Figure 5.17. *PAGE1* (a), *IGFBP5* (b), *CRYZ* (c), and *C1QL1* (d) mRNA expression levels in CHP-134 wild-type and E2F1 KO cells. Experiments were run in n=3 biological and technical replicates. Mean values were presented. Results shown are average of three independent experiments with standard error of mean, analysed by one-way ANOVA. ns: p>0.05, *** p<0.001, **** p<0.0001.

5.4.3. The genome wide splicing events decrease in the absence of E2F1 in CHP-134 cells

We next conducted splicing analysis of the isogenic wild-type and E2F1 knockout CHP-134 neuroblastoma cells that were treated with T1-44. Wild-type and E2F1 knockout cells had a distinct transcriptome, characterized by unique changes in RNA splicing. When differentially spliced events in T1-44 treated cells were compared to the wild-type control, there were clear differences between splicing events of CHP-134 E2F1 KO cells versus wild-type cells as it was presented as Venn diagram and Canberra heat-map (Figure 5.18, Figure 5.19). 142 splicing events from the alternative splicing analysis were above significance threshold for differential expression ($p<0.01$) in E2F1 knockout versus wild-type CHP-134 cell line. The number of significantly differentially spliced events were 3196 in wild-type T1-44 treated cells, whereas that number decreased into 2523 in E2F1 KO T1-44 treated cells for the same dose of the drug treatment (Figure 5.18).

A heat-map displaying the statistically significant alternative splicing event changes in DMSO and T1-44 treated wild-type and E2F1 KO CHP-134 cell lines was derived by analysing the RNA-seq data with rMATS algorithm were represented at Figure 5.19 (FDR >0.01).

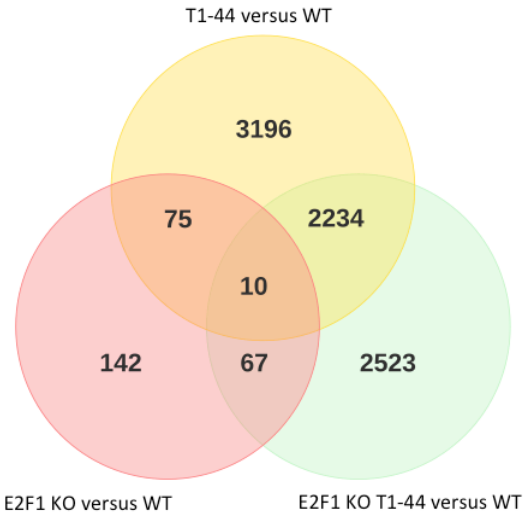

Figure 5.18. Venn diagram of differentially spliced events in wild-type and E2F1 KO CHP-134 cells upon treatment with 200 nM treatment with T1-44 for 72 hours (FDR >0.01). Venn diagrams representing the differential expression analysis as being up- or down-regulated (regulated greater than two-fold) and those identified as being differentially or alternatively spliced. This data was generated from three biological replicates. The number of differentially spliced events decreased from 3196 to 2523 after the same T1-44 treatment in the absence of E2F1. Considering the E2F1 KO effect alone, only 142 splicing events were affected depending on E2F1 presence. 2234 splicing events were shared both in CHP-134 WT and E2F1 KO cells upon T1-44 treatment.

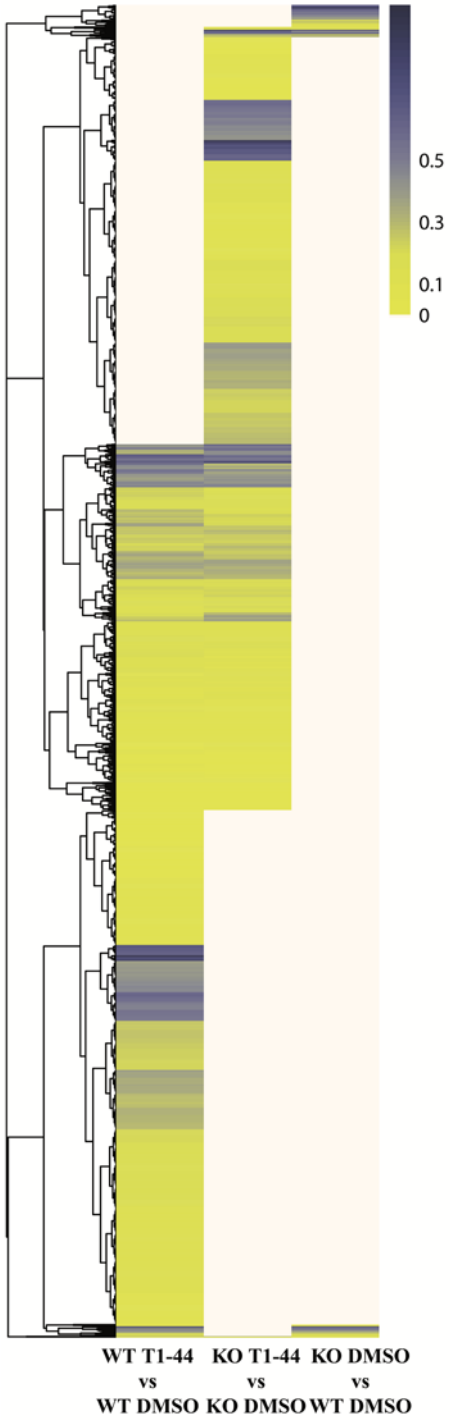

Figure 5.19. Canberra heat-map of differential splicing in wild-type and E2F1 KO CHP-134 cells upon treatment with 200 nM treatment with T1-44 for 72 hours. A heat-map representing absolute values of ΔΨ (percent spliced in) for cell lines, corresponding to statistically significant alternative splicing event changes with respect to the DMSO and T1-44 treated wild-type and E2F1 KO CHP-134 cell lines derived by analysing the RNA-seq data with rMATS algorithm. Yellow colour represents the lowest difference and blue colour represents the highest (FDR >0.01).

We found that E2F1 KO CHP-134 cells had lower number of differentially spliced genes when compared to wild-type counterparts upon T1-44 treatment, pointing out E2F1's role in the regulation of genome-wide global splicing effects (Figure 5.20). However, when we compare E2F1 knockout effect with T1-44 treatment, T1-44 treatment led more splicing events when compared with E2F1 knockout alone.

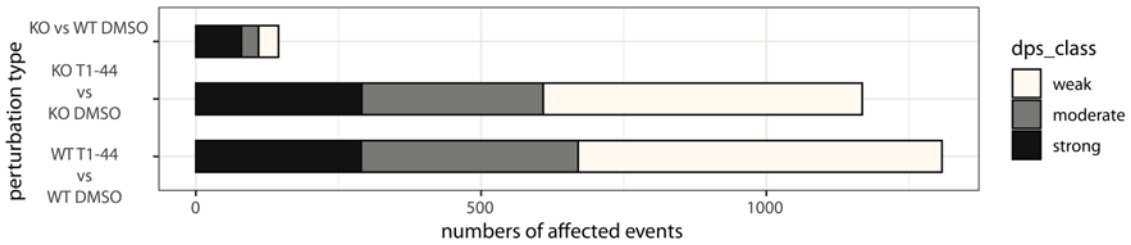

Figure 5.20. Splicing events dpsi score percentages after treatments. Bar chart displaying the statistically significant alternative splicing perturbation types in wild-type and E2F1 KO CHP-134 cells upon treatment with 200 nM T1-44 for 72 hours. Delta psi scores were used as following: delta psi <0.1 insignificant; 0.1-0.3 low weak; 0.3-0.5 moderate; >0.5 strong (FDR > 0.01).

We then performed gene ontology (GO) analyses for the differentially expressed spliced genes, GO enrichment analysis were run using all selected genes and up- and down-regulated differentially spliced genes (Figure 5.21). GO terms enriched in genes uniquely upregulated in wild-type T1-44 treatment compared to wild-type DMSO were regulation of establishment of cell polarization, positive regulation of vacuole organization, positive regulation of axon extension, positive regulation of Arp2/3 complex, negative regulation of insulin secretion, mitotic spindle midzone assembly, mitotic G2 DNA damage signalling checkpoint, mitotic chromosome condensation, mitotic chromosome segregation, IRES-dependent viral translational initiation, interstrand cross link repair, glycine biosynthetic process, folic acid metabolic process,

establishment of RNA localization, CTP biosynthetic process, chromosome segregation, and centrosome duplication (Figure 5.21).

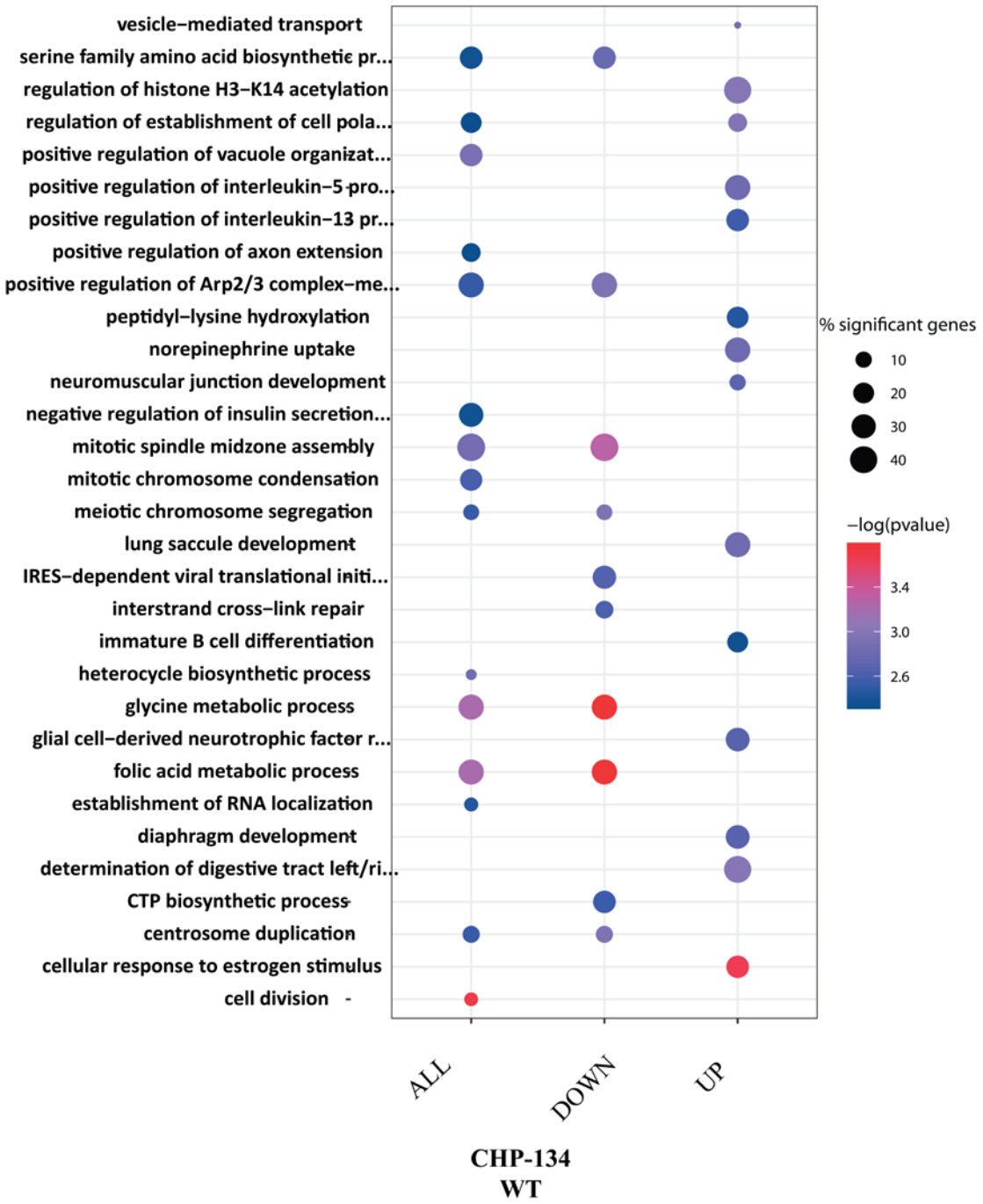

Figure 5.21. GO categories of differentially spliced genes in wild-type CHP-134 cells upon 200 nM T1-44 treatment for 72 hours.

However, E2F1 KO led to a decrease in the intensity of differentially spliced genes upon the same dose of T1-44 treatment (200 nM) suggesting a genome-wide role for E2F1 in these pathways. GO terms enriched in genes uniquely upregulated in E2F1 KO T1-44 treatment compared to E2F1 KO DMSO were t-circle formation, negative regulation of microtubule polymerization, mitotic cell cycle, DNA repair, DNA-duplex unwinding, DNA damage checkpoint signalling, chromatin organization cell division, and astral microtubule organization (Figure 5.22).

These gene set enrichment analysis reveals that E2F1 is involved in the splicing regulation of establishment of cell polarization, positive regulation of vacuole organization, positive regulation of axon extension, positive regulation of Arp2/3 complex, negative regulation of insulin secretion, mitotic spindle midzone assembly, mitotic G2 DNA damage signalling checkpoint, mitotic chromosome condensation, mitotic chromosome segregation, IRES-dependent viral translational initiation, interstrand cross link repair, glycine biosynthetic process, folic acid metabolic process, establishment of RNA localization, CTP biosynthetic process, chromosome segregation, and centrosome duplication pathways in general. Overall, RNA sequencing results revealed that E2F1 deficiency decreased the splicing events in these pathways significantly, which indicates E2F1's role in splicing regulation.

In GO analysis, histone H3-K27 tri-methylation relevant genes were uniquely spliced and down-regulated in E2F1 KO CHP-134 cells treated with T1-44 versus DMSO comparison (Figure 5.22). However, negative regulation of microtubule polymerization category was uniquely up-regulated in E2F1 KO T1-44 treated cells versus E2F1 KO DMSO comparison (Figure 5.22).

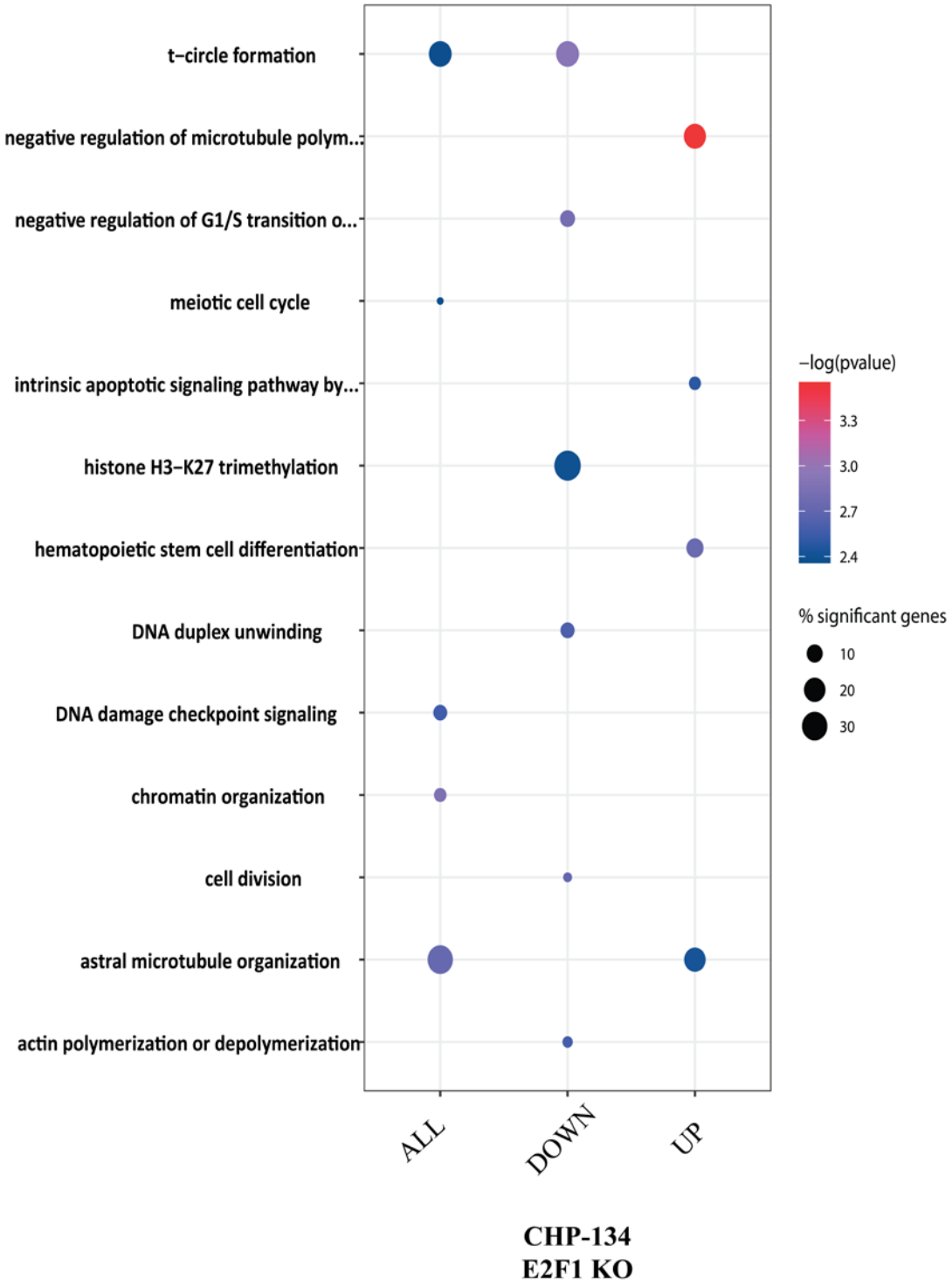

Figure 5.22. GO categories of differentially spliced genes in E2F1 KO CHP-134 cells upon 200 nM T1-44 treatment for 72 hours.

It is noteworthy that CHP-134 E2F KO cell line influenced the intensity of splicing upon the same concentration of T1-44 treatment. Comparison of GO categories after E2F1 knockout identified that the cells were not responding the PRMT5 inhibition at the same level which might conclude E2F1's role in the genome wide regulation of splicing.

5.5. Chapter conclusions

Although CHP-134 - GI-ME-N cell line comparison enabled us to work on E2F1's role in sensitivity to PRMT5 inhibition (CHP-134 has higher levels of E2F1, whereas GI-ME-N has lower levels of E2F1), we knocked out E2F1 in CHP-134 cells in order to rule out the lineage specific effects. To further understand the mechanistic insights into E2F1-PRMT5 axis that leads to sensitivity to PRMT5 inhibition in MYCN amplified neuroblastoma cells, we performed RNA sequencing analysis of isogenic CHP-134 E2F1 knockout cells and its wild-type counterpart after treatment with DMSO and 200 nM of T1-44 in order to make a robust comparison with our first RNA-seq data.

Gene ontology analysis revealed that histone modification and protein phosphorylation pathways were significantly enriched in the absence of E2F1 as differentially expressed gene level. This finding suggests E2F1's role in posttranslational modification processes (Figure 5.12, Figure 5.13).

Heat-map analysis showed cluster of genes that are positively or negatively regulated depending on E2F1 (Cluster 1 and 2 genes) and by investigating these gene clusters, we identified some potential non-canonical E2F1 target genes like *PAGE1* and *CRYZ* (Figure 5.14-Figure 5.17).

Then, we checked differential splicing events in CHP-134 wild-type and E2F1 knockout cells treated with T1-44. E2F1 knockout and wild-type cells had a distinct transcriptome characterized by unique changes in RNA splicing. Consistent with our first RNA-seq data for CHP-134 and GI-ME-N comparison, the second RNA-seq data revealed an increase in the number of splicing events upon treatment with T1-44 compared with DMSO treated cells. This was the case for both wild-type and E2F1 knockout CHP-134 cells. We also found that E2F1 knockout CHP-134 cells had lower number of differentially spliced genes when compared to wild-type counterparts upon T1-44

treatment, pointing out the E2F1's role in the regulation of genome-wide global splicing effects (Figure 5.18-Figure 5.20).

Chapter 6. Differential apoptotic response in MYCN amplified CHP-134 versus non-MYCN amplified GI-M-EN cell line upon PRMT5 inhibition

6.1. Introduction

While we were validating CHP-134 and GI-ME-N RNA-sequencing data, where we compared the effect of PRMT5 inhibition in two different cell lines, we found that PRMT5 inhibition led to significant differential splicing events in the MYCN amplified CHP-134 cell line. Once we delved deeper into the differentially spliced genes, we found that some of these genes were involved in the apoptotic pathway.

Although, the symmetrical dimethyl inhibition was achieved in both cells (inhibition of SDMA mark), the consequence was quite different in terms of cell fate. To characterize the relevance of the differential apoptotic response seen between MYCN-amplified and non-MYCN amplified neuroblastoma cells, we analysed differentially spliced apoptotic genes upon 200 nM treatment with T1-44 for 72 hours as these genes might have a functional impact on the cell fate.

Some of the candidate genes that we identified from the RMATs data were *BCL2L11* and *CDK10* (Cyclin Dependent Kinase 10). *BCL2* gene family member *BCL2L11* had increased levels of exon 2 skipping upon 200 nM treatment with T1-44 for 72 hours in MYCN amplified CHP-134 cells but not in GI-ME-N cells. Another apoptosis relevant gene *CDK10* had increased retained intron levels upon 200 nM treatment with T1-44 for 72 hours.

6.2. T1-44 induced *BCL2L11* exon 2 skipping that might lead to differential apoptosis

One of the most significantly spliced genes was *BCL2L11* in the RNA-seq data where we compared CHP-134 versus GI-ME-N upon T1-44 treatment. *BCL2L11* (also known as *BIM*) is a member of the BCL-2 protein family. BCL-2 family members form hetero- and homodimers that act as anti- or pro-apoptotic regulators that are involved in a wide variety of cellular activities (Kale et al., 2018). Alternative splicing patterns of the *BIM* gene were previously shown as an important mediator of cell fate by regulating apoptosis-related splicing events (Lin et al., 2016). *BCL2L11* exon 3 and 4 were shown to be involved in generating two distinct transcripts that confer drug resistance. A change in the cytosine-to-thymidine base in the *BCL2L11* exon 4 gene (rs724710) caused a decrease in the selection of exon 4 in lymphoblastic leukemia cells which contributed to drug resistance (Lin et al., 2016). It was shown that *BCL2L11* splice switching induced proapoptotic isoforms that resensitized resistant *BCL2L11* deletion containing chronic myeloid leukemia cell lines to imatinib (Liu et al., 2017).

In our first RNA-seq data, we found that *BCL2L11* exon 2 was skipped significantly upon PRMT5 inhibition (Figure 6.1). Previous findings about splicing isoforms in *BCL2L11* made us curious about to investigate this splicing event in further detail. We validated this exon-skipping event in CHP-134 and GI-ME-N cells by qPCR and we found that *BCL2L11* exon 2 skipping increased significantly in CHP-134 cells, whereas it decreased in GI-ME-N cells (Figure 6.1).

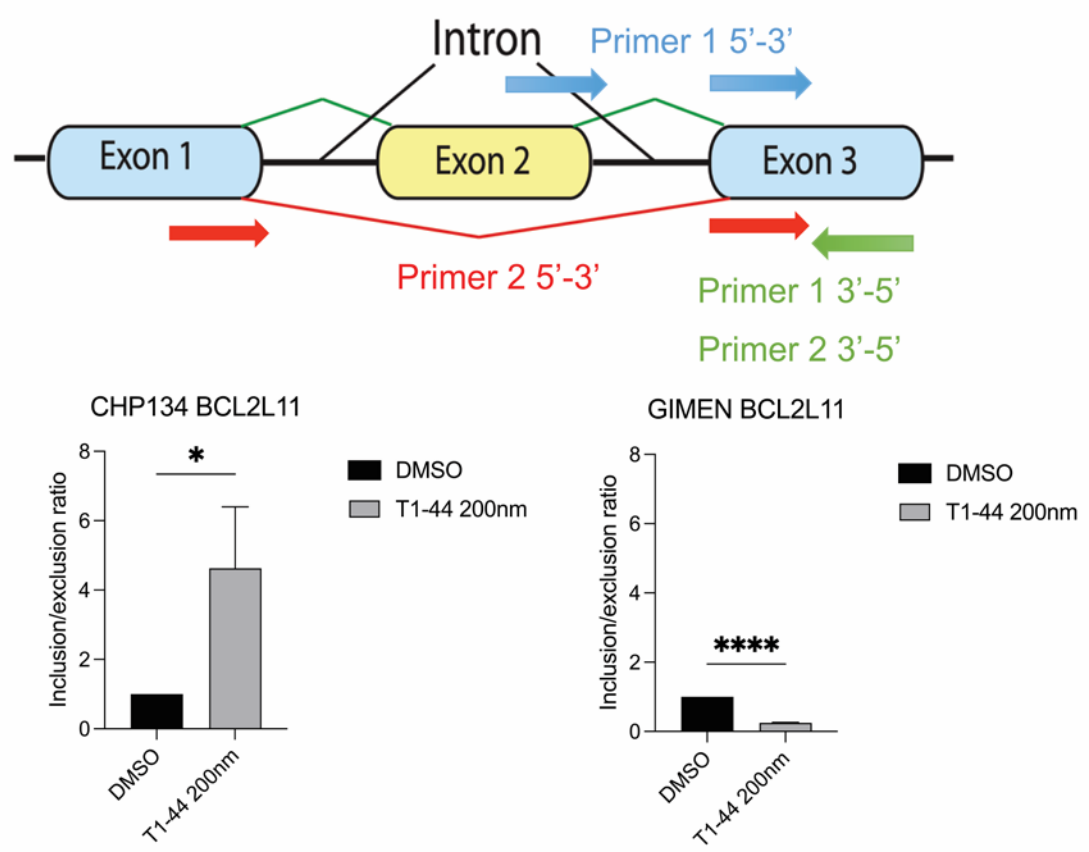

Figure 6.1. *BCL2L11* exon 2 inclusion/exclusion ratio upon 200 nM T1-44 treatment for 72 hours in CHP-134 and GI-ME-N cells. Values represent the ratio of exon inclusion versus exon exclusion as mRNA expression. Data are presented as mean ± SD. Error bars indicate the SD of three independent experiments. Statistical analyses were performed using a two-tailed, unpaired student's t-test. * $p<0.05$, **** $p<0.0001$.

6.3. E2F1 knockout led to decrease in *BCL2L11* exon 2 skipping event upon in CHP-134 cells

E2F1's involvement in the regulation of apoptotic events has been known for many years now. E2F1 has also shown to up-regulate *BCL2L11* (Gogada et al, 2013). As our aim was to understand E2F1's role in the regulation of splicing events, we wanted to check how this specific splicing event changes once we knockout E2F1 expression in CHP-134 cells. We measured the skipped exon levels in the absence of E2F1 in CHP-134 cells. We found that E2F1 KO led to the increased inclusion of *BCL2L11* exon 2, resulting in less exon 2 skipping in the absence of E2F1 (Figure 6.2). T1-44 effect is lost in E2F1 KO cells in terms of the skipped exon 2 levels. That should also be noted that E2F1 knockout also decreased total *BCL2L11* mRNA expression levels in CHP-134 cells (Figure 6.2).

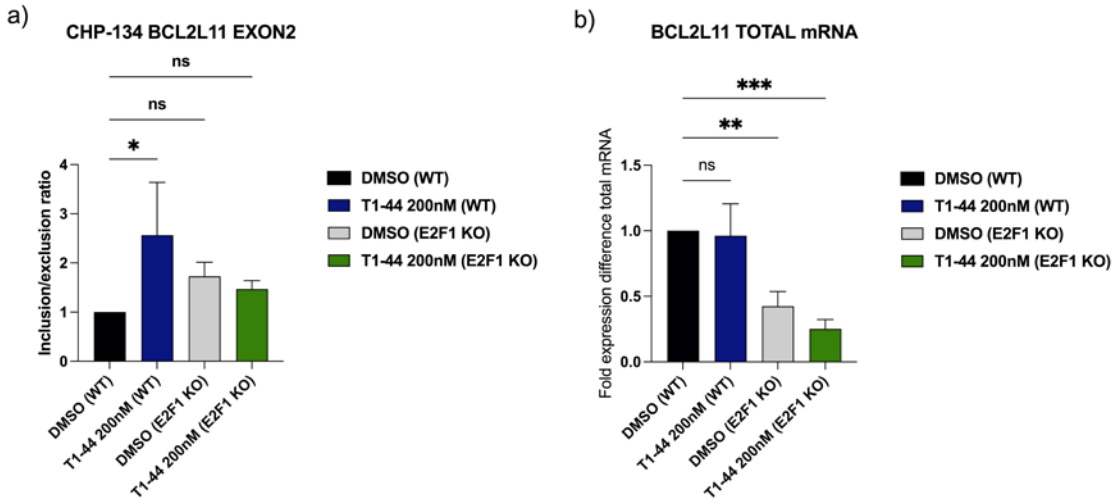

Figure 6.2. a) *BCL2L11* exon 2 skipping inclusion/exclusion ratio upon 200 nM T1-44 treatment in CHP-134 WT and CHP-134 E2F1 KO cells. Values represent the ratio of exon inclusion versus exon exclusion as mRNA expression. b) Total mRNA expression of *BCL2L11* upon 200 nM T1-44 treatment in CHP-134 WT and CHP-134 E2F1 KO cells. Data are presented as mean ± SD. Error bars indicate the SD of three independent experiments. Statistical analyses were performed using one-way ANOVA. ns: $p>0.05$, * $p<0.05$, ** $p<0.01$, *** $p<0.001$.

6.4. BCL2L11 exon 2 skipping effect is exclusive to PRMT5 inhibition by T1-44

We also questioned whether other splicing inhibitors could mimic the effect of PRMT5 inhibitor T1-44 in terms of the effect on *BCL2L11* exon skipping. Therefore, we treated CHP-134 cells with 100 nM pladienolide B for 4 hours and then we checked our differentially spliced apoptotic gene target *BCL2L11* after confirming the pladienolide B's effect via measuring the *DNAJB1* intronic region. This intronic region is used in order to measure splicing inhibition by monitoring failure to splice out an intron. Pladienolide B is an *SF3B1* inhibitor that impairs U2 snRNP interaction with pre-mRNA (Kotake et al., 2007). We found that pladienolide B did not induce *BCL2L11* exon 2 skipping as T1-44 showing that, the effect was exclusive to T1-44 (Figure 6.3).

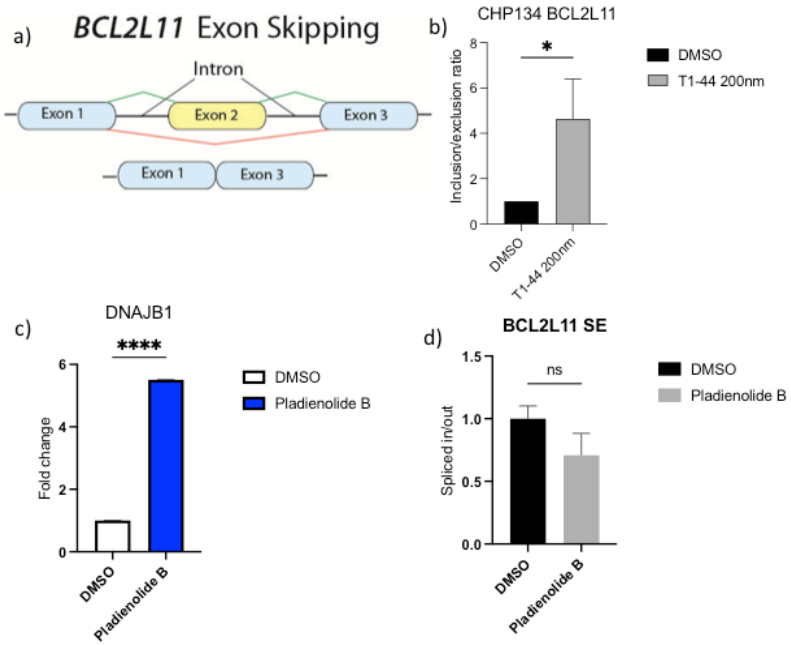

Figure 6.3. a) Schematic representation of T1-44 induced exon 2 skipping in *BCL2L11* gene, b) *BCL2L11* exon 2 skipping ratio upon 200 nM T1-44 treatment in CHP-134 cells, c) *DNAJB1* mRNA expression levels were measured by qRT-PCR after 4 h pladienolide B treatment in CHP-134 cells as a pharmacologic indicator of pladienolide B activity, d) *BCL2L11* exon 2 skipping ratio upon pladienolide B treatment in CHP-134 cells. Data are presented as mean ± SD. Error bars indicate the SD of three independent experiments. Statistical analyses were performed using a two-tailed, unpaired student's t-test. ns: not significant, ns: $p>0.05$, * $p<0.05$, **** $p<0.0001$.

6.5. PRMT5 inhibition increased CDK10 retained intron mRNA expression level and reduced CDK10 protein expression level

Defects in alternative splicing regulation are frequently observed in human tumours. However, their functional impact in tumorigenesis remains mostly unknown (Climente-González, 2017). Recently, the skipping of exon 14 in the *MET* gene was found to induce impaired tyrosine kinase receptor degradation that leads to oncogenic transformation. These molecular sub-sets of lung cancer patients have higher response to tyrosine kinase receptor inhibitors like crizotinib (Drillon, 2016). Alternative splicing can also lead to the retention of introns that cause deficient nuclear export, truncated proteins or nonsense-mediated decay (NMD) (Tazi et al., 2009).

The cyclin-dependent kinase (CDK)-RB-E2F axis forms the core transcriptional machinery that is driving cell cycle progression, controlling the timing and fidelity of genome replication and ensuring genetic material is accurately transferred through each cell division (Kent and Leone, 2019). Our lab, previously identified *CDK10* as a potential functional target in HCT-116 colorectal carcinoma cell line's RNA-seq data where it was also treated with T1-44. Once we checked our MYCN amplified CHP-134 cell line and non-MYCN amplified GI-ME-N cell line, we also found *CDK10* as a significant differentially spliced gene. We measured the total *CDK10* mRNA expression and its expression level was decreased at 200 nM T1-44 treatment. However, we found that T1-44 compound increased retention of intron (intron 8) in the *CDK10* gene in a dose-dependent manner. Inversely, CDK10 total protein expression was decreased in a dose-dependent manner after 72 hours treatment with T1-44 (Figure 6.4). We hypothesized that PRMT5 inhibition initiates retained introns that leads to decline in the protein expression levels. To question whether this effect was limited to CHP-134 cell line, we also checked the CDK10 protein expression levels in another cell line, N206.

N206 cell line data was given in the Appendix A, Figure 2. Our further interest will be to explore more retained introns like the one observed in *CDK10*, that might have functional impact on protein expression.

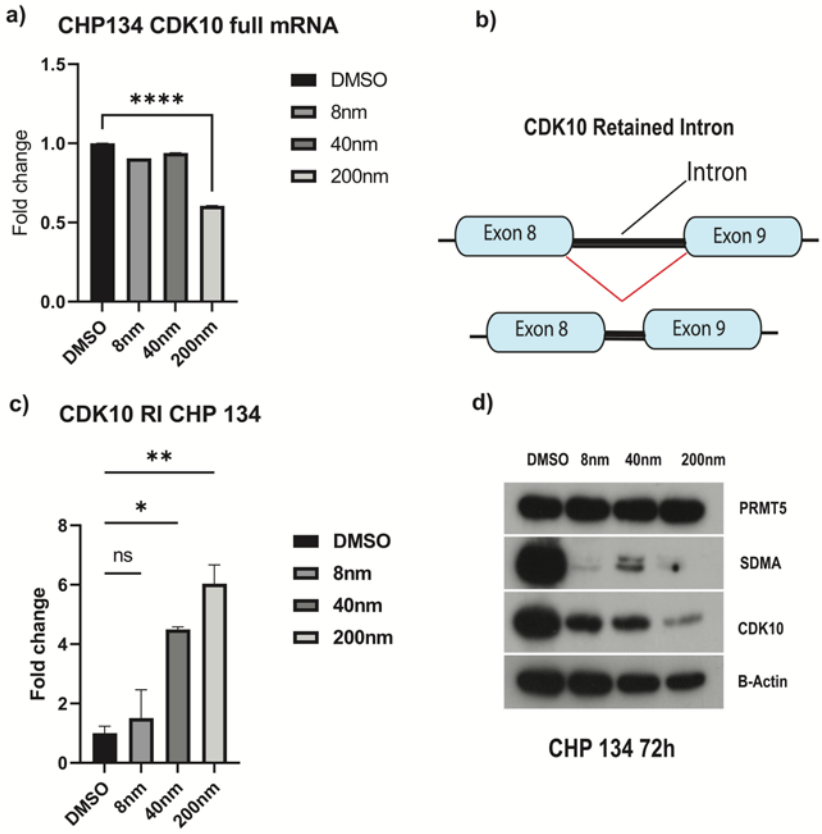

Figure 6.4. a) Total *CDK10* mRNA expression of MYCN amplified CHP-134 cell line after 72 hour treatment with 8-200 nM concentrations of compound T1-44, b) Schematic representation of *CDK10's* retained intron, c) Retained intron levels of intron 8 for *CDK10* on MYCN amplified CHP-134 cell line after 72 hours treatment with 8-200 nM concentrations of compound T1-44, d) CDK10 protein expression levels of MYCN amplified CHP-134 cell line after treatment with 8-200 nM concentrations of compound T1-44. SDMA (Symmetric Dimethylarginine Motif) antibody was used to show inhibition of methyl marks by compound T1-44. ns: $p>0.05$, * $p<0.05$, ** $p<0.01$, **** $p<0.0001$

6.6. Chapter conclusion

Several types of alternative splicing events have been described including alternative 5' or 3' splice sites, mutually exclusive exons, exon skipping, and retained introns. These different types of alternative splicing might lead different biological consequences in cells. In this chapter, we characterized a skipped exon and retained intron in order to see how abnormal splicing regulates cell behaviour.

We characterized differentially spliced apoptotic genes upon 200 nM treatment with T1-44 for 72 hours as these genes might have a functional impact on cell fate. We found that T1-44 induced higher differential splicing of apoptosis genes *BCL2L11* and *CDK10* in MYCN-amplified compared with non-MYCN amplified neuroblastoma cells.

Alternative splicing patterns of the *BCL2L11* gene were previously shown as an important mediator of cell fate by regulating apoptosis-related splicing events (Lin et al., 2016). We found that *BCL2L11* exon 2 was skipped significantly upon PRMT5 inhibition (Figure 6.1). We also found that E2F1 KO led to the increased inclusion of *BCL2L11* exon 2, resulting in less exon 2 skipping in the absence of E2F1 (Figure 6.2). T1-44 effect is lost in E2F1 KO cells in terms of the skipped exon 2 levels.

Chapter 7. Discussion

7.1. PRMT5-MYCN-E2F1 axis impacts neuroblastoma pathogenesis

Arginine methylation is a post-translational modification that plays key roles in a wide range of cellular processes like pre-mRNA splicing, DNA damage signalling, mRNA translation, cell signalling, and cell fate decision (Blanc and Richard, 2017). PRMT5 (Protein arginine methyltransferase 5) is the major type of arginine methyltransferase that is overexpressed in several cancers like ovarian, lung, multiple myeloma, breast, glioblastoma, and prostate cancers (Lattouf et al., 2019). PRMT5 has a key role in controlling the maturity of small nuclear ribonucleoproteins (snRNPs) and maintaining splicing fidelity (Guccione and Richard, 2019).

Park and colleagues previously discovered that PRMT5 plays a significant role in the post-translational regulation of MYCN and is also a poor prognostic factor as a key regulator of MYCN-dependent oncogenesis. Inhibition of PRMT5 and MYCN led to decreased proliferation and increased apoptosis in neuroblastoma cells (Park et al., 2015). Therefore, inhibiting PRMT5 may provide a novel alternative for the treatment of NB and MYCN-driven cancers.

Other members of PRMT family were also reported to have an impact on neuroblastoma pathogenicity. PRMT1 depletion reduced neuroblastoma cell viability and MYCN expression levels and PRMT1 regulates MYCN stability (Eberhardt et al., 2016). PRMT1 inhibition led to a decrease in the growth and formation of spheres in murine neuroblastoma cells. It also inhibited the proliferation and triggered cell death in human neuroblastoma cells (Hua et al. 2020).

Our group previously identified that residue-specific arginine methylation by PRMT5 enables E2F1 to regulate many genes at the alternative splicing level (Roworth et al., 2019). Many splicing regulatory elements, like the Ser-Arg (SR) rich protein family,

which act as splicing factors, are transcriptional targets of E2F1 (Edmond et al., 2013). Overexpression of positive E2F regulators (MYC or CCND1) can direct cells to proliferate via oncogenic activation of the E2F transcriptional programme (Kent and Leone, 2019). Our results showed that MYCN amplified cell lines also have higher E2F1 expression levels and they are more sensitive to PRMT5 inhibition.

It was shown that MYCN has a role in the regulation of alternative splicing in neuroblastoma (Zhang et al., 2016). However, the underlying mechanism has not yet been identified. In addition to that, non-MYCN amplified neuroblastoma often expresses C-MYC, and the expression of C-MYC and N-MYC is mutually exclusive (Rickman et al., 2018). MYC's oncogenic potential might stem from its ability to regulate splicing factors at the transcriptional level (Urbanski et al., 2018). Our results showed that the number of differentially spliced genes were higher upon PRMT5 inhibition in MYCN amplified cells when compared to non-MYCN amplified cells. Ryl et al. (2017) showed that high-MYCN cells in the G0/1 phase all proceeded to the G1/S transition state, characterized by phosphorylated RB and high E2F1 expression, whereas low MYCN cells in the G0/1 phase were recovered in two distinct molecular states: the G1/S transition state and G0 like state characterized by unphosphorylated RB and repressed E2F1 transcription. Ryl et al. (2017) validated their model using both mathematical models and experimental approaches and they found that high MYCN levels bypass G1/S restriction point in the cell cycle and sensitizes cells to the chemotherapeutic drugs. Their findings are also consistent with our results as we found that high E2F1 and MYCN expressing cells were significantly more sensitive to the PRMT5 inhibitor. It is also known that E2F transcription factors are involved in the activation and repression of MYCN in neuroblastomas. E2F1, E2F2, and E2F3 were the first identified transcription factors that regulate MYCN expression in neuroblastoma

(Strieder and Lutz, 2003). Wang and colleagues recently reported E2F1 and E2F3 as a poor prognostic factor in different paediatric neuroblastoma cohorts from publicly available datasets; Therapeutically Applicable Research to Generate Effective Treatments (TARGET), Gene Expression Omnibus (GEO), and ArrayExpress (Wang et al., 2022).

In this study, we have outlined our recent findings about PRMT5 inhibition to exploit possible vulnerabilities in MYCN amplified neuroblastoma cells. We wanted to know how inhibition of PRMT5 in MYCN amplified and high E2F1 expressing neuroblastoma cells can lead to increased sensitivity when compared to non-MYCN amplified and low E2F1 expressing neuroblastoma cells.

MYCN canonical pathway involves transcription, RNA processing, chromatin remodelling, and translational regulation (Sibley et al., 2016). One of our aims was to expand this knowledge to non-canonical pathways and their biological consequences. Mechanistically this can be explained through the inhibition of arginine post-translational modification (SDMA) of large sets of RNA-binding proteins (RBP) involved in splicing regulation. Type I PRMTs have been shown to methylate different arginine residues of RBPs involved in RNA post-transcriptional regulation (Fong et al., 2019). There are also numerous examples of how ADMA/SDMA may regulate cellular localization of RBPs (Maniaci et al., 2021).

Previous researches focused more onto the MYCN's role in splicing, however we aimed to enlighten E2F1's contribution into the regulation of splicing. We found that SR rich splicing factors that we found differentially expressed in our RNA-seq data were both E2F1 and MYCN target genes. Previous work in our lab had identified that PRMT5 mediates modulation of cell growth via a small R-rich motif located on the E2F1 that is a target for symmetric methylation by PRMT5. This R-rich domain on E2F1 is first

recognized and read by the p100/TSN. This process enables the recruitment of splicing factor to the spliceosome, driving splicing events on genes regulating cell growth and survival (Roworth et al., 2019). E2F1 can also function as a transcription factor that co-expressed with MYCN in neuroblastoma cells. Alongside, MYCN also regulates the expression of diverse splicing factors, which might be necessary for the symmetrical demethylation activation of the splicing machinery by PRMT5 (Zhang et al., 2016). Therefore, targeting PRMT5 in MYCN amplified cells might lead synthetic lethality.

MYC-driven cancers were previously shown to be dependent on the spliceosome. Therefore, targeting splicing factors in MYC-driven neuroblastoma might be an effective treatment strategy. Spliceosome assembly was found as the most significantly enriched pathway in high-risk neuroblastoma where 3000 most differentially genes were analysed in 498 primary neuroblastoma samples. They found that DNA replication and cell cycle signatures relevant gene ontology categories were enriched (Singh et al., 2021). We also found that E2F1 knockout in CHP-134 cells and following PRMT5 inhibition also led to similar gene ontology terms in our RNA-seq data. Therefore, we confirmed that E2F1 is also an important player in response to the PRMT5 inhibition. Our results demonstrated a significant role of PRMT5-E2F1-MYCN axis in targeting alternative splicing in neuroblastoma. The identification of differentially spliced genes and pathways in neuroblastoma tumours may be important in the understanding the biology and leading to the discovery of diagnostic markers or therapeutic targets in the treatment of this deadly disease.

DNA repair and cell cycle regulation related genes were found in co-expression analysis network in pan-cancer transcriptome data, suggesting a critical role for these pathways (Savary et al., 2020). Our work also indicates the importance of cell cycle relevant in neuroblastoma treatment. Our data suggests that beyond the role for MYCN in

canonical neuroblastoma progression, PRMT5-E2F1-MYCN axis hold great promise as a target in therapy. This work also highlights the potential usage of high E2F1-MYCN co-expression in order to stratify patients for PRMT5 inhibitor treatment. Noting that these potent biomarkers could also be relevant for other MYCN amplified cancers too.

MYCN amplification is observed in many other cancer types beyond neuroblastoma therefore, we believe that our findings will also contribute to the targeted therapy efforts in other cancer types as well.

7.2. E2F1 knockout led to genome wide decrease in differentially spliced genes

We found that E2F1 KO in a high E2F1/MYCN-amplified cell line induced a decrease in sensitivity to the PRMT5 inhibitor T1-44 that resulted in a decrease in PRMT5/E2F1 driven splicing events. One of the functional consequences of this change in the sensitivity was the inactivation of pro-apoptotic gene splicing in the E2F1 high/MYCN-amplified cells after E2F1 KO. Our RNA-seq results revealed the role of PRMT5 inhibitors on the splicing outcomes for pro- and anti-apoptotic target genes are dependent on E2F1 as we showed that *BCL2L11* exon skipping is no longer present after E2F1 KO.

Another important finding from our work is that the different isoforms of genes described in this work (especially for *BCL2L11*) holds great promise to improve our understanding of the biological role of E2F1 on the regulation of splicing. It is also possible that PRMT5 inhibition causes the extensive splicing of oncogenic isoforms required for the survival of MYCN amplified cells similar to what we observed with *BCL2L11* isoforms. To test this hypothesis, we focused our analysis on the aberrant splicing of the *BCL2L11* mRNA. *BCL2L11* is a canonical E2F1 target gene that is involved in apoptosis. Although multiple genes could meditate the downstream effects of PRMT5 inhibition, CRISPR/Cas9-mediated knockout of E2F1 decreased the rate of *BCL2L11* exon 2 skipping.

As our RNA sequencing results revealed, *BCL2L11* exon 2 skipping levels change in response to the PRMT5 inhibition after E2F1 knockout that could be the underlying mechanism for PRMT5 inhibitor resistance in E2F1 KO CHP-134 cells as the expression of *BIM* isoforms has been linked to drug response in tumours (Reviejo et al., 2021).

BCL2L11 plays important role in apoptosis, and it has been proposed to be a potential target in cancer treatment (Faber et al., 2012). Our results demonstrated the exon-skipping event in *BCL2L11* leveraged by PRMT5 inhibition in MYCN amplified NB cells. Our results provide useful resource for discovering diagnostic biomarkers or therapeutic targets in neuroblastoma.

We also identified E2F1 relevant unique gene expression changes in our second RNA sequencing data that might hint identifying some of the non-canonical E2F1 target genes like *PAGE1* and *CRYZ*. We believe these two genes might have important functional roles of E2F1 in neural cells especially. More functional experiments are required for further validation of these genes, as existing literature remains very limited in terms of their biological functions.

As high MYCN expression levels correspond to the high E2F1 levels that might nurture PRMT5-E2F1 pathway. As a model, E2F1 might have two major control mechanisms over crucial cellular pathways. The first one is transcriptional control where E2F1 controls cell cycle, DNA replication, DNA repair, and apoptosis. The second control mechanism is splicing control where PRMT5 methylation enables E2F1 to regulate many genes at alternative splicing level (Figure 7.1). This multi-facet mechanism might have contributed the strong PRMT5 inhibitor response in MYCN amplified cells. As we found that when E2F1 was depleted in the cells, cells become more resistant to the PRMT5 inhibition (IC_{50} was increased), and the number of differentially spliced genes decreased. What remains important is that to show the functions of these differentially spliced genes in the absence of E2F1 and their effect on apoptosis. We showed *BCL2L11* as an example, but this is not only limited to *BCL2L11* but also many other genes as well. These pro-apoptotic splicing events might be crucial as *BCL2L11*

skipped exon 2 events in terms of conferring pro-apoptotic features and enhanced drug sensitivity in cells.

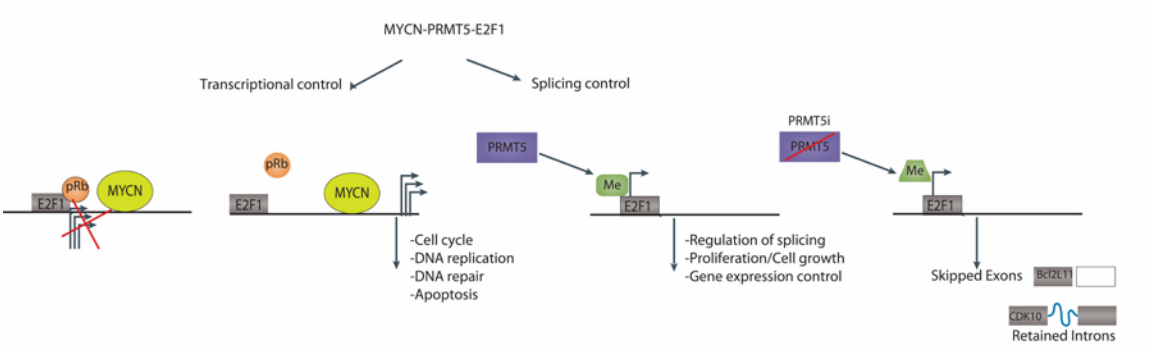

Figure 7.1. Different states of E2F1 contribute to the variety of cellular processes via major two mechanisms: Transcriptional control and splicing control.

7.3. Conclusion

To conclude, the data provided here have important bench to the bedside therapeutic implications for the use of PRMT5 inhibitors in MYCN-amplified neuroblastoma. Ongoing clinical trials are also promising regarding the future implications of PRMT5 inhibitors. We think that our results are also applicable to other MYCN amplified cancer types as well.

As childhood cancers have lower rates of mutational changes when compared to adult malignancies and lower MYCN amplified neuroblastoma harbour very few further genetic lesions and only a small subset of them is recurrent, epigenetic targeting of neuroblastoma emerges as a plausible therapeutic strategy.

It is possible that newly discovered mutations, RNA-based signatures, epigenetic alterations, or a combination of these factors would provide more details for identifying the higher-risk group of patients. Current work is focused on defining and validating the optimal gene set for targeting the right genetic stratification for PRMT5 targeted therapy in neuroblastoma in vitro.

We hypothesized that E2F1 regulates the genome wide effects in the cell cycle via two major pathways. One of them is the direct effect of E2F1 in regulating the apoptotic gene response; such as *BCL2L11* (BIM) and *CDK10*, and one of the other important effects of E2F1 is regulating splicing via post-transcriptional processes that affects RNA stability and translation. Taken together, our results suggest non-canonical features of E2F1 functioning as the regulator of post-transcriptional processes.

As more PRMT5 inhibitor heads towards clinical trials, that is much needed to stratify patients in clinic. Our preclinical results suggest that MYCN-E2F1 expression status should be considered in patient stratification to determine who is more likely to benefit

from the therapy. Future work in this area should focus on the biomarker driven stratification of patients for PRMT5 inhibitor treatment in the clinic.

References

Achbergerová M, Hederová S, Hrašková A, Kolenová A. Dinutuximab beta in the treatment of high-risk neuroblastoma: A follow-up of a case series in Bratislava. Medicine (Baltimore). 2022 Jan 28;101(4):e28716. doi: 10.1097/MD.0000000000028716. PMID: 35089239; PMCID: PMC8797591.

Ackermann S, Cartolano M, Hero B, Welte A, Kahlert Y, Roderwieser A, Bartenhagen C, Walter E, Gecht J, Kerschke L, Volland R, Menon R, Heuckmann JM, Gartlgruber M, Hartlieb S, Henrich KO, Okonechnikov K, Altmüller J, Nürnberg P, Lefever S, de Wilde B, Sand F, Ikram F, Rosswog C, Fischer J, Theissen J, Hertwig F, Singhi AD, Simon T, Vogel W, Perner S, Krug B, Schmidt M, Rahmann S, Achter V, Lang U, Vokuhl C, Ortmann M, Büttner R, Eggert A, Speleman F, O'Sullivan RJ, Thomas RK, Berthold F, Vandesompele J, Schramm A, Westermann F, Schulte JH, Peifer M, Fischer M. A mechanistic classification of clinical phenotypes in neuroblastoma. Science. 2018 Dec 7;362(6419):1165-1170. doi: 10.1126/science.aat6768. PMID: 30523111; PMCID: PMC7875194.

Al-Hamashi AA, Diaz K, Huang R. Non-Histone Arginine Methylation by Protein Arginine Methyltransferases. Curr Protein Pept Sci. 2020;21(7):699-712. doi: 10.2174/1389203721666200507091952. PMID: 32379587; PMCID: PMC7529871.

Anczuków O, Krainer AR. The spliceosome, a potential Achilles heel of MYC-driven tumors. Genome Med. 2015;7:107. Published 2015 Oct 22. doi:10.1186/s13073-015-0234-3.

Althoff K, Beckers A, Bell E, Nortmeyer M, Thor T, Sprüssel A, Lindner S, De Preter K, Florin A, Heukamp LC, Klein-Hitpass L, Astrahantseff K, Kumps C, Speleman F, Eggert A, Westermann F, Schramm A, Schulte JH. A Cre-conditional MYCN-driven neuroblastoma mouse model as an improved tool for preclinical studies. Oncogene. 2015 Jun;34(26):3357-68. doi: 10.1038/onc.2014.269. Epub 2014 Sep 1. PMID: 25174395; PMCID: PMC4487199.

Baralle FE, Giudice J. Alternative splicing as a regulator of development and tissue identity. Nat Rev Mol Cell Biol. 2017 Jul;18(7):437-451. doi: 10.1038/nrm.2017.27. Epub 2017 May 10. PMID: 28488700; PMCID: PMC6839889.

Barczak W, Jin L, Carr SM, Munro S, Ward S, Kanapin A, Samsonova A, La Thangue NB. PRMT5 promotes cancer cell migration and invasion through the E2F pathway. Cell death & disease. 2020 Jul 24;11(7):572.

Barr EK, Applebaum MA. Genetic Predisposition to Neuroblastoma. Children (Basel). 2018 Aug 31;5(9):119. doi: 10.3390/children5090119. PMID: 30200332; PMCID: PMC6162470.

Beltran H. The N-myc Oncogene: Maximizing its Targets, Regulation, and Therapeutic PotentialN-myc Oncogene. Molecular Cancer Research. 2014 Jun 1;12(6):815-22.

Bezzi M, Teo SX, Muller J, Mok WC, Sahu SK, Vardy LA, Bonday ZQ, Guccione E. Regulation of constitutive and alternative splicing by PRMT5 reveals a role for Mdm4 pre-mRNA in sensing defects in the spliceosomal machinery. Genes Dev. 2013 Sep 1;27(17):1903-16.

Blanc RS, Richard S. Arginine Methylation: The Coming of Age. Mol Cell. 2017 Jan 5;65(1):8-24.

Blanco-Luquin I, Lázcoz P, Celay J, Castresana JS, Encío IJ. In Vitro Assessment of the Role of p53 on Chemotherapy Treatments in Neuroblastoma Cell Lines. Pharmaceuticals (Basel). 2021 Nov 19;14(11):1184. doi: 10.3390/ph14111184. PMID: 34832966; PMCID: PMC8624165.

Bluhm E, McNeil DE, Cnattingius S, Gridley G, El Ghormli L, Fraumeni JF Jr. Prenatal and perinatal risk factors for neuroblastoma. Int J Cancer. 2008 Dec 15;123(12):2885-90. doi: 10.1002/ijc.23847. PMID: 18798548; PMCID: PMC6276802.

Board PP. Neuroblastoma Treatment (PDQ®). InPDQ Cancer Information Summaries [Internet] 2022 Jun 9. National Cancer Institute (US).

Bourdeaut F, Ferrand S, Brugières L, Hilbert M, Ribeiro A, Lacroix L, Bénard J, Combaret V, Michon J, Valteau-Couanet D, Isidor B, Rialland X, Poirée M, Defachelles AS, Peuchmaur M, Schleiermacher G, Pierron G, Gauthier-Villars M, Janoueix-Lerosey I, Delattre O; Comité Neuroblastome of the Société Francaise de Cancérologie. ALK germline mutations in patients with neuroblastoma: a rare and weakly penetrant syndrome. Eur J Hum Genet. 2012 Mar;20(3):291-7. doi: 10.1038/ejhg.2011.195. Epub 2011 Nov 9. PMID: 22071890; PMCID: PMC3283184.

Brady SW, Liu Y, Ma X, Gout AM, Hagiwara K, Zhou X, Wang J, Macias M, Chen X, Easton J, Mulder HL. Pan-neuroblastoma analysis reveals age-and signature-associated driver alterations. Nature communications. 2020 Oct 14;11(1):5183.

Braunschweig U, Barbosa-Morais NL, Pan Q, Nachman EN, Alipanahi B, Gonatopoulos-Pournatzis T, Frey B, Irimia M, Blencowe BJ. Widespread intron retention in mammals functionally tunes transcriptomes. Genome Res. 2014 Nov;24(11):1774-86. doi: 10.1101/gr.177790.114. Epub 2014 Sep 25. PMID: 25258385; PMCID: PMC4216919.

Bretones G, Delgado MD, León J. Myc and cell cycle control. Biochimica et Biophysica Acta (BBA)-Gene Regulatory Mechanisms. 2015 May 1;1849(5):506-16.

Broeker, CD, Andrechek ER. E2F Transcription Factors in Cancer, More than the Cell Cycle, Reference Module in Biomedical Sciences, Elsevier, 2021. doi.org/10.1016/B978-0-12-820472-6.00102-X.

Buongervino S, Lane MV, Garrigan E, Zhelev DV, Dimitrov DS, Bosse KR. Antibody-drug conjugate efficacy in neuroblastoma-role of payload, resistance mechanisms, target density, and antibody internalization. Molecular cancer therapeutics. 2021 Nov;20(11):2228.

Carpenter EL, Mossé YP. Targeting ALK in neuroblastoma--preclinical and clinical advancements. Nat Rev Clin Oncol. 2012 May 15;9(7):391-9. doi: 10.1038/nrclinonc.2012.72. PMID: 22585002; PMCID: PMC3683972.

Carr SM, Roworth AP, Chan C, La Thangue NB. Post-translational control of transcription factors: methylation ranks highly. FEBS J. 2015 Dec;282(23):4450-65.

Chan-Penebre E, Kuplast KG, Majer CR, Boriack-Sjodin PA, Wigle TJ, Johnston LD, Rioux N, Munchhof MJ, Jin L, Jacques SL, West KA. A selective inhibitor of PRMT5 with in vivo and in vitro potency in MCL models. Nature chemical biology. 2015 Jun;11(6):432-7.

Cho EC, Zheng S, Munro S, Liu G, Carr SM, Moehlenbrink J, Lu YC, Stimson L, Khan O, Konietzny R, McGouran J, Coutts AS, Kessler B, Kerr DJ, Thangue NB. Arginine methylation controls growth regulation by E2F-1. EMBO J. 2012 Apr 4;31(7):1785-97.

Chu CM, Rasalkar DD, Hu YJ, Cheng FW, Li CK, Chu WC. Clinical presentations and imaging findings of neuroblastoma beyond abdominal mass and a review of imaging algorithm. Br J Radiol. 2011 Jan;84(997):81-91.

Chung C, Boterberg T, Lucas J, Panoff J, Valteau-Couanet D, Hero B, Bagatell R, Hill-Kayser CE. Neuroblastoma. Pediatr Blood Cancer. 2021 May;68 Suppl 2(Suppl 2):e28473. doi: 10.1002/pbc.28473. PMID: 33818884; PMCID: PMC8785544.

Climente-González H, Porta-Pardo E, Godzik A, Eyras E. The Functional Impact of Alternative Splicing in Cancer. Cell Rep. 2017 Aug 29;20(9):2215-2226.

Colon NC, Chung DH. Neuroblastoma. Adv Pediatr. 2011;58(1):297-311.

Dehairs J, Talebi A, Cherifi Y, Swinnen JV. CRISP-ID: decoding CRISPR mediated indels by Sanger sequencing. Sci Rep. 2016 Jul 1;6:28973.

Denechaud PD, Fajas L, Giralt A. E2F1, a Novel Regulator of Metabolism. Front Endocrinol (Lausanne). 2017 Nov 10;8:311.

Dimova DK, Dyson NJ. The E2F transcriptional network: old acquaintances with new faces. Oncogene. 2005 Apr 18;24(17):2810-26.

Dobin A, Davis CA, Schlesinger F, Drenkow J, Zaleski C, Jha S, Batut P, Chaisson M, Gingeras TR. STAR: ultrafast universal RNA-seq aligner. Bioinformatics. 2013 Jan 1;29(1):15-21.

Drilon A. MET Exon 14 Alterations in Lung Cancer: Exon Skipping Extends Half-Life. Clin Cancer Res. 2016 Jun 15;22(12):2832-4.

DuBois SG, Macy ME, Henderson TO. High-risk and relapsed neuroblastoma: Toward more cures and better outcomes. American Society of Clinical Oncology Educational Book. 2022 May 6;42:768-80.

Eberhardt A, Hansen JN, Koster J, Lotta Jr LT, Wang S, Livingstone E, Qian K, Valentijn LJ, Zheng YG, Schor NF, Li X. Protein arginine methyltransferase 1 is a novel regulator of MYCN in neuroblastoma. Oncotarget. 2016 Sep 9;7(39):63629.

Edmond V, Merdzhanova G, Gout S, Brambilla E, Gazzeri S, Eymin B. A new function of the splicing factor SRSF2 in the control of E2F1-mediated cell cycle progression in neuroendocrine lung tumors. Cell Cycle. 2013 Apr 15;12(8):1267-78.

Faber AC, Ebi H, Costa C, Engelman JA. Apoptosis in targeted therapy responses: the role of BIM. Adv Pharmacol. 2012;65:519-42.

Fackenthal JD, Godley LA. Aberrant RNA splicing and its functional consequences in cancer cells. Dis Model Mech. 2008 Jul-Aug;1(1):37-42.

Fong JY, Pignata L, Goy PA, Kawabata KC, Lee SC, Koh CM, Musiani D, Massignani E, Kotini AG, Penson A, Wun CM, Shen Y, Schwarz M, Low DH, Rialdi A, Ki M, Wollmann H, Mzoughi S, Gay F, Thompson C, Hart T, Barbash O, Luciani GM, Szewczyk MM, Wouters BJ, Delwel R, Papapetrou EP, Barsyte-Lovejoy D, Arrowsmith CH, Minden MD, Jin J, Melnick A, Bonaldi T, Abdel-Wahab O, Guccione E. Therapeutic Targeting of RNA Splicing Catalysis through Inhibition of Protein Arginine Methylation. Cancer Cell. 2019 Aug 12;36(2):194-209.e9.

Gallego-Paez LM, Bordone MC, Leote AC, Saraiva-Agostinho N, Ascensão-Ferreira M, Barbosa-Morais NL. Alternative splicing: the pledge, the turn, and the prestige: the key role of alternative splicing in human biological systems. Human genetics. 2017 Sep;136:1015-42.

Gogada R, Yadav N, Liu J, Tang S, Zhang D, Schneider A, Seshadri A, Sun L, Aldaz CM, Tang DG, Chandra D. Bim, a proapoptotic protein, up-regulated via transcription factor E2F1-dependent mechanism, functions as a prosurvival molecule in cancer. J Biol Chem. 2013 Jan 4;288(1):368-81. doi: 10.1074/jbc.M112.386102. Epub 2012 Nov 14. PMID: 23152504; PMCID: PMC3537034.

Grabski DF, Broseus L, Kumari B, Rekosh D, Hammarskjold ML, Ritchie W. Intron retention and its impact on gene expression and protein diversity: A review and a practical guide. Wiley Interdisciplinary Reviews: RNA. 2021 Jan;12(1):e1631.

Gregorio A, Corrias MV, Castriconi R, Dondero A, Mosconi M, Gambini C, Moretta A, Moretta L, Bottino C. Small round blue cell tumours: diagnostic and prognostic usefulness of the expression of B7-H3 surface molecule. Histopathology. 2008 Jul;53(1):73-80. doi: 10.1111/j.1365-2559.2008.03070.x. PMID: 18613926; PMCID: PMC2658025.

Guccione E, Richard S. The regulation, functions and clinical relevance of arginine methylation. Nat Rev Mol Cell Biol. 2019 Oct;20(10):642-657.

Guo X, Chen QR, Song YK, Wei JS, Khan J. Exon array analysis reveals neuroblastoma tumors have distinct alternative splicing patterns according to stage and MYCN amplification status. BMC Med Genomics. 2011 Apr 18;4:35.

Hallberg B, Palmer RH. The role of the ALK receptor in cancer biology. Ann Oncol. 2016 Sep;27 Suppl 3:iii4-iii15. doi: 10.1093/annonc/mdw301. PMID: 27573755.

Hallstrom TC, Nevins JR. Balancing the decision of cell proliferation and cell fate. Cell Cycle. 2009 Feb 15;8(4):532-5.

Hartlieb SA, Sieverling L, Nadler-Holly M, Ziehm M, Toprak UH, Herrmann C, Ishaque N, Okonechnikov K, Gartlgruber M, Park YG, Wecht EM, Savelyeva L, Henrich KO, Rosswog C, Fischer M, Hero B, Jones DTW, Pfaff E, Witt O, Pfister SM, Volckmann R, Koster J, Kiesel K, Rippe K, Taschner-Mandl S, Ambros P, Brors B, Selbach M, Feuerbach L, Westermann F. Alternative lengthening of telomeres in childhood neuroblastoma from genome to proteome. Nat Commun. 2021 Feb 24;12(1):1269. doi: 10.1038/s41467-021-21247-8. PMID: 33627664; PMCID: PMC7904810.

Heck JE, Ritz B, Hung RJ, Hashibe M, Boffetta P. The epidemiology of neuroblastoma: a review. Paediatric and perinatal epidemiology. 2009 Mar;23(2):125-43.

Hong E, Barczak W, Park S, Heo JS, Ooshima A, Munro S, Hong CP, Park J, An H, Park JO, Park SH. Combination treatment of T1-44, a PRMT5 inhibitor with Vactosertib, an inhibitor of TGF-β signaling, inhibits invasion and prolongs survival in a mouse model of pancreatic tumors. Cell Death & Disease. 2023 Feb 10;14(2):93.

Howard JM, Sanford JR. The RNAissance family: SR proteins as multifaceted regulators of gene expression. Wiley Interdiscip Rev RNA. 2015 Jan-Feb;6(1):93-110.

Hsu CL, Chang HY, Chang JY, Hsu WM, Huang HC, Juan HF. Unveiling MYCN regulatory networks in neuroblastoma via integrative analysis of heterogeneous genomics data. Oncotarget. 2016 Jun 6;7(24):36293.

Hua ZY, Hansen JN, He M, Dai SK, Choi Y, Fulton MD, Lloyd SM, Szemes M, Sen J, Ding HF, Angelastro JM, Fei X, Li HP, Wu CR, Yang SY, Malik K, Bao X, George Zheng Y, Liu CM, Schor NF, Li ZJ, Li XG. PRMT1 promotes neuroblastoma cell survival through ATF5. Oncogenesis. 2020 May 15;9(5):50. doi: 10.1038/s41389-020-0237-9. PMID: 32415090; PMCID: PMC7229216.

Huang DW, Sherman BT, Lempicki RA. Systematic and integrative analysis of large gene lists using DAVID Bioinformatics Resources. Nature Protoc. 2009;4(1):44-57.

Huang DW, Sherman BT, Lempicki RA. Bioinformatics enrichment tools: paths toward the comprehensive functional analysis of large gene lists. Nucleic Acids Res. 2009;37(1):1-13.

Huang M, Weiss WA. Neuroblastoma and MYCN. Cold Spring Harb Perspect Med. 2013 Oct 1;3(10):a014415.

Hwang JW, Cho Y, Bae GU, Kim SN, Kim YK. Protein arginine methyltransferases: Promising targets for cancer therapy. Experimental & molecular medicine. 2021 May;53(5):788-808.

Jansson M, Durant ST, Cho EC, Sheahan S, Edelmann M, Kessler B, La Thangue NB. Arginine methylation regulates the p53 response. Nature cell biology. 2008 Dec;10(12):1431-9.

Jarrold J, Davies CC. PRMTs and Arginine Methylation: Cancer's Best-Kept Secret? Trends Mol Med. 2019 Nov;25(11):993-1009.

Johnsen JI, Dyberg C, Wickström M. Neuroblastoma—A neural crest derived embryonal malignancy. Frontiers in molecular neuroscience. 2019 Jan 29;12:9.

Kale J, Osterlund EJ, Andrews DW. BCL-2 family proteins: changing partners in the dance towards death. Cell Death Differ. 2018 Jan;25(1):65-80.

Kalev P, Hyer ML, Gross S, Konteatis Z, Chen CC, Fletcher M, Lein M, Aguado-Fraile E, Frank V, Barnett A, Mandley E. MAT2A inhibition blocks the growth of MTAP-deleted cancer cells by reducing PRMT5-dependent mRNA splicing and inducing DNA damage. Cancer Cell. 2021 Feb 8;39(2):209-24.

Kent LN, Bae S, Tsai SY, Tang X, Srivastava A, Koivisto C, Martin CK, Ridolfi E, Miller GC, Zorko SM, Plevris E, Hadjiyannis Y, Perez M, Nolan E, Kladney R, Westendorp B, de Bruin A, Fernandez S, Rosol TJ, Pohar KS, Pipas JM, Leone G. Dosage-dependent copy number gains in E2f1 and E2f3 drive hepatocellular carcinoma. J Clin Invest. 2017 Mar 1;127(3):830-842.

Kent LN, Leone G. The broken cycle: E2F dysfunction in cancer. Nat Rev Cancer. 2019 Jun;19(6):326-338.

Koh CM, Sabò A, Guccione E. Targeting MYC in cancer therapy: RNA processing offers new opportunities. Bioessays. 2016;38(3):266-275. doi:10.1002/bies.201500134.

Koneru B, Lopez G, Farooqi A, Conkrite KL, Nguyen TH, Macha SJ, Modi A, Rokita JL, Urias E, Hindle A, Davidson H, Mccoy K, Nance J, Yazdani V, Irwin MS, Yang S, Wheeler DA, Maris JM, Diskin SJ, Reynolds CP. Telomere Maintenance Mechanisms Define Clinical Outcome in High-Risk Neuroblastoma. Cancer Res. 2020 Jun 15;80(12):2663-2675. doi: 10.1158/0008-5472.CAN-19-3068. Epub 2020 Apr 14. PMID: 32291317; PMCID: PMC7313726.

Kotake Y, Sagane K, Owa T, Mimori-Kiyosue Y, Shimizu H, Uesugi M, Ishihama Y, Iwata M, Mizui Y. Splicing factor SF3b as a target of the antitumor natural product pladienolide. Nat Chem Biol. 2007 Sep;3(9):570-5. doi: 10.1038/nchembio.2007.16. Epub 2007 Jul 22. PMID: 17643112.

Kroesen M, Nierkens S, Ansems M, Wassink M, Orentas RJ, Boon L, den Brok MH, Hoogerbrugge PM, Adema GJ. A transplantable TH-MYCN transgenic tumor model in C57Bl/6 mice for preclinical immunological studies in neuroblastoma. Int J Cancer. 2014 Mar 15;134(6):1335-45. doi: 10.1002/ijc.28463. Epub 2013 Sep 14. PMID: 24038106.

Kryukov GV, Wilson FH, Ruth JR, Paulk J, Tsherniak A, Marlow SE, Vazquez F, Weir BA, Fitzgerald ME, Tanaka M, Bielski CM, Scott JM, Dennis C, Cowley GS, Boehm JS, Root DE, Golub TR, Clish CB, Bradner JE, Hahn WC, Garraway LA. MTAP deletion confers enhanced dependency on the PRMT5 arginine methyltransferase in cancer cells. Science. 2016 Mar 11;351(6278):1214-8. doi: 10.1126/science.aad5214. Epub 2016 Feb 11. PMID: 26912360; PMCID: PMC4997612.

La Thangue NB. DP and E2F proteins: components of a heterodimeric transcription factor implicated in cell cycle control. Curr Opin Cell Biol. 1994 Jun;6(3):443-50.

Lattouf H, Poulard C, Le Romancer M. PRMT5 prognostic value in cancer. Oncotarget. 2019 May 7;10(34):3151-3153.

Li Y, Diehl JA. PRMT5-dependent p53 escape in tumorigenesis. Oncoscience. 2015 Aug 31;2(8):700-2.

Lin JC, Tsao MF, Lin YJ. Differential Impacts of Alternative Splicing Networks on Apoptosis. Int J Mol Sci. 2016 Dec 14;17(12):2097.

Liu J, Bhadra M, Sinnakannu JR, Yue WL, Tan CW, Rigo F, Ong ST, Roca X. Overcoming imatinib resistance conferred by the BIM deletion polymorphism in chronic myeloid leukemia with splice-switching antisense oligonucleotides. Oncotarget. 2017 Sep 9;8(44):77567.

Llombart V, Mansour MR. Therapeutic targeting of “undruggable” MYC. EBioMedicine. 2022 Jan 1;75:103756.

Long JC, Caceres JF. The SR protein family of splicing factors: master regulators of gene expression. Biochem J. 2009 Jan 1;417(1):15-27. doi: 10.1042/BJ20081501. PMID: 19061484.

Look AT, Hayes FA, Shuster JJ, Douglass EC, Castleberry RP, Bowman LC, Smith EI, Brodeur GM. Clinical relevance of tumor cell ploidy and N-myc gene amplification in childhood neuroblastoma: a Pediatric Oncology Group study. J Clin Oncol. 1991 Apr;9(4):581-91. doi: 10.1200/JCO.1991.9.4.581. PMID: 2066755.

Lorton BM, Shechter D. Cellular consequences of arginine methylation. Cell Mol Life Sci. 2019 Aug;76(15):2933-2956. doi: 10.1007/s00018-019-03140-2. Epub 2019 May 17. PMID: 31101937; PMCID: PMC6642692.

Louis CU, Shohet JM. Neuroblastoma: molecular pathogenesis and therapy. Annual review of medicine. 2015 Jan 14;66:49-63.

Love MI, Huber W, Anders S. Moderated estimation of fold change and dispersion for RNA-seq data with DESeq2. Genome Biol. 2014;15(12):550.

Lundberg KI, Treis D, Johnsen JI. Neuroblastoma Heterogeneity, Plasticity, and Emerging Therapies. Curr Oncol Rep. 2022 Aug;24(8):1053-1062. doi: 10.1007/s11912-022-01270-8. Epub 2022 Apr 1. PMID: 35362827; PMCID: PMC9249718.

Mahapatra S, Challagundla KB. Neuroblastoma. [Updated 2023 Feb 6]. In: StatPearls [Internet]. Treasure Island (FL): StatPearls Publishing; 2023 Jan-. Available from: https://www.ncbi.nlm.nih.gov/books/NBK448111/

Maniaci M, Boffo FL, Massignani E, Bonaldi T. Systematic Analysis of the Impact of R-Methylation on RBPs-RNA Interactions: A Proteomic Approach. Front Mol Biosci. 2021 Sep 7;8:688973.

Mathieu LN, Larkins E, Akinboro O, Roy P, Amatya AK, Fiero MH, Mishra-Kalyani PS, Helms WS, Myers CE, Skinner AM, Aungst S, Jin R, Zhao H, Xia H, Zirkelbach JF, Bi Y, Li Y, Liu J, Grimstein M, Zhang X, Woods S, Reece K, Abukhdeir AM, Ghosh S, Philip R, Tang S, Goldberg KB, Pazdur R, Beaver JA, Singh H. FDA Approval Summary: Capmatinib and Tepotinib for the Treatment of Metastatic NSCLC Harboring MET Exon 14 Skipping Mutations or Alterations. Clin Cancer Res. 2022 Jan 15;28(2):249-254.

Matsuo M. Antisense oligonucleotide-mediated exon-skipping therapies: precision medicine spreading from Duchenne muscular dystrophy. JMA journal. 2021 Jul 15;4(3):232-40.

Matthay KK, Maris JM, Schleiermacher G, Nakagawara A, Mackall CL, Diller L, Weiss WA. Neuroblastoma. Nat Rev Dis Primers. 2016 Nov 10;2:16078.

Matys V, Kel-Margoulis OV, Fricke E, Liebich I, Land S, Barre-Dirrie A, Reuter I, Chekmenev D, Krull M, Hornischer K, Voss N, Stegmaier P, Lewicki-Potapov B, Saxel H, Kel AE, Wingender E. TRANSFAC and its module TRANSCompel: transcriptional gene regulation in eukaryotes. Nucleic Acids Res. 2006 Jan 1;34(Database issue):D108-10.

Meena JP, Seth R, Chakrabarty B, Gulati S, Agrawala S, Naranje P. Neuroblastoma presenting as opsoclonus-myoclonus: A series of six cases and review of literature. J Pediatr Neurosci. 2016 Oct-Dec;11(4):373-377. doi: 10.4103/1817-1745.199462. PMID: 28217170; PMCID: PMC5314861.

Meng P, Ghosh R. Transcription addiction: can we garner the Yin and Yang functions of E2F1 for cancer therapy? Cell Death Dis. 2014 Aug 7;5(8):e1360.

Merdzhanova G, Edmond V, De Seranno S, Van den Broeck A, Corcos L, Brambilla C, Brambilla E, Gazzeri S, Eymin B. E2F1 controls alternative splicing pattern of genes involved in apoptosis through upregulation of the splicing factor SC35. Cell Death Differ. 2008 Dec;15(12):1815-23.

Milton A, Luoto K, Ingram L, Munro S, Logan N, Graham AL, Brummelkamp TR, Hijmans EM, Bernards R, La Thangue NB. A functionally distinct member of the DP family of E2F subunits. Oncogene. 2006 May 25;25(22):3212-8.

Nagy Á, Munkácsy G, Győrffy B. Pancancer survival analysis of cancer hallmark genes. Scientific reports. 2021 Mar 15;11(1):6047.

NIH (2017) NANT 2015-02: A Phase 1 Study of Lorlatinib (PF-06463922) Retrieved from: https://www.clinicaltrials.gov/ct2/show/NCT03107988 [Accessed 30 March 2023].

NIH (2019) A Study of PRT811 in Participants with Advanced Solid Tumors, CNS Lymphoma and Gliomas. Retrieved from: https://clinicaltrials.gov/ct2/show/NCT04089449?term=PRT811&draw=2&rank=1 [Accessed 30 March 2023].

NIH (2019) A Study of PRT543 in Participants with Advanced Solid Tumors and Hematologic Malignancies Retrieved from: https://clinicaltrials.gov/ct2/show/NCT03886831?term=PRT543&draw=1&rank=1 [Accessed 30 March 2023].

NIH (2022) A Dose Escalation Study of PF-06939999 In Participants with Advanced or Metastatic Solid Tumors. Retrieved from: https://clinicaltrials.gov/ct2/show/NCT03854227 [Accessed 30 March 2023].

Palais G, Nguyen Dinh Cat A, Friedman H, Panek-Huet N, Millet A, Tronche F, Gellen B, Mercadier JJ, Peterson A, Jaisser F. Targeted transgenesis at the HPRT locus: an efficient strategy to achieve tightly controlled in vivo conditional expression with the tet system. Physiol Genomics. 2009 Apr 10;37(2):140-6. doi: 10.1152/physiolgenomics.90328.2008. Epub 2009 Jan 13. PMID: 19141541.

Park JH, Szemes M, Vieira GC, Melegh Z, Malik S, Heesom KJ, Von Wallwitz-Freitas L, Greenhough A, Brown KW, Zheng YG, Catchpoole D, Deery MJ, Malik K. Protein arginine methyltransferase 5 is a key regulator of the MYCN oncoprotein in neuroblastoma cells. Mol Oncol. 2015 Mar;9(3):617-27. doi: 10.1016/j.molonc.2014.10.015. Epub 2014 Nov 15. PMID: 25475372; PMCID: PMC4359099.

Pastore F, Bhagwat N, Pastore A, Radzisheuskaya A, Karzai A, Krishnan A, Li B, Bowman RL, Xiao W, Viny AD, Zouak A, Park YC, Cordner KB, Braunstein S, Maag JL, Grego A, Mehta J, Wang M, Lin H, Durham BH, Koche RP, Rampal RK, Helin K, Scherle P, Vaddi K, Levine RL. PRMT5 Inhibition Modulates E2F1 Methylation and Gene-Regulatory Networks Leading to Therapeutic Efficacy in JAK2V617F-Mutant

MPN. Cancer Discov. 2020 Nov;10(11):1742-1757. doi: 10.1158/2159-8290.CD-20-0026. Epub 2020 Jul 15. PMID: 32669286; PMCID: PMC7642059.

Pathan M, Keerthikumar S, Ang CS, Gangoda L, Quek CY, Williamson NA, Mouradov D, Sieber OM, Simpson RJ, Salim A, Bacic A, Hill AF, Stroud DA, Ryan MT, Agbinya JI, Mariadason JM, Burgess AW, Mathivanan S. FunRich: An open access standalone functional enrichment and interaction network analysis tool. Proteomics. 2015 Aug;15(15):2597-601.

Pohl M, Bortfeldt RH, Grützmann K, Schuster S. Alternative splicing of mutually exclusive exons—A review. Biosystems. 2013 Oct 1;114(1):31-8.

Polager S, Kalma Y, Berkovich E, Ginsberg D. E2Fs up-regulate expression of genes involved in DNA replication, DNA repair and mitosis. Oncogene. 2002 Jan 17;21(3):437-46.

Ponzoni M, Bachetti T, Corrias MV, Brignole C, Pastorino F, Calarco E, Bensa V, Giusto E, Ceccherini I, Perri P. Recent advances in the developmental origin of neuroblastoma: an overview. J Exp Clin Cancer Res. 2022 Mar 11;41(1):92. doi: 10.1186/s13046-022-02281-w. PMID: 35277192; PMCID: PMC8915499.

Ran FA, Hsu PD, Wright J, Agarwala V, Scott DA, Zhang F. Genome engineering using the CRISPR-Cas9 system. Nat Protoc. 2013 Nov;8(11):2281-2308.

Raposo AE, Piller SC. Protein arginine methylation: an emerging regulator of the cell cycle. Cell Div. 2018 Mar 20;13:3.

Ratovitski T, Arbez N, Stewart JC, Chighladze E, Ross CA. PRMT5- mediated symmetric arginine dimethylation is attenuated by mutant huntingtin and is impaired in Huntington's disease (HD). Cell Cycle. 2015;14(11):1716-29.

Reviejo M, Soto M, Lozano E, Asensio M, Martínez-Augustin O, Sánchez de Medina F, Marin JJG. Impact of alternative splicing on mechanisms of resistance to anticancer drugs. Biochem Pharmacol. 2021 Nov;193:114810. doi: 10.1016/j.bcp.2021.114810. Epub 2021 Oct 19. PMID: 34673012.

Richardson DN, Rogers MF, Labadorf A, Ben-Hur A, Guo H, Paterson AH, Reddy AS. Comparative analysis of serine/arginine-rich proteins across 27 eukaryotes: insights into sub-family classification and extent of alternative splicing. PloS one. 2011 Sep 14;6(9):e24542.

Rickman DS, Schulte JH, Eilers M. The Expanding World of N-MYC-Driven Tumors. Cancer Discov. 2018 Feb;8(2):150-163.

Rowland BD, Bernards R. Re-evaluating cell-cycle regulation by E2Fs. Cell. 2006 Dec 1;127(5):871-4.

Roworth AP, Ghari F, La Thangue NB. To live or let die - complexity within the E2F1 pathway. Mol Cell Oncol. 2015 Jan 30;2(1):e970480.

Roworth AP, Carr SM, Liu G, Barczak W, Miller RL, Munro S, Kanapin A, Samsonova A, La Thangue NB. Arginine methylation expands the regulatory mechanisms and extends the genomic landscape under E2F control. Sci Adv. 2019 Jun 26;5(6):eaaw4640.

Ryl T, Kuchen EE, Bell E, Shao C, Flórez AF, Mönke G, Gogolin S, Friedrich M, Lamprecht F, Westermann F, Höfer T. Cell-Cycle Position of Single MYC-Driven Cancer Cells Dictates Their Susceptibility to a Chemotherapeutic Drug. Cell Syst. 2017 Sep 27;5(3):237-250.e8.

Sachamitr P, Ho JC, Ciamponi FE, Ba-Alawi W, Coutinho FJ, Guilhamon P, Kushida MM, Cavalli FM, Lee L, Rastegar N, Vu V. PRMT5 inhibition disrupts splicing and stemness in glioblastoma. Nature communications. 2021 Feb 12;12(1):979.

Samoyedny A, Srinivasan A, States L, Mosse YP, Alai E, Pawel B, Pogoriler J, Shellikeri S, Vatsky S, Acord M, Escobar F, Edgar JC, Maris JM, Cahill AM. Image-Guided Biopsy for Relapsed Neuroblastoma: Focus on Safety, Adequacy for Genetic Sequencing, and Correlation of Tumor Cell Percent With Quantitative Lesion MIBG Uptake. JCO Precis Oncol. 2021 Jan 28;5:PO.20.00171.

Savary C, Kim A, Lespagnol A, Gandemer V, Pellier I, Andrieu C, Pagès G, Galibert MD, Blum Y, de Tayrac M. Depicting the genetic architecture of pediatric cancers through an integrative gene network approach. Sci Rep. 2020 Jan 27;10(1):1224.

Scaglione A, Patzig J, Liang J, Frawley R, Bok J, Mela A, Yattah C, Zhang J, Teo SX, Zhou T, Chen S, Bernstein E, Canoll P, Guccione E, Casaccia P. PRMT5-mediated regulation of developmental myelination. Nat Commun. 2018 Jul 19;9(1):2840.

Schleiermacher G, Mosseri V, London WB, Maris JM, Brodeur GM, Attiyeh E, Haber M, Khan J, Nakagawara A, Speleman F, Noguera R. Segmental chromosomal

alterations have prognostic impact in neuroblastoma: a report from the INRG project. British journal of cancer. 2012 Oct;107(8):1418-22.

Schmelz K, Toedling J, Huska M, Cwikla MC, Kruetzfeldt LM, Proba J, Ambros PF, Ambros IM, Boral S, Lodrini M, Chen CY, Burkert M, Guergen D, Szymansky A, Astrahantseff K, Kuenkele A, Haase K, Fischer M, Deubzer HE, Hertwig F, Hundsdoerfer P, Henssen AG, Schwarz RF, Schulte JH, Eggert A. Spatial and temporal intratumour heterogeneity has potential consequences for single biopsy-based neuroblastoma treatment decisions. Nat Commun. 2021 Nov 23;12(1):6804.

Sengupta R, Zaidi SK. AACR Cancer Progress Report 2021: discovery science driving clinical breakthroughsAACR cancer progress report 2021. Clinical Cancer Research. 2021 Nov 1;27(21):5757-9.

Shats I, Deng M, Davidovich A, Zhang C, Kwon JS, Manandhar D, Gordân R, Yao G, You L. Expression level is a key determinant of E2F1-mediated cell fate. Cell Death Differ. 2017 Apr;24(4):626-637.

Shen S, Park JW, Lu ZX, Lin L, Henry MD, Wu YN, Zhou Q, Xing Y. rMATS: robust and flexible detection of differential alternative splicing from replicate RNA-Seq data. Proc Natl Acad Sci U S A. 2014 Dec 23;111(51):E5593-601.

Shi Y, Yuan J, Rraklli V, Maxymovitz E, Cipullo M, Liu M, Li S, Westerlund I, Bedoya-Reina OC, Bullova P, Rorbach J, Juhlin CC, Stenman A, Larsson C, Kogner P, O'Sullivan MJ, Schlisio S, Holmberg J. Aberrant splicing in neuroblastoma generates RNA-fusion transcripts and provides vulnerability to spliceosome inhibitors. Nucleic Acids Res. 2021 Mar 18;49(5):2509-2521.

Sibley CR, Blazquez L, Ule J. Lessons from non-canonical splicing. Nat Rev Genet. 2016 Jul;17(7):407-421.

Singh S, Quarni W, Goralski M, Wan S, Jin H, Van de Velde LA, Fang J, Wu Q, Abu-Zaid A, Wang T, Singh R, Craft D, Fan Y, Confer T, Johnson M, Akers WJ, Wang R, Murray PJ, Thomas PG, Nijhawan D, Davidoff AM, Yang J. Targeting the spliceosome through RBM39 degradation results in exceptional responses in high-risk neuroblastoma models. Sci Adv. 2021 Nov 19;7(47):eabj5405.

Sivanandhan D, Garapaty S, Vadivelu S, Seerapu GP, Das R, Kar R, Singh AK, Venkateshappa VA, Tamizharasan N, Swamy IN, Nagaraju N. Novel, small-molecule

PRMT5 inhibitors for treatment of cancer. Cancer Research. 2018 Jul 1;78(13_Supplement):4856-.

Smith CR, Aranda R, Bobinski TP, Briere DM, Burns AC, Christensen JG, Clarine J, Engstrom LD, Gunn RJ, Ivetac A, Jean-Baptiste R. Fragment-based discovery of MRTX1719, a synthetic lethal inhibitor of the PRMT5• MTA complex for the treatment of MTAP-deleted cancers. Journal of Medicinal Chemistry. 2022 Jan 18;65(3):1749-66.

Smith V, Foster J. High-Risk Neuroblastoma Treatment Review. Children (Basel). 2018 Aug 28;5(9):114.

Stanelle J, Stiewe T, Theseling CC, Peter M, Pützer BM. Gene expression changes in response to E2F1 activation. Nucleic Acids Res. 2002 Apr 15;30(8):1859-67.

Stark R, Grzelak M, Hadfield J. RNA sequencing: the teenage years. Nat Rev Genet. 2019 Nov;20(11):631-656.

Strenger V, Kerbl R, Dornbusch HJ, Ladenstein R, Ambros PF, Ambros IM, Urban C. Diagnostic and prognostic impact of urinary catecholamines in neuroblastoma patients. Pediatr Blood Cancer. 2007 May;48(5):504-9.

Strieder V, Lutz W. E2F proteins regulate MYCN expression in neuroblastomas. J Biol Chem. 2003 Jan 31;278(5):2983-9.

Subramanian A, Tamayo P, Mootha VK, Mukherjee S, Ebert BL, Gillette MA, Paulovich A, Pomeroy SL, Golub TR, Lander ES, Mesirov JP. Gene set enrichment analysis: a knowledge-based approach for interpreting genome-wide expression profiles. Proc Natl Acad Sci U S A. 2005 Oct 25;102(43):15545-50.

Swiss VA, Casaccia P. Cell-context specific role of the E2F/Rb pathway in development and disease. Glia. 2010 Mar;58(4):377-90.

Swiss VA, Casaccia P. Cell-context specific role of the E2F/Rb pathway in development and disease. Glia. 2010 Mar;58(4):377-90.

Taylor J, Lee SC. Mutations in spliceosome genes and therapeutic opportunities in myeloid malignancies. Genes Chromosomes Cancer. 2019 Dec;58(12):889-902.

Tazi J, Bakkour N, Stamm S. Alternative splicing and disease. Biochim Biophys Acta. 2009 Jan;1792(1):14-26.

Tolbert VP, Matthay KK. Neuroblastoma: clinical and biological approach to risk stratification and treatment. Cell Tissue Res. 2018 May;372(2):195-209.

Trigg RM, Turner SD. ALK in Neuroblastoma: Biological and Therapeutic Implications. Cancers (Basel). 2018 Apr 10;10(4):113. doi: 10.3390/cancers10040113. PMID: 29642598; PMCID: PMC5923368.

Urbanski LM, Leclair N, Anczuków O. Alternative-splicing defects in cancer: Splicing regulators and their downstream targets, guiding the way to novel cancer therapeutics. Wiley Interdiscip Rev RNA. 2018 Jul;9(4):e1476.

Vélez-Cruz R, Johnson DG. The Retinoblastoma (RB) Tumor Suppressor: Pushing Back against Genome Instability on Multiple Fronts. Int J Mol Sci. 2017 Aug 16;18(8):1776.

Villar MV, Spreafico A, Moreno V, Braña I, Hernandez T, Razak AA, Wang J, Haddish-Berhane N, Mehta J, Johnson A, Maes A. 537MO First-in-human study of JNJ-64619178, a protein arginine methyltransferase 5 (PRMT5) inhibitor, in patients with advanced cancers. Annals of Oncology. 2020 Sep 1;31:S470.

Voeller J, Sondel PM. Advances in anti-GD2 immunotherapy for treatment of high-risk neuroblastoma. Journal of pediatric hematology/oncology. 2019 Apr;41(3):163.

Wang H, Wang X, Xu L, Zhang J. Prognostic analysis of E2F transcription factors E2F1 and E2F3 in four independent pediatric neuroblastoma cohorts. BMC pediatrics. 2022 Dec;22(1):1-5.

Weiss WA, Aldape K, Mohapatra G, Feuerstein BG, Bishop JM. Targeted expression of MYCN causes neuroblastoma in transgenic mice. EMBO J. 1997 Jun 2;16(11):2985-95. doi: 10.1093/emboj/16.11.2985. PMID: 9214616; PMCID: PMC1169917.

Wolpaw AJ, Bayliss R, Büchel G, Dang CV, Eilers M, Gustafson WC, Hansen GH, Jura N, Knapp S, Lemmon MA, Levens D, Maris JM, Marmorstein R, Metallo SJ, Park JR, Penn LZ, Rape M, Roussel MF, Shokat KM, Tansey WP, Verba KA, Vos SM, Weiss WA, Wolf E, Mossé YP. Drugging the "Undruggable" MYCN Oncogenic Transcription Factor: Overcoming Previous Obstacles to Impact Childhood Cancers. Cancer Res. 2021 Apr 1;81(7):1627-1632. doi: 10.1158/0008-5472.CAN-20-3108. Epub 2021 Jan 28. PMID: 33509943; PMCID: PMC8392692.

Worst BC, van Tilburg CM, Balasubramanian GP, Fiesel P, Witt R, Freitag A, Boudalil M, Previti C, Wolf S, Schmidt S, Chotewutmontri S, Bewerunge-Hudler M, Schick M, Schlesner M, Hutter B, Taylor L, Borst T, Sutter C, Bartram CR, Milde T, Pfaff E, Kulozik AE, von Stackelberg A, Meisel R, Borkhardt A, Reinhardt D, Klusmann JH, Fleischhack G, Tippelt S, Dirksen U, Jürgens H, Kramm CM, von Bueren AO, Westermann F, Fischer M, Burkhardt B, Wößmann W, Nathrath M, Bielack SS, Frühwald MC, Fulda S, Klingebiel T, Koscielniak E, Schwab M, Tremmel R, Driever PH, Schulte JH, Brors B, von Deimling A, Lichter P, Eggert A, Capper D, Pfister SM, Jones DT, Witt O. Next-generation personalised medicine for high-risk paediatric cancer patients - The INFORM pilot study. Eur J Cancer. 2016 Sep;65:91-101.

Wu H, Zheng W, Eram MS, Vhuiyan M, Dong A, Zeng H, He H, Brown P, Frankel A, Vedadi M, Luo M, Min J. Structural basis of arginine asymmetrical dimethylation by PRMT6. Biochem J. 2016 Oct 1;473(19):3049-63. doi: 10.1042/BCJ20160537. Epub 2016 Aug 1. PMID: 27480107; PMCID: PMC5280038.

Wu JY, Maniatis T. Specific interactions between proteins implicated in splice site selection and regulated alternative splicing. Cell. 1993 Dec 17;75(6):1061-70.

Xiao W, Chen X, Liu L, Shu Y, Zhang M, Zhong Y. Role of protein arginine methyltransferase 5 in human cancers. Biomed Pharmacother. 2019 Jun;114:108790.

Yu AL, Gilman AL, Ozkaynak MF, London WB, Kreissman SG, Chen HX, Smith M, Anderson B, Villablanca JG, Matthay KK, Shimada H. Anti-GD2 antibody with GM-CSF, interleukin-2, and isotretinoin for neuroblastoma. New England Journal of Medicine. 2010 Sep 30;363(14):1324-34.

Zhang S, Wei JS, Li SQ, Badgett TC, Song YK, Agarwal S, Coarfa C, Tolman C, Hurd L, Liao H, He J, Wen X, Liu Z, Thiele CJ, Westermann F, Asgharzadeh S, Seeger RC, Maris JM, Guidry Auvil JM, Smith MA, Kolaczyk ED, Shohet J, Khan J. MYCN controls an alternative RNA splicing program in high-risk metastatic neuroblastoma. Cancer Lett. 2016 Feb 28;371(2):214-24.

Zhang Y, Qian J, Gu C, Yang Y. Alternative splicing and cancer: a systematic review. Signal transduction and targeted therapy. 2021 Feb 24;6(1):78.

Zheng S, Moehlenbrink J, Lu YC, et al. Arginine methylation-dependent reader-writer interplay governs growth control by E2F-1. Mol Cell. 2013;52(1):37-51. doi:10.1016/j.molcel.2013.08.039

Zhou Y, Zhou B, Pache L, Chang M, Khodabakhshi AH, Tanaseichuk O, Benner C, Chanda SK. Metascape provides a biologist-oriented resource for the analysis of systems-level datasets. Nature communications. 2019 Apr 3;10(1):1523.

Appendix A

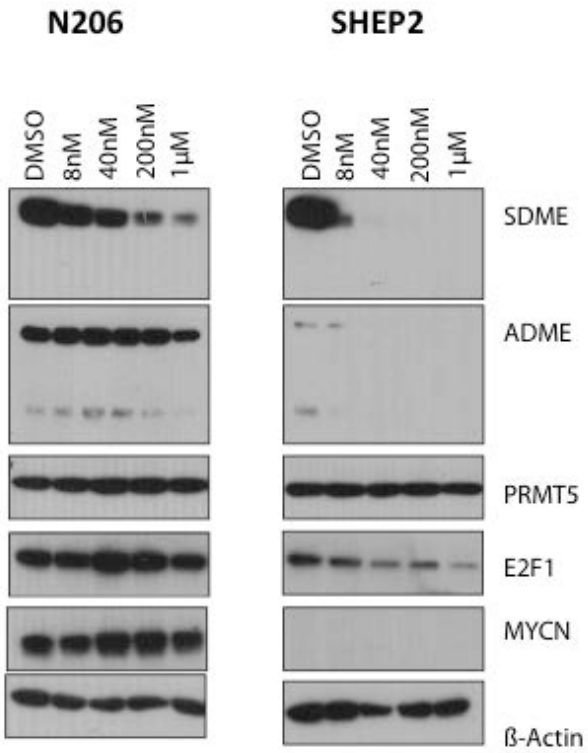

Figure 1. MYCN amplified N206 and non-MYCN amplified SHEP-2 cell lines were treated with 8 nM-1 μM concentrations of T1-44 compound treatment after 6 days. Representative image of western blots for 3 different biological replicates was represented. 20μg total protein was loaded onto the gels. β-actin was used as a loading control.

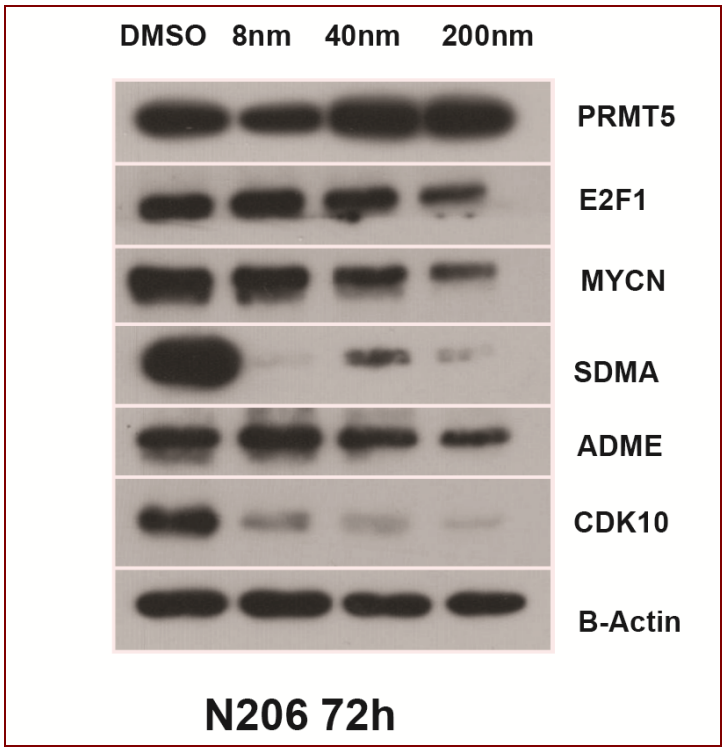

Figure 2. CDK10 protein expression levels of MYCN amplified N206 cell line after treatment with 8-200 nM concentrations of compound T1-44, SDMA (Symmetric Dimethylarginine) motif antibody was used to show inhibition of methyl marks by compound T1-44.

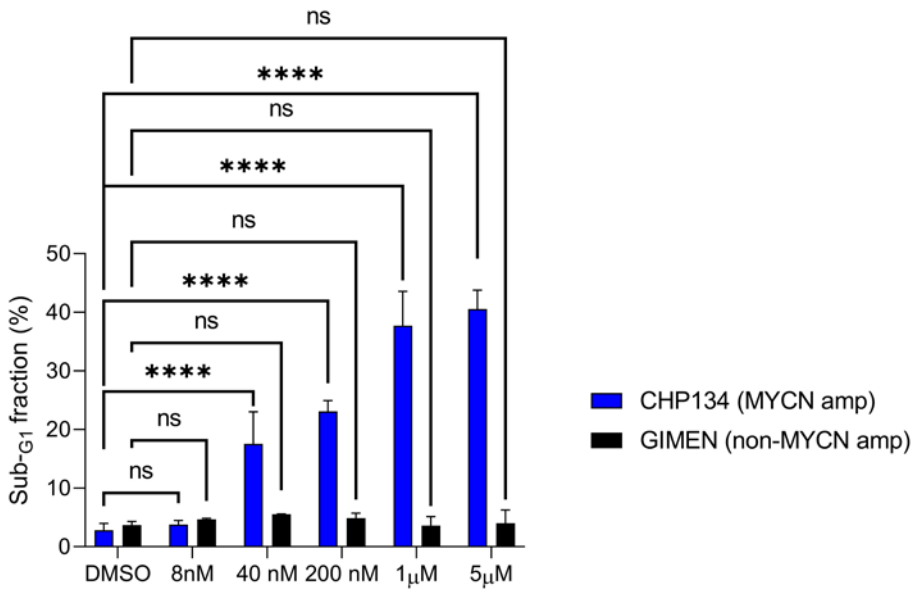

Figure 3. MYCN amplified CHP-134 and non-MYCN amplified GI-ME-N cell lines were treated with 8 nM-5 µM concentrations of T1-44 compound treatment for 6 days and SubG1 was analysed by flow cytometer. Results shown are average of three independent experiments. Data were analysed by two-way ANOVA test. ns: $p>0.05$, **** $p<0.0001$ (Data was kindly provided from Dr. Laurel Bate-Eya).

Appendix B

Table 1. Differentially expressed gene list in CHP-134 DMSO versus CHP-134 200 nM T1-44 treatment after 72 hours (Limited to 100 genes and sorted by log2 fold changes).

Base mean	Log2 fold change	padj	ENSEMBL	Symbol
28.7192545	6.947212468	4.94E-06	ENSG00000224294	PINCR
8.276383632	6.520720488	8.63E-05	ENSG00000180921	FAM83H
35.42714139	6.265644929	8.46E-05	ENSG00000268812	LOC91370
296.2212496	5.45780513	2.78E-24	ENSG00000130513	GDF15
42.16847938	5.230853352	0.000223909	ENSG00000250337	PURPL
534.145758	5.017672529	3.45E-07	ENSG00000128342	LIF
10.82181499	4.882184924	5.08E-06	ENSG00000186529	CYP4F3
30.10267086	4.862573214	3.57E-16	ENSG00000177098	SCN4B
9.104149751	4.839394086	6.13E-05	ENSG00000174898	CATSPERD
280.7578321	4.838713038	1.66E-19	ENSG00000180139	ACTA2-AS1
364.6714507	4.818239429	0.000224612	ENSG00000154127	UBASH3B
137.1539795	4.816465519	1.33E-47	ENSG00000168918	INPP5D
7.541908014	4.752197538	0.009073331	ENSG00000228496	LOC100506405
11.24304858	4.708985551	1.27E-06	ENSG00000183072	NKX2-5
574.811942	4.55055854	1.98E-28	ENSG00000107796	ACTA2
105.3168817	4.401747036	0.006482142	ENSG00000087589	CASS4
76.65464655	4.20721395	0.000383917	ENSG00000138347	MYPN
719.4643603	4.182549596	1.31E-41	ENSG00000120875	DUSP4
172.6264832	4.134597245	4.04E-05	ENSG00000187678	SPRY4
601.7953927	4.006089158	9.94E-45	ENSG00000131080	EDA2R
44.99094463	3.893779497	1.23E-12	ENSG00000143217	NECTIN4
2680.261626	3.887233507	2.09E-06	ENSG00000146674	IGFBP3
656.6957904	3.73814601	0.007023945	ENSG00000102452	NALCN
492.2941304	3.660972344	6.62E-49	ENSG00000142627	EPHA2
9.126854353	3.584412205	0.000157082	ENSG00000162511	LAPTM5
54.91832633	3.566663849	6.68E-14	ENSG00000257202	NA
539.8387773	3.493089626	2.96E-10	ENSG00000185432	METTL7A
17.70641875	3.475980539	0.003340019	ENSG00000205592	MUC19

12.42489102	3.446367957	0.002574788	ENSG00000233218	NA
7.397193217	3.343205621	0.001044702	ENSG00000150394	CDH8
6.603677974	3.327604002	0.002704874	ENSG00000182040	USH1G
73.15596326	3.269468745	6.77E-19	ENSG00000198075	SULT1C4
96.68879523	3.245479956	1.23E-21	ENSG00000163071	SPATA18
6.830089308	3.18778931	0.001881765	ENSG00000148734	NPFFR1
244.2066487	3.135979666	1.52E-31	ENSG00000244694	PTCHD4
31.06354483	3.095052402	3.30E-08	ENSG00000101198	NKAIN4
11.85128007	3.08882973	0.000213598	ENSG00000237512	UNC5B-AS1
550.698796	3.077449129	8.30E-39	ENSG00000136048	DRAM1
112.1963173	3.052437337	0.000203973	ENSG00000202198	RN7SK
58.74532863	3.029844975	2.22E-10	ENSG00000118898	PPL
41.28214177	3.023989325	6.46E-09	ENSG00000260412	NA
5950.381807	2.998828044	8.34E-30	ENSG00000124762	CDKN1A
77.50678583	2.905677747	1.46E-16	ENSG00000040731	CDH10
117.3794282	2.883384425	2.70E-25	ENSG00000224818	NA
779.6826141	2.847746995	2.81E-22	ENSG00000174307	PHLDA3
14.03732499	2.829285743	0.000225963	ENSG00000266680	NA
190.8852805	2.80561675	2.37E-07	ENSG00000173546	CSPG4
276.3294043	2.759485684	1.30E-10	ENSG00000076356	PLXNA2
29.38629361	2.751856856	4.42E-05	ENSG00000161509	GRIN2C
10.0991358	2.727193812	0.00069104	ENSG00000235098	ANKRD65
148.1199885	2.697865957	2.84E-11	ENSG00000105327	BBC3
817.9357121	2.689600555	4.54E-09	ENSG00000099204	ABLIM1
14.24898598	2.676837863	0.001718054	ENSG00000162009	SSTR5
35.34545257	2.665512906	4.62E-07	ENSG00000262766	NA
1817.93822	2.636601683	8.03E-12	ENSG00000145632	PLK2
25.88127853	2.598765391	8.20E-06	ENSG00000073282	TP63
11.24187723	2.547164125	0.002747596	ENSG00000117595	IRF6
143.3109179	2.526432267	1.57E-12	ENSG00000026103	FAS
17.11734083	2.525127799	0.001069405	ENSG00000184599	TAFA3
22.98260178	2.501137054	1.84E-07	ENSG00000141579	ZNF750
28.77165748	2.495862092	3.91E-07	ENSG00000157445	CACNA2D3
10.29656486	2.468481942	0.003328587	ENSG00000070193	FGF10

68.72999981	2.466460561	6.88E-09	ENSG00000150594	ADRA2A
1056.392271	2.460152649	2.16E-05	ENSG00000184371	CSF1
78.72515995	2.45667328	3.88E-10	ENSG00000165973	NELL1
128.1353092	2.44447633	2.19E-05	ENSG00000172572	PDE3A
21.45461344	2.412128525	7.33E-05	ENSG00000188993	LRRC66
23.56839954	2.409129153	1.61E-05	ENSG00000123454	DBH
29.71690069	2.397598642	0.003396695	ENSG00000224945	NA
29.58192761	2.396118424	0.007104902	ENSG00000188175	HEPACAM2
35.19244413	2.392682028	2.05E-05	ENSG00000248587	NA
73.82484337	2.382832502	0.00451935	ENSG00000172927	MYEOV
394.2874063	2.382255444	0.00058038	ENSG00000115896	PLCL1
16.09622005	2.367363918	0.000481053	ENSG00000099338	CATSPERG
27.45518943	2.361783521	2.16E-05	ENSG00000169116	PARM1
143.5442871	2.356242089	0.000534535	ENSG00000198753	PLXNB3
134.977924	2.352358022	8.44E-06	ENSG00000173114	LRRN3
81.27529498	2.301613102	1.53E-07	ENSG00000198576	ARC
203.0137675	2.286379195	6.93E-06	ENSG00000158125	XDH
12.4034192	2.277930239	0.001559543	ENSG00000166145	SPINT1
8.3351459	2.270828742	0.008102554	ENSG00000225156	NA
49.93410928	2.262943747	1.38E-05	ENSG00000261490	NA
15.1249721	2.210701389	0.003949694	ENSG00000168274	NA
53.47283514	2.207481185	5.84E-07	ENSG00000151136	BTBD11
16.73928814	2.20166353	0.000243618	ENSG00000128276	RFPL3
74.85669113	2.187304188	2.69E-12	ENSG00000171246	NPTX1
15.19079394	2.182977668	0.001044702	ENSG00000156564	LRFN2
12.94710408	2.16575345	0.003536974	ENSG00000170835	CEL
17.49415473	2.165703808	0.008389033	ENSG00000116147	TNR
30.05359527	2.160916884	0.000380182	ENSG00000177106	EPS8L2
29.27344023	2.15646664	1.50E-06	ENSG00000260023	NA
13.45787161	2.152573763	0.0038476	ENSG00000212766	EWSAT1
18.94203331	2.146080448	0.000193298	ENSG00000128739	SNRPN
81.55993782	2.11374329	0.008826424	ENSG00000184564	SLITRK6
90.47223085	2.111506951	2.90E-10	ENSG00000271730	NA
213.7889504	2.087944897	0.00412388	ENSG00000175832	ETV4

12.96308665	2.087079298	0.001541253	ENSG00000062038	CDH3
10.90709973	2.083979456	0.00427994	ENSG00000225756	DBH-AS1
12.61951615	2.075008013	0.003624449	ENSG00000264232	NA

Table 2. Differentially expressed gene list in GI-ME-N DMSO versus GI-ME-N 200 nM T1-44 treatment after 72 hours (Top genes list).

Base mean	Log2 fold change	padj	ENSEMBL	Symbol
35.34545257	2.189349072	0.002320436	ENSG00000262766	NA
143.9251561	2.118719911	6.55E-11	ENSG00000162630	B3GALT2
149.1772509	1.223443337	6.22E-05	ENSG00000135407	AVIL
388.4565329	1.214336249	0.000860672	ENSG00000166261	ZNF202
737.242652	1.097989782	1.09E-05	ENSG00000147454	SLC25A37
413.8895887	1.053384321	0.007792446	ENSG00000006016	CRLF1
623.6094987	1.024969121	0.000498967	ENSG00000044446	PHKA2
2451.389979	0.922720184	0.000154149	ENSG00000074054	CLASP1
131.6698358	0.902412289	0.005403017	ENSG00000239779	WBP1
4267.033443	0.900834555	0.001281755	ENSG00000124181	PLCG1
1674.45669	0.831665198	0.007792446	ENSG00000134186	PRPF38B
494.425255	0.80610166	0.002320436	ENSG00000092094	OSGEP
1326.167961	0.781585471	0.005403017	ENSG00000111641	NOP2
1781.686742	0.779171502	0.008536751	ENSG00000126773	PCNX4
514.5615137	0.723070696	0.002907111	ENSG00000119953	SMNDC1
712.1602438	-0.69253457	0.003433013	ENSG00000187239	FNBP1
530.5218939	-0.81415353	0.008230156	ENSG00000128973	CLN6
353.6597465	-0.823979831	0.002320436	ENSG00000167272	POP5
523.7553206	-0.856375442	0.001478403	ENSG00000135414	GDF11
544.3171747	-0.899301529	6.22E-05	ENSG00000092330	TINF2
832.3226771	-1.052643843	0.007989984	ENSG00000189306	RRP7A
1072.443384	-1.140672572	0.000372376	ENSG00000044090	CUL7
1916.022969	-1.303835431	6.55E-11	ENSG00000172660	NA
148.7961715	-1.450641912	0.000501613	ENSG00000102854	MSLN
192.6507324	-1.538529296	3.33E-07	ENSG00000156398	SFXN2
136.380619	-1.542095423	0.009167331	ENSG00000230487	PSMG3-AS1
301.786096	-1.555365381	3.88E-06	ENSG00000134575	ACP2
115.6597216	-1.612066504	0.001836569	ENSG00000269837	NA
296.2542411	-1.677545961	0.000176514	ENSG00000178057	NDUFAF3
35.34545257	2.189349072	0.002320436	ENSG00000262766	NA

143.9251561	2.118719911	6.55E-11	ENSG00000162630	B3GALT2
149.1772509	1.223443337	6.22E-05	ENSG00000135407	AVIL
388.4565329	1.214336249	0.000860672	ENSG00000166261	ZNF202
737.242652	1.097989782	1.09E-05	ENSG00000147454	SLC25A37
413.8895887	1.053384321	0.007792446	ENSG00000006016	CRLF1
623.6094987	1.024969121	0.000498967	ENSG00000044446	PHKA2
2451.389979	0.922720184	0.000154149	ENSG00000074054	CLASP1
131.6698358	0.902412289	0.005403017	ENSG00000239779	WBP1
4267.033443	0.900834555	0.001281755	ENSG00000124181	PLCG1
1674.45669	0.831665198	0.007792446	ENSG00000134186	PRPF38B
494.425255	0.80610166	0.002320436	ENSG00000092094	OSGEP
1326.167961	0.781585471	0.005403017	ENSG00000111641	NOP2
1781.686742	0.779171502	0.008536751	ENSG00000126773	PCNX4
514.5615137	0.723070696	0.002907111	ENSG00000119953	SMNDC1
712.1602438	-0.69253457	0.003433013	ENSG00000187239	FNBP1

Table 3. Differentially expressed gene list in CHP-134 E2F1 KO DMSO versus CHP-134 E2F1 KO 200 nM T1-44 treatment for 72 hours (Limited to 100 genes and sorted by log2 fold changes).

Base mean	Log2 fold change	padj	ENSEMBL	E2F1_flag	Symbol
3.051418657	5.10515109	0.007755119	ENSG00000238097	0	LINC02037
5.45113713	3.986120195	0.009925442	ENSG00000227852	0	NA
4.685330689	3.749653171	0.037254064	ENSG00000183662	0	TAFA1
6.870621519	3.719998846	0.006198296	ENSG00000188424	0	NA
4.240142966	3.598966074	0.032965551	ENSG00000260305	0	NTRK3-AS1
9.939221509	3.517359447	0.000511425	ENSG00000253553	1	NA
9.292951743	3.396940582	0.00089447	ENSG00000181323	0	SPEM1
3.705097641	3.38791278	0.057575165	ENSG00000253068	0	NA
8.77885349	3.313385018	0.001430944	ENSG00000261783	0	NA
6.698754008	3.225352554	0.013089238	ENSG00000120500	0	ARR3
3.05204118	3.093668881	0.096008757	ENSG00000215498	0	FAM230B
3.041870533	3.089321593	0.095100189	ENSG00000259792	0	NA
10.73145251	3.078602002	0.002581668	ENSG00000123080	1	CDKN2C
3.001187943	3.072381446	0.108376205	ENSG00000270571	1	NA
3.041460871	3.063022592	0.113513455	ENSG00000271367	0	NA
3.015746853	3.058583718	0.11954166	ENSG00000237487	0	VN1R48P
8.743447696	3.029320762	0.003532886	ENSG00000260423	0	LINC02367
4.389060404	3.018654491	0.041613728	ENSG00000228043	1	NA
6.919471755	2.93031998	0.009372779	ENSG00000197635	1	DPP4
4.032586904	2.869373044	0.082056278	ENSG00000204361	0	NXPE2
3.844775359	2.837767763	0.087587707	ENSG00000268654	0	MIMT1
20.63858205	2.817827791	0.000235553	ENSG00000184979	1	USP18
6.246625183	2.751828866	0.020791711	ENSG00000134042	0	MRO
3.687874289	2.735372737	0.083946423	ENSG00000244009	0	NA
3.655697666	2.723097993	0.109708397	ENSG00000188051	1	TMEM221
6.072147448	2.708078009	0.023799241	ENSG00000254332	0	NA
4.838593996	2.704440513	0.057511659	ENSG00000254141	0	NA
5.719338527	2.628850054	0.036240962	ENSG00000259216	0	LOC645405
3.38988366	2.593139792	0.125512734	ENSG00000260490	0	NA

12.21366796	2.566238894	0.002786093	ENSG00000227091	0	NA
3.363956095	2.561641077	0.13068903	ENSG00000256508	0	MRGPRF-AS1
3.357114807	2.558731209	0.133646699	ENSG00000249694	0	NA
3.262435629	2.504413953	0.169359779	ENSG00000008196	0	TFAP2B
3.206913503	2.500718496	0.146846264	ENSG00000251126	0	NA
13.8114682	2.490844073	0.000747854	ENSG00000129167	0	TPH1
3.206405784	2.481681478	0.148513843	ENSG00000257954	0	NA
16.90768135	2.467980635	0.001103304	ENSG00000171502	0	COL24A1
6.203501767	2.461522463	0.037309062	ENSG00000234264	1	DEPDC1-AS1
47.56349907	2.445124916	9.62E-09	ENSG00000165806	1	CASP7
3.004488455	2.408118964	0.205630194	ENSG00000232027	0	NA
6.039759409	2.397323572	0.038937333	ENSG00000200879	0	SNORD14E
11.66868012	2.342085981	0.007126219	ENSG00000175445	0	LPL
11.55718515	2.317011734	0.004909674	ENSG00000231424	0	NA
3.869323417	2.310523886	0.1393054	ENSG00000272002	0	NA
31.4775772	2.305792989	2.49E-06	ENSG00000212232	0	SNORD17
27.01356104	2.303655052	0.004464821	ENSG00000161103	0	LOC102725072
3.855935014	2.295740723	0.177339588	ENSG00000259030	1	FPGT-TNNI3K
37.82733569	2.279626236	4.63E-07	ENSG00000204228	0	HSD17B8
5.487929241	2.246922924	0.097380426	ENSG00000200090	0	NA
17.59477041	2.244893863	0.001801863	ENSG00000269113	0	TRABD2B
4.604139418	2.228662502	0.117454458	ENSG00000199890	0	NA
10.85484208	2.213772364	0.010675409	ENSG00000186369	0	NA
36.33032884	2.20823571	6.32E-06	ENSG00000074416	1	MGLL
5.385999114	2.198253304	0.075526817	ENSG00000250061	0	NA
8.120159741	2.195277327	0.030380587	ENSG00000203546	1	NA
3.553275496	2.169920351	0.178926281	ENSG00000231007	0	CDC20P1
4.399853575	2.164741909	0.138110327	ENSG00000269845	0	CCNYL6
348.1221897	2.133848019	2.64E-19	ENSG00000123610	0	TNFAIP6
409.8632992	2.132801733	7.47E-16	ENSG00000170801	0	HTRA3
10.39889148	2.131826155	0.012949388	ENSG00000261560	0	NA
17.44897542	2.12961165	0.003053042	ENSG00000232093	1	NA
4392.568221	2.118013587	6.45E-26	ENSG00000171848	1	RRM2
629.0281424	2.103568959	4.55E-16	ENSG00000144824	1	PHLDB2

4.98586243	2.084337813	0.130605512	ENSG00000228763	0	LIMS1-AS1
13.41286242	2.081405563	0.007491658	ENSG00000152208	0	GRID2
4.146014036	2.081062883	0.182444775	ENSG00000227167	0	NA
10.13153794	2.078796662	0.02876569	ENSG00000251271	0	NA
4.181292925	2.076458145	0.142790456	ENSG00000250081	0	NA
3.353279858	2.075299385	0.221381351	ENSG00000232893	0	NA
7.592622377	2.074356897	0.061064834	ENSG00000135547	1	HEY2
114.8547768	2.070104552	0.013668012	ENSG00000162407	1	PLPP3
7.528776852	2.070031294	0.070470854	ENSG00000240522	0	RPL7AP10
7.54325125	2.064156745	0.077348771	ENSG00000123388	1	HOXC11
12.48745625	2.058844085	0.019013437	ENSG00000149646	0	CNBD2
6.510891444	2.02861612	0.068372785	ENSG00000268402	0	NA
40.13662682	2.026291704	3.67E-06	ENSG00000110675	0	ELMOD1
5.741418259	2.011831682	0.110550163	ENSG00000273366	0	NA
7.238950668	2.00823781	0.053256897	ENSG00000250167	0	NA
3.98699516	2.00757791	0.178771826	ENSG00000197142	0	ACSL5
4.018846632	2.004751682	0.187162811	ENSG00000249249	0	NA
50.71975436	2.002061766	1.93E-07	ENSG00000235423	0	NA
597.4233982	2.000372563	2.01E-34	ENSG00000160867	1	FGFR4
4.070166542	1.993831099	0.200034759	ENSG00000272979	0	NA
3.160940946	1.981621636	0.259611413	ENSG00000182824	0	FAM230E
3.159276266	1.980861902	0.257659801	ENSG00000184984	1	CHRM5
3.222600526	1.97895476	0.249101363	ENSG00000232648	1	NA
4.672524546	1.967531339	0.149440322	ENSG00000189269	0	DRICH1
58.37240962	1.967200664	7.61E-08	ENSG00000178343	0	SHISA3
7.891189935	1.965561079	0.044039073	ENSG00000197465	0	GYPE
3.190339392	1.961545782	0.261750768	ENSG00000219016	0	NA
4.710232845	1.960783026	0.169474206	ENSG00000149305	0	HTR3B
10.19264503	1.96074218	0.021786068	ENSG00000247877	0	NA
1488.375089	1.959933388	1.13E-33	ENSG00000121691	0	CAT
55.59885815	1.953616672	1.05E-05	ENSG00000123685	1	BATF3
55.78863601	1.950169012	1.89E-05	ENSG00000135272	1	MDFIC
31.14286779	1.949300066	6.08E-05	ENSG00000259495	0	NA
60.40379179	1.94837121	0.069765725	ENSG00000137693	1	YAP1

6.99268617	1.943382527	0.076409619	ENSG00000236364	0	NA
7.034721835	1.941583272	0.071823533	ENSG00000124429	0	POF1B